Many-Body Dynamics of Atoms and Molecules

2

2.1 Precision Nuclear Ground-State Properties

Photo of the high-precision hyperbolic Penning trap of TRIGA-TRAP installed at the nuclear research reactor TRIGA in Mainz (Photo: G. Otto, GSI Darmstadt).

Introduction

Mass can be considered as an ID card for a nucleus in the world of physics. The mass is not merely "dead weight" but a source of valuable information about the internal structure of a nuclide and the forces which form the nuclide. The mass defines the place of residence of a nuclide on the nuclear chart of matter. It gives insight into the life expectancy of a nuclide and defines how its life ends.

The more precisely the mass of a nuclide is known, the more comprehensively one can study the laws of nature that govern the life of nuclides. Knowing the mass with a relatively moderate precision of 1000 parts-per-billion (ppb) is sufficient to study such collective effects of nuclear matter as the existence of shell closures, shell quenching, regions of nuclear deformation, drip lines, halos and the island of stability of super-heavy elements. A precision of 100 ppb already allows for a separation of nuclear excited states, so called isomers, and opens the door to the realm of nuclear astrophysics, which describes the synthesis of nuclides in nature. Measurements of masses of certain nuclides on the 10 ppb level enable investigating such aspects of the standard model as the conserved vector current hypothesis and the unitarity of the Cabibbo-Kobayashi-Maskawa quark mixing matrix. Particularly high-precision below 1 ppb is required for mass measurements of specific nuclides in order to address fundamental questions on the value of the neutrino mass and the validity of quantum electrodynamics in strong electro-magnetic fields.

At present, three complementary techniques are applied in high-precision mass measurements of exotic nuclides: Isochronous and Schottky Mass Spectrometry (IMS and SMS, respectively) in storage rings, and Penning-trap mass spectrometry (PT-MS). These techniques are favoured since they are based on a determination of the mass of a nuclide via a measurement of either its revolution frequency in a storage ring or its cyclotron frequency in a strong homogeneous magnetic field. Although, IMS offers only a moderate precision of slightly better than 1000 ppb, this is the only mass measurement technique that provides access to very short-lived nuclides with half-lives in the microsecond range and that requires only several particles for a successful mass determination. SMS allows for mass measurements at the 100 ppb level of nuclides with half-lives as short as several seconds. As soon as masses with a precision of below 100 ppb are required, Penning-trap mass spectrometry becomes the method of choice. Recently, first results from a fourth technique called multi-reflection time-of-flight mass spectrometry have become available. Its appeal lies in the fact that mass measurements on a 100 ppb level become possible for nuclides with minute production rates and half-lives below 100 ms. It thus nicely bridges the gap between the low precision but fast IMS technique and the slower and more precise SMS or PT-MS techniques.

Fig. 1: TRIGA-SPEC: A setup for mass spectrometry and laser spectroscopy at the research reactor TRIGA Mainz.

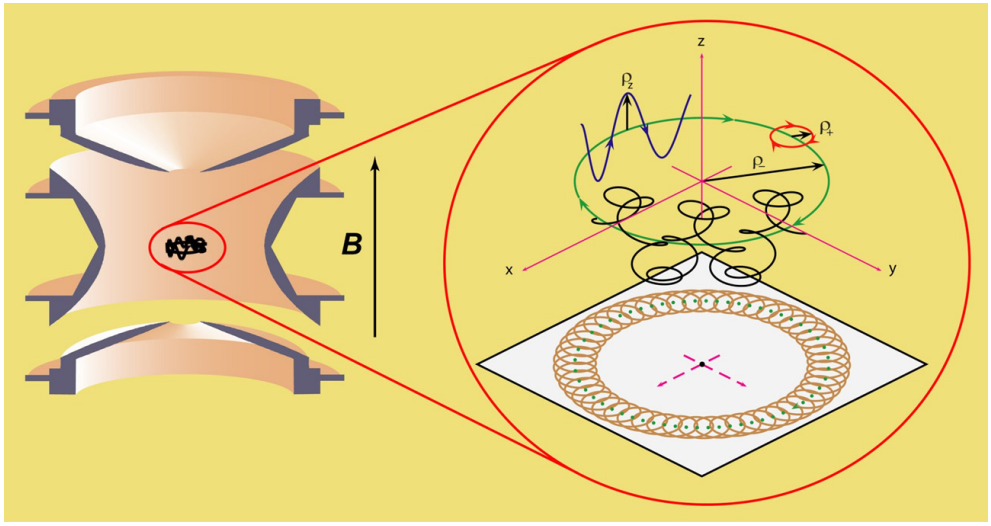

Fig. 2: Schematic ion trajectory in space and projection onto the x-y plane in a Penning trap.

In a Penning trap (Fig. 2) a charged particle (ion) is bound radially on the cyclotron orbit by a homogeneous magnetic field, while an electrostatic potential between the trap electrodes provides axial confinement. Since the ion is trapped in three dimensions, it exhibits three independent eigenmotions. The eigenmotion frequencies and hence the cyclotron frequency of the ion can be measured via observing the response of the ion to an applied radio-frequency field with a certain frequency and a certain spatial and temporal structure. Two cyclotron-frequency-measurement techniques are employed in high-precision Penning-trap mass spectrometry: A technique known as Time-of-Flight Ion-Cyclotron-Resonance (ToF-ICR) has proven to be the most suitable method for mass measurements on short-lived nuclides with uncertainties down to 10 ppb. It is based on the measurement of the time of flight of an ion between a Penning trap and an ion counting detector placed outside of the strong magnetic field. Before sending the ion to the detector, its radial motions are resonantly excited. On the way to the detector the ion passes the region with a strong magnetic field gradient and thus experiences acceleration due to a conversion of its radial into axial energy. The measurement of the ion's time of flight versus the frequency of the applied radial-motion excitation allows for a determination of the ion cyclotron frequency. This technique is presently employed at every Penning-trap installation dedicated to experiments on unstable nuclides. However, for many aspects of fundamental physics the relevant mass measurements are related to long-lived nuclides. In these studies ultra-high mass precisions well below 1 ppb are required. Such uncertainties can only be reached with cryogenic Penning traps in which a single highly-charged ion is confined for an extended period of time to a volume of just a few cubic micrometers. The mass is determined via measuring the frequency of the current induced by the moving ion in the segmented trap electrodes. This complementary technique has been given the name Fourier-Transform Ion-Cyclotron-Resonance (FT-ICR) method and it is superior to the ToF-ICR method in terms of achievable mass precision although it can only be applied on nuclides with relatively long lifetimes.

The division of *Stored and Cooled Ions* at the Max-Planck-Institute for Nuclear Physics is one of the leading groups in the field of high-precision Penning-trap mass spectrometry. The three in-house Penning-trap mass spectrometry projects are: TRIGA-TRAP at the reactor TRIGA in Mainz for experiments on short-lived neutron-rich nuclides, THe-Trap at MPIK for the measurement of the *Q*-value of the tritium β-decay, and PENTATRAP at MPIK for ultra-precise mass measurements of long-lived highly charged nuclides relevant for fundamental physics. The members of the division also actively participate in or even provide the spokesperson of experiments at SHIPTRAP (GSI Darmstadt) and ISOLTRAP (ISOLDE/CERN, Geneva). Furthermore, the division is deeply involved in all experiments on storage-ring mass spectrometry, which are currently conducted at two accelerator facilities, namely at the Experimental Storage Ring (ESR) at GSI and experimental Cooler-Storage Ring (CSRe) at the IMP in Lanzhou, China. In the following, highlights of recent results obtained at these experiments are presented.

Mass Measurements of Neutron-Deficient Nuclei and the rp-Process of Nucleosynthesis

Widely observed in space X-ray bursts are interpreted as being generated by thermonuclear explosions in the atmosphere of a neutron star accreting matter from a companion star in a close binary system. In between the bursts, the energy is generated at a constant rate by the hot CNO cycle driven by the in-flow of hydrogen and helium material from the less evolved companion star. A breakout from the CNO cycle leads to the rapid-proton capture process (rp-process), which is a sequence of proton-capture reactions and beta-decays along the proton drip-line. The X-ray bursts can result in the production of neutron-deficient nuclei, possibly up to Sn–Sb elements.

Precise knowledge of nuclear masses is essential for modelling the rp-process of nucleosynthesis in X-ray bursts, and in turn for the understanding of the observed light curves. Both, storage-ring and Penning-trap mass spectrometry have provided essential contributions in the last years.Proceeding along the proton drip line, the rp-process encounters the exceptionally long-lived positron emitters ^{64}Ge, ^{68}Se, and ^{72}Kr. They were thus identified as waiting points in the rp-process because they cannot be bypassed and, thus, the process has to "wait" until they decay by the slow positron emission. By measuring the mass of ^{65}As in the CSRe, surprising evidence was provided that ^{64}Ge is not a significant waiting point in the rp-process for the majority of relevant temperature-density conditions in X-ray bursts [1]. Furthermore, masses of short-lived ^{41}Ti, ^{45}Cr, ^{49}Fe and ^{53}Ni were recently determined at the CSRe. Based on the new mass of ^{45}Cr, it was shown that the formation of any strong Ca-Sc cycle, which could prevent matter from flowing to heavier-mass nuclei, can basically be excluded.

Through accurate measurements of masses of ^{85}Mo and ^{87}Tc at SHIPTRAP, a systematic shift (by up to 1.6 MeV) of the measured mass surface as compared to the tabulated Atomic-Mass Evaluation 2003 was identified [2]. This led to dramatic modifications in the calculated element abundances and moreover pointed to a possible formation of a Zr-Nb cycle in the rp-process. The latter constrains the temperature-density conditions for the rp-process to be able to proceed to elements beyond Nb.

Although the masses for the majority of nuclides involved in the rp-process are known experimentally, several important masses of heavy $N \approx Z$ nuclides are known only from theory. Therefore tests of underlying basic principles of modern models are needed. With a new mass of ^{53}Ni measured at CSRe it became possible to address the fundamental isospin symmetry. A 3.5 σ deviation from the quadratic form of the Isobaric Multiplet Mass Equation was found [3], which presently can not be explained by the state-of-the-art theoretical calculations.

Yuri Litvinov, Sergey Eliseev, Klaus Blaum

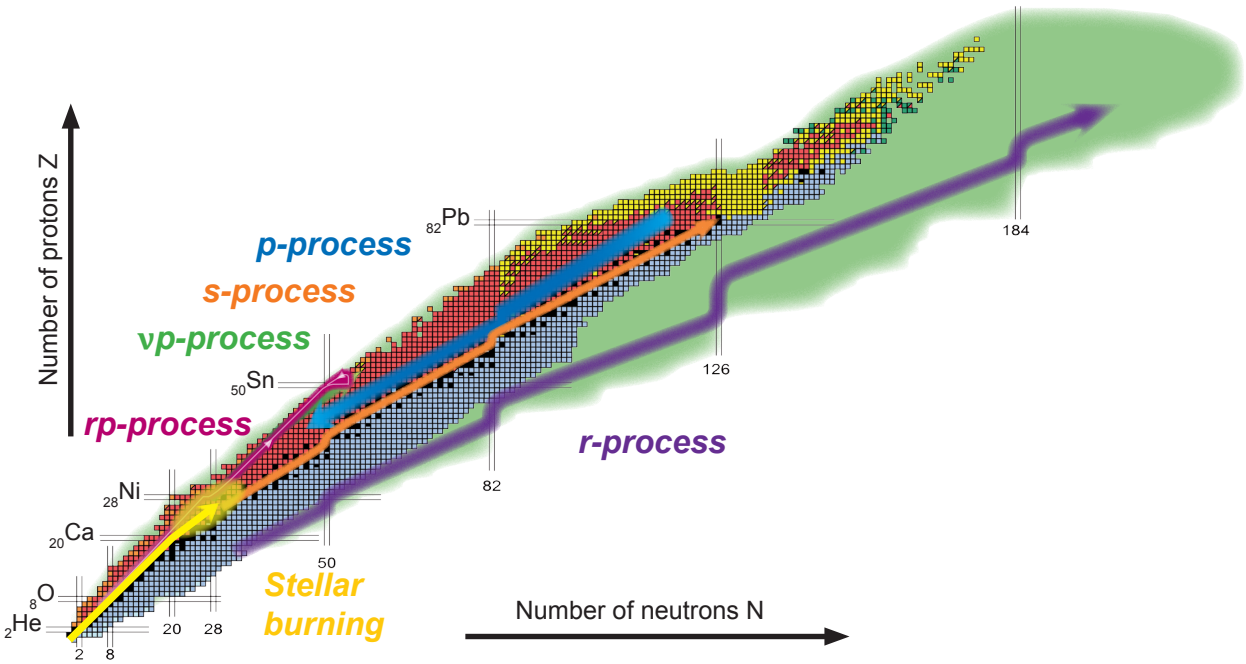

Fig. 3: Chart of isotopes and the different nucleosynthesis paths (GSI-EMMI / Different Arts).

Measurement of the Mass of ^{82}Zn for Modelling the Crustal Composition of Neutron Stars

The rapid neutron-capture process (r-process) of stellar nucleosynthesis is considered to be responsible for the production of more than half of the heavy elements in nature. However, the exact astrophysical site for this process has not been identified yet. Modeling of the r-process path depends strongly on the employed astrophysical model and the supposed stellar condition. Nevertheless, the underlying structure of nuclei plays its role also in stellar environments, making nuclei around the closed neutron shells $N = 50$ and $N = 82$ prominently appear. Penning-trap mass measurements touched the r-process path for nuclides around ^{80}Zn and ^{132}Sn, which are essential for constraining nuclear mass models that in turn are needed as input for astrophysical models whenever experimental masses are not (yet) available. Since most of nuclides on the envisioned r-process path were not even observed in the laboratory, using mass models for astrophysical modeling remains indispensable. Accurate mass measurements are also needed to reliably compare the calculated r-process abundances to observations. A possible theory, alternative to the supernova-induced r-process, is the decompression of neutron-star matter by its merger with another neutron star. In the neutron-star crust, exotic rare isotopes transform into the so-called equilibrium nuclei and contribute to the elemental abundance.

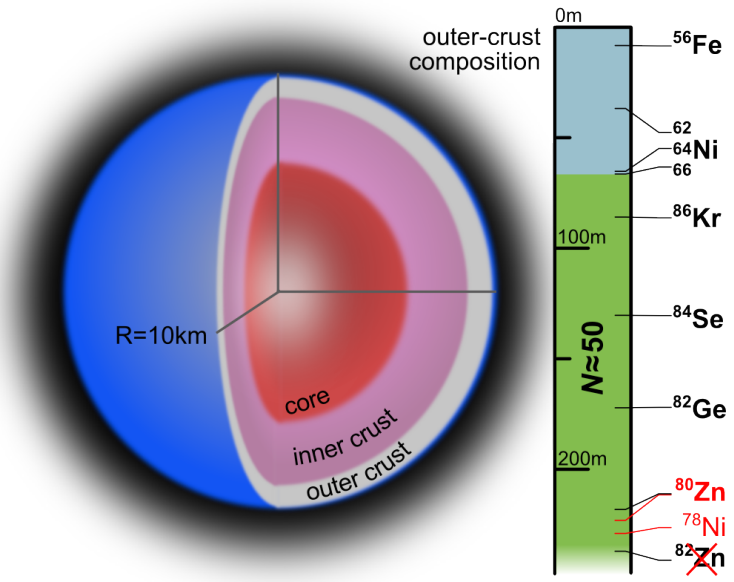

Fig. 4: Composition of a neutron star with a radius of 10 km and a mass of 1.4 solar masses. The depth profile of the outer crust shows experimentally known masses in bold. Marked in red are the changes resulting from the ^{82}Zn mass measurement. Adapted from [4].

A recent example is the mass measurement of ^{82}Zn with ISOLTRAP, which is important for understanding the crustal composition of neutron stars [4]. Through the precisely determined mass value and by testing 25 different mass models it was possible to establish that ^{82}Zn is not present in the outer crust of a neutron star [5] (see Fig. 4). Based on the new experimental mass the neutron-star crust composition has been calculated anew. The composition profile is not only altered but now constrained by experimental data deeper into the crust than before.

Susanne Kreim, Robert Wolf, Klaus Blaum

Search for New Nuclear Magic Numbers

Far from the valley of β-stability, the highly asymmetric neutron-to-proton ratio within the nucleus determines the nuclear interaction to such an extent that magic numbers can disappear or new magic numbers can emerge. Magic nuclei are nuclei, which exhibit an enhanced binding compared to their neighbors and manifest a filled proton or neutron shell. Recently, a series of experiments have been carried out with SHIPTRAP and ISOLTRAP investigating shell structure in neutron-rich nuclei, which have resulted in the discovery of new magic neutron numbers at $N = 32$ and $N = 152$.

At the Penning-trap installation SHIPTRAP two successful experiments on mass measurements on nobelium and lawrencium isotopes have been conducted [6]. The masses of six trans-uranium nuclides, $^{252–255}$No and ^{155,156}Lr, have been determined. It is worthwhile to note, that ^{256}Lr is presently the heaviest radionuclide and has the lowest production rate, for which a direct mass measurement with a Penning trap has ever been performed. The obtained results have revealed the existence of a deformed shell gap at $N = 152$. Furthermore, the combination of the present results with spectroscopic data has fixed the masses of certain nuclides up to as heavy as ^{270}Ds ($Z = 110$) [6].

Another new magic number at $N = 32$ has recently been experimentally observed at ISOLTRAP through mass measurements of calcium isotopes. This experiment has been triggered by a recent development of a new class of ab-initio calculations with realistic potentials, which includes not only two-body but also three-body nuclear forces. This nuclear theory not only successfully described the known neutron magic numbers in the

proton-magic calcium isotopic chain but also predicted a new magic number at $N = 32$. To test these predictions, the masses of $^{51-54}$Ca have been determined. The mass of ^{53,54}Ca could be obtained for the first time using the MR-ToF MS as a mass spectrometer [7]. Fig. 5 shows the two-neutron separation energy of the calcium chain as a function of neutron number. The experimental data agree well with the different calculations illustrating the importance of this new theory in nuclear physics.

To judge on the level of magicity of the new magic number $N = 32$ the size of the so-called empirical neutron shell gap has to be considered. With a gap size of about 4 MeV, the magicity of calcium ($Z = 20$, $N = 32$) becomes comparable to the well-established shell gaps at magic numbers $N = 28$ in iron, $N = 50$ in selenium, and $N = 20$ in titanium. Furthermore, the gap size at $N = 32$ is the largest in calcium and is reduced for its two neighbors, scandium and potassium, corroborating ^{52}Ca as a doubly-magic nucleus. The masses of the potassium isotopes $^{51-53}$K, required for the above conclusions, have also been measured for the first time with the ISOLTRAP Penning-trap mass spectrometer.

Sergey Eliseev, Susanne Kreim, Robert Wolf

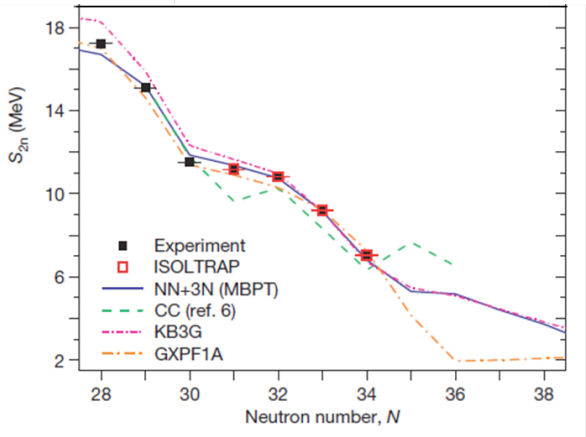

Fig. 5: Two-neutron separation energies S_{2n} of the neutron-rich calcium isotopes as a function of neutron number N, where the new ISOLTRAP values are shown in red. The ISOLTRAP masses are compared among others to predictions from microscopic valence-shell calculations with three-nucleon forces (NN + 3N) based on chiral effective field theory (solid line, MBPT). Taken from [8].

Mass and Nature of Neutrinos

Impressive progress of high-precision Penning-trap mass spectrometry in recent years has opened the door to ultra-precise mass measurements of long-lived nuclides with an aim to determine the mass and nature of the electron neutrino.

The long standing question of fundamental physics whether neutrinos and antineutrinos are identical or different particles can be answered by investigations of neutrinoless double-electron capture transitions. Double-electron capture is such an extremely rare nuclear process that despite persistent attempts it has not been observed yet. This process of capturing two atomic orbital electrons by a nucleus can either happen with an emission of two neutrinos or be neutrinoless. Of particular interest is the neutrinoless mode. Its mere observation would be an unambiguous proof that neutrinos and antineutrinos are identical particles. By knowing the half-life of the process, one would be able to assess the value of the effective Majorana neutrino mass. Theoretical calculations estimate the expected half-life of the neutrinoless mode well beyond 10^{30} years, which renders this process in general unobservable. Nevertheless, if the initial and the final states of the transition happen to be degenerate in energy, the probability of the neutrinoless mode can resonantly be enhanced by orders of magnitude and become in fact reachable by modern detection techniques. Recently, a joint measurement campaign at SHIPTRAP, TRIGA-TRAP and ISOLTRAP has been carried out to search for such resonantly enhanced transitions by determining the Q-values of several potential candidate-transitions. As a result, two cases have been found whose transitions should be resonantly enhanced, namely ^{152}Gd and ^{156}Dy [8]. In ^{156}Dy a unique multiple resonance enhancement to four nuclear excited states has been discovered. This phenomenon may allow for an assessment of the realization of different mechanisms of neutrinoless double-electron capture. Although, in search of resonantly enhanced neutrinoless double-electron capture these transitions with an expected half-life of 10^{27}–10^{28} years pose a formidable challenge for the present experimental techniques.Nevertheless, they are feasible – the CANDELS and CARVEL experiments, which are currently under construction, are good examples of such projects.

Another intriguing characteristic of the neutrino is its mass. It is so tiny that it was long thought that neutrinos were massless particles. Nevertheless, the striking discovery of the neutrino oscillations has assigned neutrinos to the family of massive particles. In spite of persistent attempts to measure the neutrino mass, it still remains unknown. At present, several experiments, e.g., KATRIN and ECHo, are under development with the goal to reach a sub-eV level neutrino mass measurement sensitivity. In these projects the neutrino mass is planned to be determined from the analysis of three nuclear processes – β-decays of tritium and ^{187}Re, and electron capture in ^{163}Ho. Success of these projects requires direct measurements of the Q-values with an extraordinarily small uncertainty of

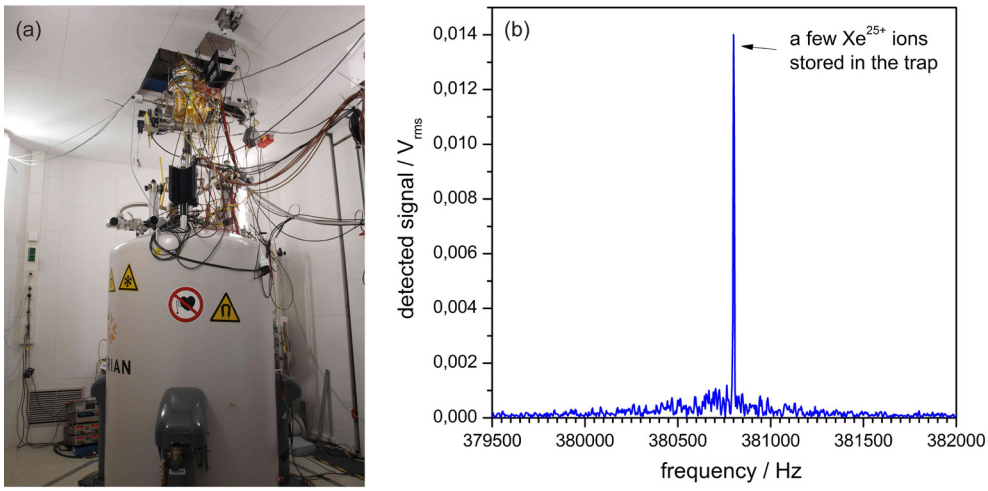

Fig. 6: (a) Penning-trap mass spectrometer PENTATRAP. (b) Signal induced in the cryogenic high-quality resonator by the axial motion of a few xenon atoms in a charge state of 25+ stored in the trap of the mass spectrometer.

100 meV or smaller. Although the Penning-trap technique (and only this technique) is in general capable of providing such accuracies for mass-difference measurements, none of the existing Penning-trap experiments is able to carry out such ultra-precise measurements in the mass regions of interest. In order to satisfy the growing requirements of fundamental physics in very precise mass-difference values, researchers at the Max Planck Institute for Nuclear Physics are building the novel Penning-trap mass spectrometers THe-Trap and PENTATRAP.

THe-Trap is optimized for the Q-value determination of the β-decay of tritium by measuring the mass difference of tritium and its β-decay daughter ^{3}He. The experiment is expected to reach 30 meV precision in the Q-value, which requires 10 ppt precision in the parent-daughter mass ratio. The setup has been undergoing constant development to meet the precision requirements. Ability to work with a single stored ion is perhaps the most significant milestone reached in late 2011. This does not only demonstrate the detection system sensitivity but also eliminates any ion-cloud related systematic uncertainty. Additionally, unavoidable systematic shifts due to finite motional amplitudes have been characterized, enabling frequency ratio measurements at the desired 10 ppt level. Recently, a proof-of-principle mass ratio measurement of ^{12}C to ^{16}O has been performed [9]. The result with 63 ppt statistical uncertainty (120 ppt total uncertainty) is in excellent agreement with the literature value and reassures that the experiment is getting close to a tritium Q-value measurement. The current precision of the Q-value is 1.2 eV, which is yet insufficient for the KATRIN experiment (located in Karlsruhe Institute of Technology) dedicated to deducing the neutrino mass from the endpoint and the shape of the energy spectrum of electrons emitted in tritium β-decay. KATRIN aims at reaching the 0.2 eV/c^2 limit for the neutrino mass at 95% confidence level, which would be a tenfold improvement over the current value.

The aim of the PENTATRAP project is to measure mass differences of a broad range of long-lived and stable nuclides, e. g., the Q-values of the β–decay of ^{187}Re and of the electron capture in ^{163}Ho, with an uncertainty of about 1 eV. The uniqueness and complexity of the Penning-trap mass spectrometer PENTATRAP stems from the unprecedented precision requirements needed for these measurements. To achieve such ultra-low uncertainties, the PENTATRAP project incorporates such state-of-the-art techniques and methods as, e. g., a cryogenic multi-trap design, the novel PnA detection technique, employment of highly-charged ions, and a permanent monitoring of magnetic field fluctuations in the trap volume. After several years of designing, construction and extensive testing, PENTATRAP has now reached the operational stage (see Fig. 6). A production of highly-charged ions of various nuclides, their transport towards the trap region and their capture in the trap are performed now routinely. For example, a few ions of xenon in a charge state of 25+ can be stored in the trap for at least half an hour and their presence in the trap can be monitored via detecting their axial motion by its locking to a high-quality cryogenic resonator. Thus, the project has recently entered the final phase – the commissioning of the experiment and the preparation for first mass measurements.

Sergey Eliseev, Tommi Eronen, Szilard Nagy

Development of a Novel Mass Measurement Technique

Impressive progress has recently been made at SHIPTRAP with the development of a novel mass-measurement approach, which was named as phase-imaging ion-cyclotron-resonance technique (PI-ICR) [10]. This novel approach is based on the determination of the nuclide's mass via counting the number of revolutions of the ion's cyclotron motion in the trap. By "imprinting" two motional phases separated by a predefined time on a high-resolution position-sensitive micro-channel-plate detector (see Fig. 7), one can directly determine the total accumulated phase and finally the ion's cyclotron frequency. The PI-ICR technique is substantially faster and offers an about 40-fold gain in resolving power compared to the presently used ToF-ICR approach and is, thus, ideally suited for mass measurements of short-living nuclides. The PI-ICR was employed at SHIPTRAP for measuring at SHIPTRAP by measuring the mass difference of ^{130}Xe and ^{129}Xe atoms. Merely a 3-day measurement of the mass difference is now sufficient to reach the statistical uncertainty of 55–60 eV, which corresponds to the relative accuracy of about 4×10^{-10}. For comparison, with the ToF-ICR technique even a substantially larger uncertainty of 200 eV can only be achieved after a week-long measurement. Presently, the new technique is a subject of the extensive experimental characterization at SHIPTRAP with the goal to investigate the maximum resolving power and accuracy achievable in practice and to create a comprehensive picture of all systematic effects.

The virtue of the new technique is that its implementation at other on-line Penning-trap facilities is rather straightforward and requires only minor modifications to the existing installations. At the same time, it allows for mass measurements on a sub keV-level of nuclides with half-lives down to a few ten milliseconds. The implementation of the technique is already in progress, e.g., at ISOLTRAP/CERN and at TRIGATRAP/Mainz.

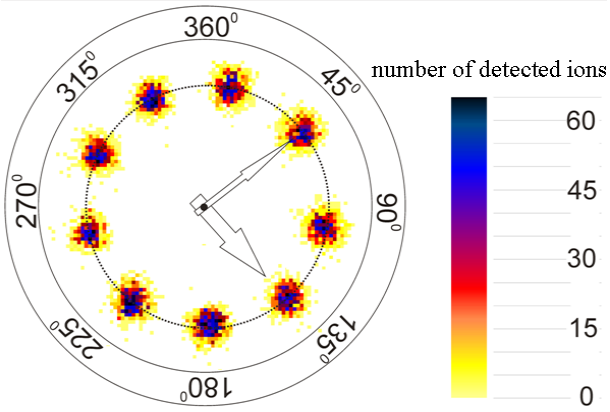

Fig. 7: A projection of the ion's motion on the detector for different ion trapping times. One revolution of the ion's motion corresponds to approximately 1 µs.

Sergey Eliseev, Klaus Blaum

References:

[1] X. L. Tu et al., Phys. Rev. Lett. 106 (2011) 112501.
[2] E. Haettner et al., Phys. Rev. Lett. 106 (2011) 122501.
[3] Y. H. Zhang et al., Phys. Rev. Lett. 109 (2012) 102501.
[4] R. N. Wolf et al., Phys. Rev. Lett. 110 (2013) 041101.
[5] S. Kreim, M. Hempel, D. Lunney and J. Schaffner-Bielich, Int. J. Mass Spectrom. 349-350 (2013) 63.
[6] E. Minaya Ramirez et al., Science 337 (2012) 1207.
[7] F. Wienholtz et al., Nature 498 (2013) 346.
[8] S. Eliseev et al., Phys. Rev. Lett. 106, 052504 (2011).
[9] S. Streubel, T. Eronen, M. Höcker, J. Ketter, M. Schuh, R. S. Van Dyck Jr., K. Blaum , Appl. Phys. B (2013) DOI 10.1007/s00340-013-5669-x (in print).
[10] S. Eliseev, K. Blaum, M. Block, C. Droese, M. Goncharov, E. Minaya Ramirez, D. A. Nesterenko, Yu. N. Novikov and L. Schweikhard, Phys. Rev. Lett. 110 (2013) 082501.

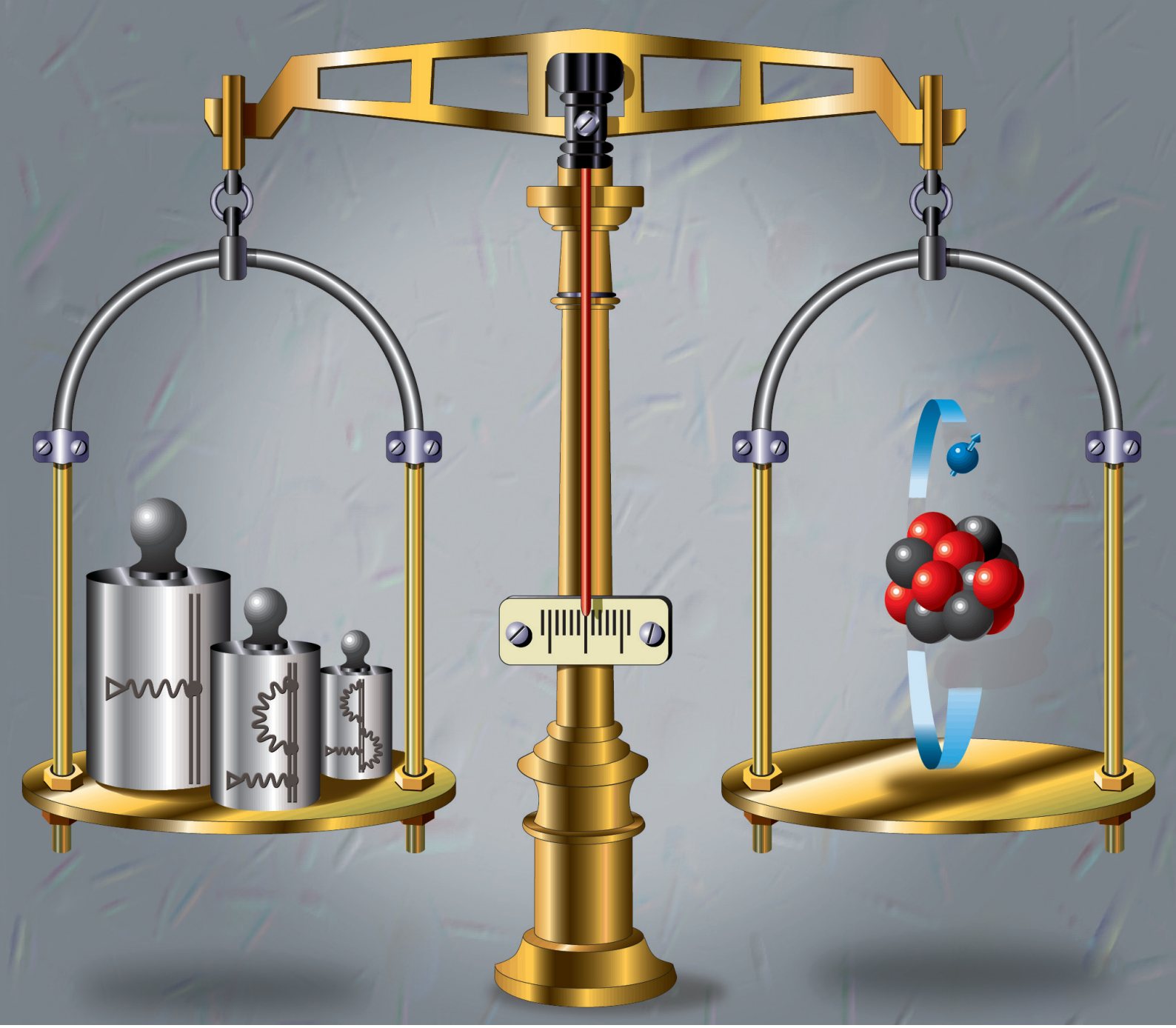

2.2 Fundamental Tests with Trapped Ions

The principle of high-precision mass measurements for a test of fundamental constants can be illustrated in form of a scale: The atomic mass of a bound electron (right) is balanced by QED contributions in increasing order playing the role of a precision mass set (left).

Introduction

Over the past few years, novel ion trapping techniques and developments have not only pushed the accuracy of pivotal tests of the fundamental interactions and symmetries into previously unprecedented regimes, but have also laid the foundations of new and intriguing experiments. MPIK constitutes an ideal environment by combining on its site both experimental and theoretical expertise. MPIK offers uniquely advanced experimental opportunities, from highly charged ions (HCI) in electron beam ion traps (EBITs) to various other techniques for precision measurements using Penning traps. Complementing these efforts, the theory division specializes in calculations needed to analyze and interpret those results with ultimate precision. This symbiosis has enabled, among others, a stringent test of quantum electrodynamics (QED) in strong fields by a comparison of experimental *g* factors of HCI determined with the highest accuracy to QED predictions. Furthermore, based on this work, the atomic mass of the electron has been determined with a 13-fold better accuracy than previously achieved. Advances in X-ray spectroscopy have yielded absolute values for transition energies in few-electron HCI. From these measurements, QED contributions can be extracted and probed. Sophisticated ion trapping and manipulation techniques are also at the center of the AEGIS experiment for the study of antimatter in gravitational fields. Its aims are to use antihydrogen created from trapped antiprotons and positrons in order to directly test the weak equivalence principle.

Calculation of Nuclear and QED Effects on the Bound Electron *g*-Factor

Electrons possess an intrinsic magnetic moment, characterized by a dimensionless quantity called the gyromagnetic factor (*g*-factor). This number describes how the quantum states of the electron behave in an externally applied magnetic field. Recent years have witnessed a remarkable improvement in the theoretical description of the *g*-factor of an electron bound in the attractive potential of an atomic nucleus. These studies are paralleled with and motivated by a quantum leap in the experimental accuracy in the investigation of the *g*-factor, especially in Penning trap measurements performed by the division headed by Klaus Blaum [1].

Measuring the electron's *g*-factor in highly charged ions (HCI) provides an exciting possibility for testing fundamental theories. The strong Coulomb force of the nucleus renders the electron dynamics relativistic, which necessitates a description based on Dirac's equation, and effects of strong-field quantum electrodynamics (QED) are increasingly relevant at higher and higher ionic charges. Experiments on the bound electron *g*-factor with ever-improving accuracy represent a continuing challenge for theory. Bound-state QED effects are scrutinized to the highest precision in recent Penning trap experiments, which have reached the 10^{-11} level in terms of relative precision with hydrogenlike carbon and silicon ions.

These experiments will be extended to heavier and heavier ions in the near future. An essential motivation of such studies is that *g*-factor measurements with heavy ions are anticipated to yield a new value of the fine-structure constant, i. e. a fundamental constant defining the strength of any kind of electromagnetic interaction in the Universe. Besides

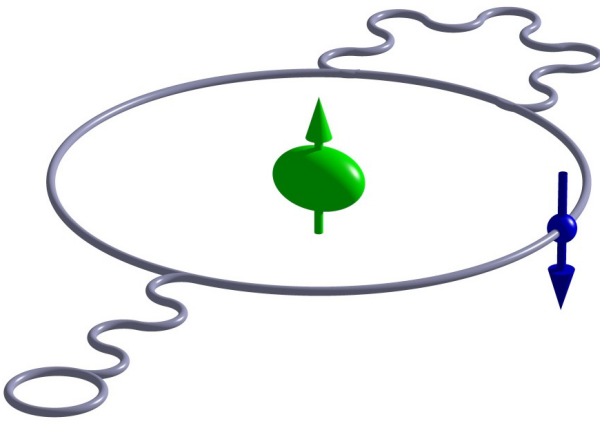

Fig. 1: An illustration of the physical effects appearing when a bound electron is orbiting a nucleus. The electron (blue) interacts with an external magnetic field, the strength of which is described by the electron's g factor. During its cycling around the nucleus, the electron may emit and reabsorb an arbitrary number of virtual photons (wave line), and may create virtual electron-positron pairs (closed loop), changing its wave function. The atomic nucleus (green) may be extended, deformed, and it may possess a non-zero spin.

that, as with the increasing strength of the binding Coulomb field the electronic wave functions have a larger and larger overlap with the nucleus, accurate measurements with such systems will also deliver new insights into nuclear structural properties. These nuclear contributions are not only interesting on their own, but they are necessary to complete the overall theoretical understanding for a broad range of charge numbers.

The most dominant nuclear structural effect, namely, the finite size effect is well understood. It can be calculated by means of perturbation theory, yielding easily evaluable analytical formulas, or numerically in an all-order fashion by including the potential corresponding to the extended nucleus into the radial Dirac equation. The comparison of theoretical and experimental *g* factors may provide one with a new tool of determining nuclear radii: the accuracy of the recent Penning trap experiment with Si^{13+} even allowed us to extract the value of the nuclear radius. This proof-of-principle study encourages one to further improve the accuracy and to extend the investigations to higher charges and to different isotopes of the same element.

In very recent studies, we have also considered the nuclear shape (or deformation) effect, i.e. the deviation of the nuclear shape from a perfectly spherical one [2]. While part of the nuclear deformation effect can be incorporated into the spherically averaged radius and thus can be understood as a constituent of the dominant finite size effect, some terms explicitly depending on the nuclear deformation parameters prevail and show a relative contribution to the *g*-factor that is visible for elements with an intermediate nuclear charge Z already. Our calculations confirm that the effect is negligible for the elements experimentally studied so far, i. e., for hydrogenlike carbon and silicon ions (Z = 6,14, respectively), therefore, it does not influence the interpretation of those results. However, the nuclear shape contribution grows quickly with Z and it is visible e. g. for strontium isotopes (Z = 38). The deformation effect becomes prominent for heavy ions, e. g. it is of the order of 10^{-6} for elements as heavy as uranium. Its contribution will be relevant in the interpretation of planned near-future experiments at the MPIK with heavy highly charged hydrogenic ions extracted from an electron beam ion trap and guided into a Penning trap, and also for the projected HITRAP experiment at the FAIR facility. A combination of theory with the experimental data may allow in the future the extraction of deformation parameters of the nucleus, relevant for explaining shape phase transitions in nuclear structure theory.

The studies mentioned so far have been restricted to elements with a vanishing nuclear spin. In ions in which the nucleus possesses an intrinsic angular momentum, i.e. a non-vanishing nuclear spin *I*, the electronic angular momentum *j* needs to be coupled to a total quantum number *F*. The associated g_F factor may be easily constructed in a first approximation from the electronic g_j factor and the nuclear g_I factor. However, at the present, improved experimental accuracy, also mixed Zeeman-hyperfine terms need to be taken into account. These nuclear magnetic shielding terms in hydrogenic ions have been calculated before in a relativistic manner. In our very recent investigations, a more accurate theory of the nuclear magnetic shielding was developed, taking into account the self-energy and vacuum polarization QED corrections to the shielding parameter [3]. As we theoretically suggested, experiments extended to ions with nonzero nuclear spin may even deliver more accurate or so far even unknown nuclear magnetic moments. These basic nuclear properties are relevant in testing nuclear structure models, and are also constituents of nuclear magnetic resonance techniques of medical imaging.

In summary, we can conclude that theoretical studies on the *g*-factor of bound electrons, given the support of corresponding experimental results, provide us with a great tool to push forward the boundaries of knowledge about quantum electrodynamics and about the influence of nuclear structural effects on atomic properties.

Zoltán Harman, Jacek Zatorski, Vladimir A. Yerokhin, Christoph H. Keitel

Experimental Determination of the Bound Electron *g*-Factor in Highly Charged Ions

A high-precision test of the standard model of physics, in this case especially bound-state quantum electrodynamics (BS-QED), requires a quantity which can be both calculated and measured to highest precision. Such a quantity is, e.g., the *g*-factor of the electron. By investigating the *g*-factor of an electron bound in highly charged ions, high electric field strengths at the position of the electron can be achieved, allowing to test the theory under extreme conditions, where possible deviations from known theoretical models are most likely to emerge.

Experimentally, the *g*-factor of the electron can be determined by measuring the spin-precession frequency (Larmor frequency) of the electron in a well-known magnetic field. To obtain the magnetic field at the position of the electron, the ion itself is utilized as a magnetic field probe by measuring its free cyclotron frequency. For a precision of $\delta g/g \leq 10^{-9}$ the ion has to be investigated over several months, which is achieved by storing the single ion in a cylindrical Penning-trap system at cryogenic temperatures. The development of a new detection technique for the cyclotron frequency, which utilizes the phase information of the single-ion signal, enabled *g*-factor determinations of the bound electron with unprecedented uncertainties. In this regard, the *g*-factor of the electron bound in hydrogenlike silicon $^{28}Si^{13+}$ has been determined with a relative statistical precision of 4×10^{-11} [4]. However, the final uncertainty of the *g*-factor was limited to 4×10^{-10} by the uncertainty of the electron mass, which is, as well as the ion mass, a required input parameter for the experimental *g*-factor. The experimental value is in excellent agreement with the theoretical prediction and constitutes the most stringent test of BS-QED calculations in strong fields [1].

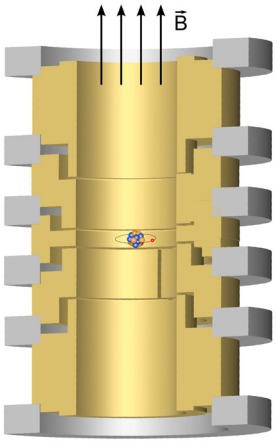

Fig. 2: Ion stored in a cylindrical Penning trap

Since the experimental uncertainty was limited by the electron mass, the measurement principle was inverted to determine the atomic mass of the electron. To this end, hydrogenlike carbon was used, where the theoretical *g*-factor was calculated within the division of Christoph Keitel to a relative precision of 3.5×10^{-12} and the ion mass is known to 1×10^{-13}. The required frequency ratio of Larmor frequency and free cyclotron frequency was measured with a precision of 3×10^{-11}, resulting in an improved precision of the atomic mass of the electron by a factor of 13 (accepted for publication in Nature).

Besides hydrogenlike ions, where a single electron is left, lithiumlike ions, with three remaining electrons, are of special interest, since these systems allow for a test of the relativistic electron-electron interaction. For this purpose, the g-factor of the outermost electron of lithiumlike silicon $^{28}Si^{11+}$ has been determined with a precision of 1.1×10^{-9} [5]. The comparison with the theoretical value yields the most precise test of relativistic many-electron calculations in a magnetic field up to date. Currently, the *g*-factor measurement of lithiumlike calcium is in progress, being the heaviest system under investigation in the present setup. Since the individual contributions to the *g*-factor increase with nuclear charge, the same experimental precision as for silicon will result in an even more sensitive test of QED calculations.

Anke Wagner, Florian Köhler, Sven Sturm, Klaus Blaum

QED Tests with Highly Charged Ions

Highly charged ions (HCI) are magnifying glasses for relativistic, quantum electrodynamic, and nuclear size effects. The energy shifts and splittings caused by such effects scale at least with the fourth power of the atomic number Z, what means a factor of seventy million across the periodic table of the elements. Extracting these enlarged effects is by no means trivial, since they affect primarily the most deeply bound electrons in the K shell. In neutral atoms, directly addressing such electrons by some excitation processes leads to rapid ionization by Auger processes, which remove a not well defined number of electrons in a matter of femtoseconds. The corresponding loss of resolution makes exploiting the full information from such experiments very difficult. A practicable solution is to work with HCI: they do not change their charge state under a wide range of collision conditions, and can be excited with X-rays without loss of integrity. Due to their inherent simplicity, hydrogenlike and heliumlike ions are ideally suited for fundamental physics studies. For the two-body systems constituted by hydrogenlike ions, the largest part of the electronic energy can be calculated using the Dirac equation. Additional contributions from, e.g.,

QED are extracted by subtracting the theoretical value from the experimental results. We have developed a novel system for the absolute measurement of the Bragg angle in crystal spectrometers [6], a quantity which gives access to a direct and independent determination of the absolute X-ray wavelength and thus transition energy. The accuracy achieved reaches 1 ppm, the highest reported for X-ray studies in atomic systems. This level of accuracy does not allow for in-depth tests of the one-electron QED predictions, which would require at least a tenfold reduction of our experimental uncertainty. Nonetheless, our absolute results for hydrogenic ions perfectly agree with theory.

The situation is different, and more interesting, for heliumlike ions. Here, the bound-state QED can be tested in a system where two electrons are sensitive to the screening of their interaction with the vacuum fluctuations by the other electron. These interactions belong to a very general class of quantum-field many-body interactions, and are the most accurately testable examples of them. For instance, Ar^{16+} ions show a one-electron Lamb shift of 1.13 eV, and a two-electron contribution of 0.095 eV in their ground state of approximately 1.13 eV. Our experiments (see Fig. 3) measure the transition energy from the first excited state $^1P_1$ of 3139.581(5) eV with an uncertainty of 5 meV. The uncertainty of our present result [6] is a factor of ≈ 20 smaller than all of the two-electron QED corrections to the $^1S_0$ ground state energy and a factor of 2 smaller than the corrections caused by the exchange of two virtual photons (9 meV). Consequently, the experiment probes these QED contributions as well as the total one-electron contribution of the excited $^1P_1$ state (6 meV), however it is not yet sensitive to its total two-electron term (3 meV). Future, improved measurements will probe QED in hydrogenlike ions in order to establish their Lyman-α lines as atomic X-ray standards at synchrotrons and free-electron lasers.

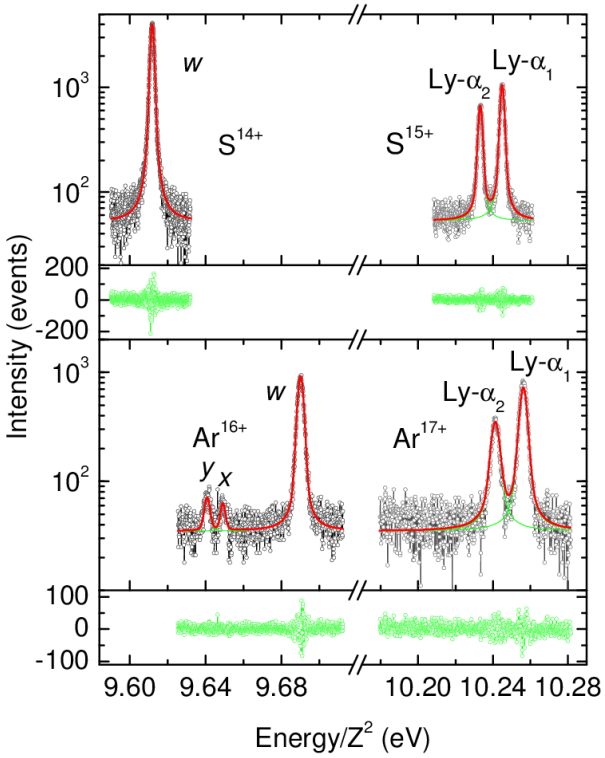

Fig. 3: X-ray spectra obtained with a crystal spectrometer showing the strongest transitions of the hydrogenic and heliumlike ions of sulfur and argon scaled by their atomic number Z.

Another approach we are presently pursuing is the application of synchrotron radiation sources for this type of studies, as shown in Fig. 4. Modern undulators provide X-ray fluxes which have been shown to be sufficient for narrow-band excitation of electronic transitions in HCI by our experiments. We have developed an electron beam ion trap, FLASH-EBIT, to this end. An electron beam produces the ions and confines their motion to a narrow cylindrical volume that is very well suited for this purpose. Instead of observing X-ray photons emitted by trapped ions after excitation by the electron beam, we produce the ions but do not excite them. This is achieved by keeping the electron energy below a certain level. Under these conditions, the electronic transitions of interest are excited by overlapping an X-ray photon beam with the trapped ion ensemble. When the photon energy is exactly resonant with an electronic transition, its excitation follows, and subsequently also the emission of a fluorescence photon. Detection of such photons reveals the level energy. The great advantage of synchrotron radiation is the superior performance of beamline monochromators at such facilities, which results from the large linear dispersion achievable with narrowly collimated photon beams over distances of tens of meters. Such long observation distances would make weak signals impossible to detect in a spectroscopic setup collecting isotropically emitted radiation from an ion trap. With this technique, we are able to improve the resolution and quality of the signal. The data obtained for, e. g., Fe^{24+} ions allows one to determine the natural width of the resonantly excited transitions at 6.7 keV photon energy to 0.311(10) eV, and yields a calibrated energy value of 6700.549(5)(70) eV [7]. These results show an excellent agreement with state-of-the-art calculations based on the bound-state QED method and confirm that an apparent trend to a deviation from QED, which had been recently claimed, is related to the significantly larger uncertainties of older experimental values.

Our novel experimental method can still be further improved by using ultra-high resolution crystal monochromators in the photon beamline, and by cooling the trapped ions. It is planned to utilize nearly perfect crystals prepared by the German metrology institute PTB and Mößbauer samples in combination with FLASH-EBIT in order to improve the accuracy by at least one order of magnitude in the near future. With the use of sympathetically cooled HCI, the perspective of reaching even further, into the regime of a few parts per billion seems to be within reach in the next years.

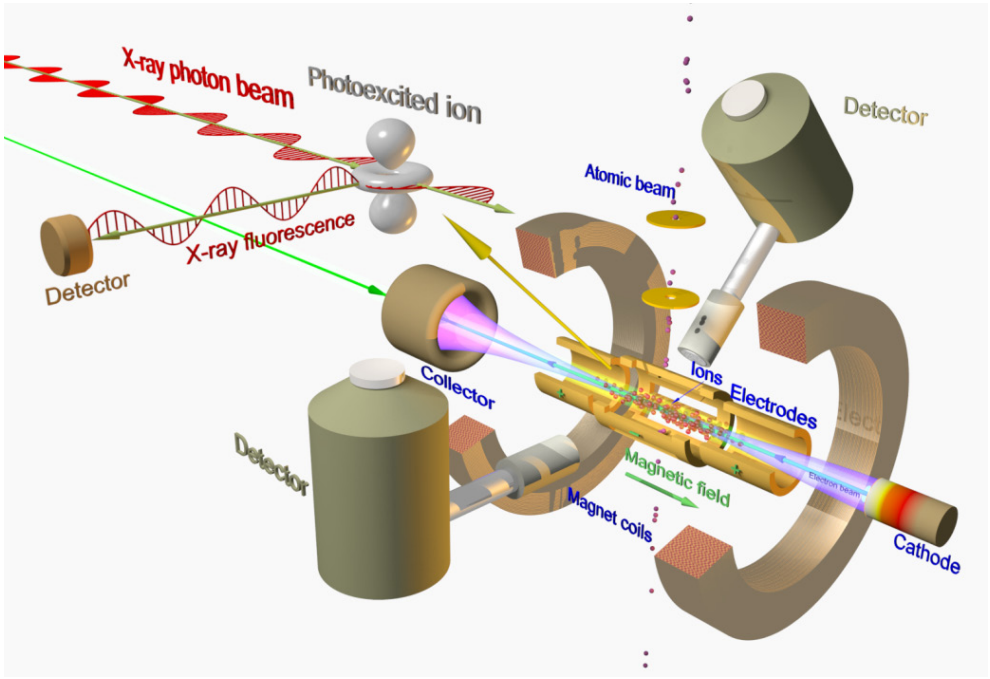

Fig. 4: Principle of photon resonant excitation spectroscopy with trapped highly charged ions. The ions are exposed to and resonantly excited by intense, monochromatic X-rays from a source such as a synchrotron or a free-electron laser. After excitation, the populated upper states emit fluorescence radiation which is collected with appropriate detectors arranged around the trap.

One important advantage of EBITs is the possibility of tuning the electron beam energy, adjusting it precisely to a value needed for resonant excitation of doubly excited states. Continuous improvements in our energy selectivity have allowed us to find strong but hitherto unrecognized electronic recombination channels that populate states having three and more excited electrons with very high efficiency. They result from higher-order electronic correlations interplaying with radiative decay channels, and theory had until now neglected them [8]. A more complete description of the electron-photon interactions in ionic systems was achieved in collaboration with the theory division, and the experimental findings were explained with the help of improved calculations encompassing several isoelectronic sequences.

José R. Crespo López-Urrutia

A Test of the Weak Equivalence Principle with Antimatter

The weak equivalence principle (WEP) is one of the cornerstones of General Relativity (GR). It states that the trajectory of a falling test body in a gravitational field is independent of its composition. While the WEP has been very well tested with ordinary matter, a verification with antimatter has never been performed. Over the years, many arguments have been brought forward against an anomalous gravitational acceleration of antimatter. However, all of these arguments rely on assumptions, such as the validity of CPT or the relevance (and choice) of an absolute gravitational potential. Therefore, a deviation from WEP for antimatter cannot currently be ruled out. Ultimately, the question of antimatter gravity can only be answered by a dedicated, direct experiment.

Gravity is the only fundamental interaction which is not currently expressed as a quantum field theory. With a view to a possible unification of GR with the Standard Model of particle physics (SM), various quantum gravity theories are being discussed. In quantum gravity, the exchange of a tensor (spin-2) graviton corresponds to ordinary 'Newtonian' gravity. Additional exchange bosons with different coupling constants and ranges are conceivable. For instance, the existence of vector (spin-1) and scalar (spin-0) exchange bosons is allowed by current torsion balance measurements on ordinary matter under the condition that their coupling constants and ranges match precisely. The presence of the non-canceling vector and scalar contributions would cause an *increased force* between matter and antimatter.

The possibility of anomalous antimatter gravity may also be considered within the Standard-Model Extension (SME), a general framework to study the implications of Lorentz violation on physical observables. Within the gravitational SME, Lorentz-violating terms arise from the coupling of a particle to a field with nonmetric interaction with gravity, or from a fixed background field which modifies the effective metric. Anomalous gravitational effects on antimatter may arise from the fact that some coefficients are CPT-odd and others are CPT-even. To discuss the implications of antimatter gravity, a toy model termed the 'isotropic parachute model' has been developed, which is constructed such that the effective classical Lagrangian can be expressed in terms of effective inertial and gravitational masses, where the latter differs between matter and antimatter. In the case of antimatter the effective gravitational mass, and accordingly the acceleration, is *reduced*, hence the name 'parachute.'

Thanks to the production of copious amounts of cold, neutral antihydrogen $\bar{H}$ at CERN's Antiproton Decelerator (AD) in the past few years, an antimatter gravity experiment has finally come within reach. The AEGIS collaboration (Antimatter Experiment: Gravity, Interferometry, Spectroscopy) intends to measure the local acceleration g of antihydrogen in the gravitational field of the Earth to (initially) 1% by detecting the vertical deflection of a cold, bunched, horizontal beam of $\bar{H}$ (see Fig. 5) [9]. The AEGIS experiment involves the following main experimental steps:

1. Production of positrons (e^+) from a source of beta-decaying radioisotope;
2. Capture and accumulation of antiprotons ($\bar{p}$) from the AD in a Penning trap;
3. Production of positronium (Ps) by implanting e^+ into a nano-porous insulator material;
4. Excitation of Ps to a Rydberg state;
5. Formation of $\bar{H}$ by resonant charge exchange between excited Ps and cold $\bar{p}$ according to the reaction $Ps^* + \bar{p} \rightarrow \bar{H}^* + e^-$;
6. Formation of an $\bar{H}$ beam by Stark acceleration with inhomogeneous electric fields;
7. Measurement of g in a two-grating moiré deflectometer coupled with a position-sensitive detector.

A moiré deflectometer is the classical counterpart of a matter wave interferometer. Three identical material gratings are placed at equal distances L from each other. A particle beam passing through the first two gratings produces a shadow pattern on the third. The change in vertical position of the shadow pattern due to gravity is determined by recording the transmission as a function of the position of the third grating. Alternatively, a position-sensitive detector may be used to replace the third grating and detector. A three-grating moiré deflectometer has previously been used to measure the local gravitational accelera-

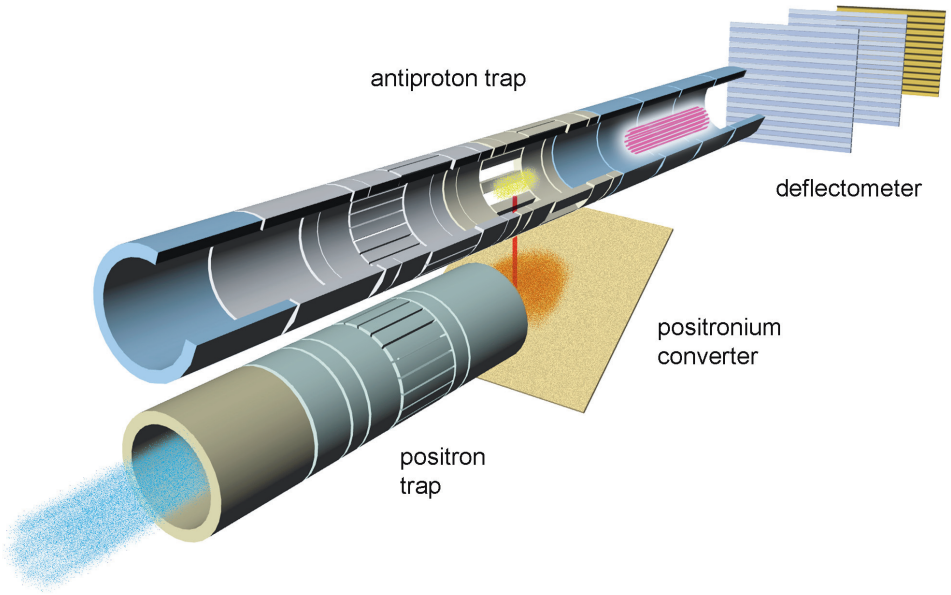

Fig. 5: Three-dimensional cut-open sketch of part of the AEGIS apparatus, showing the low-field Penning traps, the positronium converter, and the deflectometer. Illustration used with permission by Internosei/INFN.

tion of ordinary matter to a relative precision of 2×10^{-4}. Under the influence of gravity, the shadow pattern is vertically displaced by a distance $\Delta y = -gT^2$, where g is the local gravitational acceleration and T is the time of flight between each pair of gratings. The gravitational acceleration g is obtained from a quadratic fit to a plot of the vertical displacement against the mean time of flight for suitable classes of events with similar horizontal velocities.

Construction of the AEGIS experiment at the AD began in 2010. As of December 2013, the following main components are installed and operational: Positron source and accumulator; high-field (5 T) and low-field (1 T) superconducting magnets; e^+ transfer line; $\overline{p}$ capture trap; $\overline{H}$ recombination trap with Ps converter target holder; laser system for Ps excitation. A prototype of the moiré deflectometer was commissioned at the University of Heidelberg with metastable argon atoms. During beam times in June and December 2012, the capture and stacking of $\overline{p}$ was demonstrated, and a $\overline{p}$ lifetime in the capture trap of $\approx$ 10 min was observed. In addition, the feasibility of the moiré deflectometer technique was demonstrated by measuring the deviation of a horizontal $\overline{p}$ beam due to residual electromagnetic fields in a reduced-size deflectometer setup.

During the 2013/2014 shutdown of the CERN accelerators, the design and construction of the remaining components of the AEGIS apparatus are being completed. In particular, the design of the deflectometer's $\overline{H}$ detector, which will consist of a combination of nuclear emulsions [10] and Si strip detectors, is being finalized, and construction will begin shortly.

In summary, the gravitational interaction between matter and antimatter has never been studied experimentally. The AEGIS experiment will determine g for antimatter to initially 1% by measuring the vertical deflection of a horizontal $\overline{H}$ beam. Data taking is expected to begin in the second half of 2014.

Alban Kellerbauer

References

[1] S. Sturm, A. Wagner, B. Schabinger, J. Zatorski, Z. Harman, W. Quint, G. Werth, C.H. Keitel, K. Blaum, Phys. Rev. Lett. 107 (2011) 023002

[2] J. Zatorski, N. S. Oreshkina, C. H. Keitel, Z. Harman, Phys. Rev. Lett. 108 (2012) 063005.

[3] V. A. Yerokhin, K. Pachucki, Z. Harman, C. H. Keitel, Phys. Rev. Lett. 107 (2011) 043004.

[4] S. Sturm, A. Wagner, M. Kretzschmar, W. Quint, G. Werth, K. Blaum, Phys. Rev. A 87 (2013) 030501.

[5] A. Wagner, S. Sturm, F. Köhler, D.A. Glazov, A.V. Volotka, G. Plunien, W. Quint, G. Werth, V.M. Shabaev, K. Blaum, Phys. Rev. Lett. 110 (2013) 033003.

[6] K. Kubiček, J. Braun, H. Bruhns, J. R. Crespo López-Urrutia, P. H. Mokler, and J. Ullrich, Rev. Sci. Instrum. 83 (2012) 013102.

[7] J. K. Rudolph et al., Phys. Rev. Lett. 111 (2013) 103002.

[8] C. Beilmann, P. H. Mokler, S. Bernitt, C. H. Keitel, J. Ullrich, J. R. Crespo López-Urrutia, and Z. Harman, Phys. Rev. Lett. 107 (2011) 143201.

[9] A. Kellerbauer et al. (AEGIS Collaboration), Hyperfine Interact. 209 (2012) 43.

[10] S. Aghion et al. (AEGIS Collaboration), J. Instrum. 8 (2013) P08013.

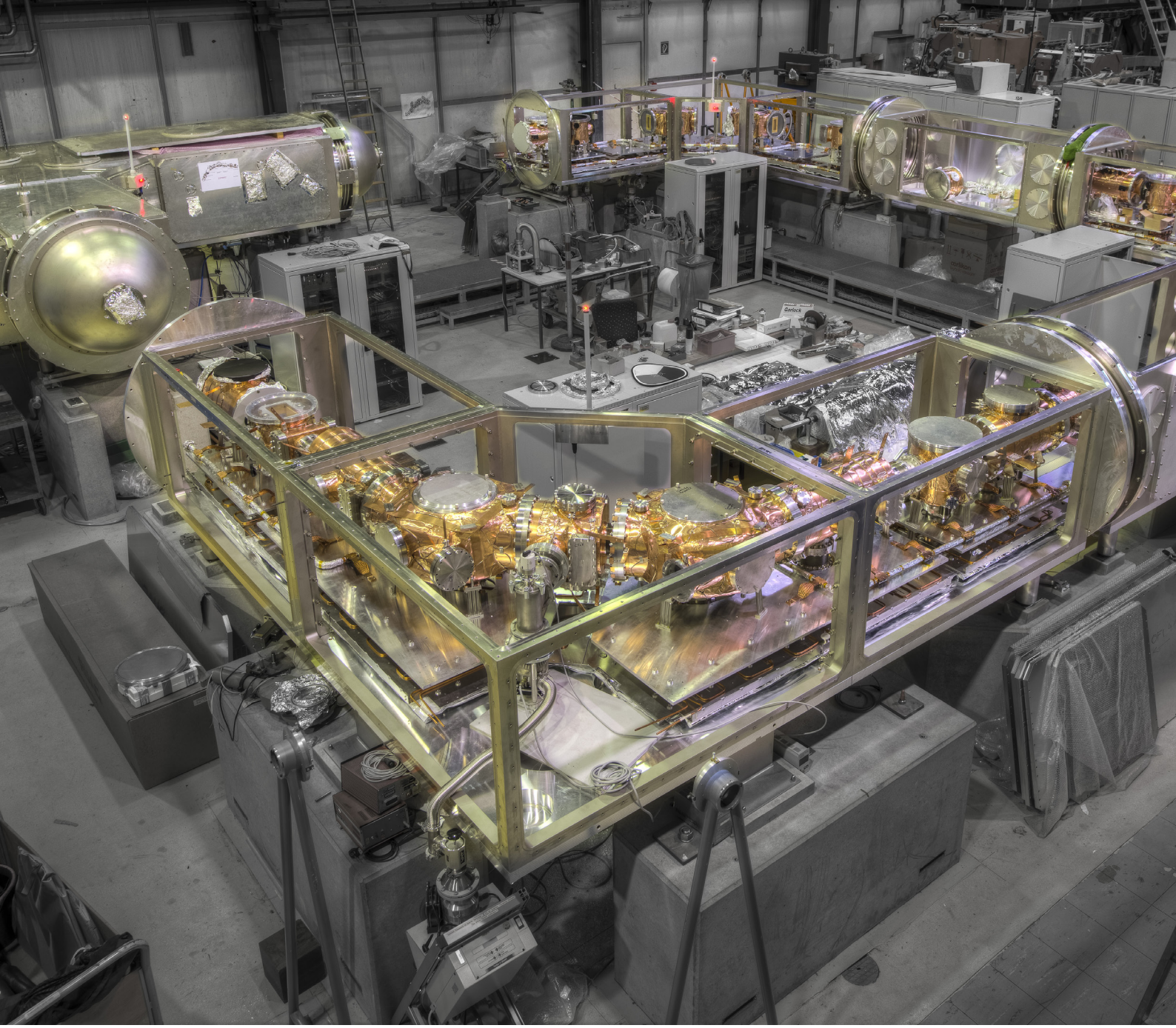

2.3 Cold Stored Ion Beams

The Cryogenic Storage Ring (CSR) during construction.

Introduction

In the physics of atoms, molecules and clusters unique advantages for detecting their reactions and for sensitively probing their internal structures are opened up by cold stored ion beams. Long storage times in ultrahigh vacuum make it possible to precisely control the motion of the ions, to prepare them in well defined internal states, and to perform precision-measurements by sensitively detecting their electric charges. Moreover, with fast beams, fragmentation reactions of the stored ions, even with collision partners at very low relative energy become observable using the merged beams technique. Charged and even neutral reaction fragments can be detected by coincidence counting and imaging on the single-particle level.

The Electrostatic Cryogenic Storage Ring CSR

The cryogenic electrostatic storage ring CSR is nearing completion. Designed to be a unique facility with extreme vacuum and a cryogenic surrounding for the beam, it will provide a wide range of atomic, molecular and cluster ions at 20–300 keV (per charge unit) for various experiments. Using liquid helium, a low temperature environment of less than 10 K – locally even 2 K – will be created along the closed round-trip orbit of the ion beam. This will also create extremely high vacuum. The ion storage times demonstrated in the cryogenic test facility CTF (>5 min) correspond to pressures below 10^{-13} mbar in an equivalent room temperature environment. These and even longer ion storage times are expected for CSR. Keeping all ion optics and the vacuum enclosure at 10 K also offers a uniquely low level of blackbody radiation in studies with ion beams. In connection with an array of ion sources and pre-cooling traps, this will efficiently prevent and control the thermal excitation of rotations, low-lying vibrations and isomeric structures for ion beams during their storage in CSR.

Deflection dipoles, focusing quadrupoles, beam pick-up electrodes and many of the detectors of CSR are situated in a cryogenic inner vacuum system of 35 m circumference. While the overall temperature here is 10 K, special cryogenic pumping surfaces are kept at 2 K. A closed-cycle refrigerator is connected to a cryostat vacuum chamber surrounding the cryogenic beam pipes, providing 10^{-6} mbar insulation vacuum. Starting with a superfluid He cycle, the cooling lines lead along the ring circumference several times at temperatures increasing from 2 K in the innermost line to ~80 K in the outermost loop. The final cooling loops are connected to radiation shield structures of 40 and 80 K, respectively, which are then surrounded by multilayer superinsulation. One of the eight quadrupoles of the CSR is shown in Fig. 1. In the four corner sections the ion beam is bent and ports are available for fragment

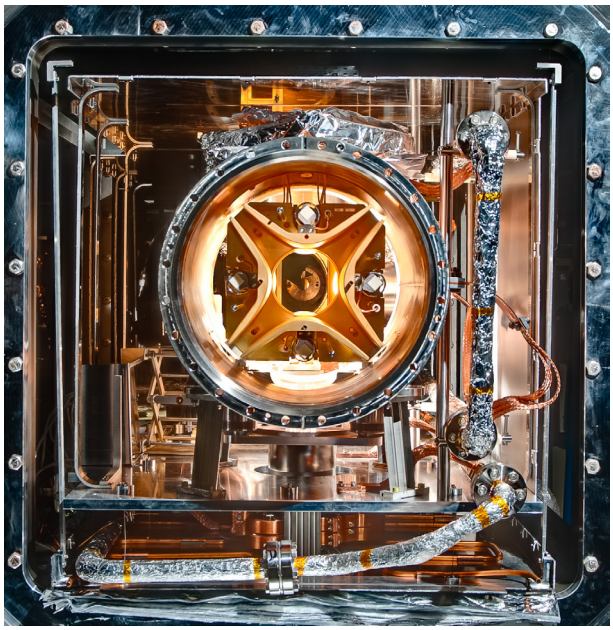

Fig. 1: View along the ion beam into a cryogenic quadrupole unit of CSR. The electrodes in the center are surrounded by the cryogenic ion beam vacuum chamber (10 K design temperature), refrigerant tubes, and two radiation shields with the inner one serving as a mechanical chassis on 40 K.

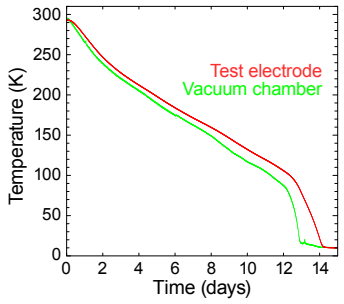

Fig. 2: Measured temperatures during CSR test-quadrant cool down. The cooling rate was throttled to minimize thermal differences. Accelerated cooling of the ion beam vacuum chambers is observed below 70 K; they finally reach 10 K with the electrodes lacking behind by about 1 day.

detectors. Straight sections of ~2.6 m length each lie between the corner sections. They house beam diagnostic elements and devices for interaction experiments, now partly being installed and partly in preparation.

The structure of the cryogenic beam optics elements and beam pipes has been finalized in all corner sections. Also in the straight sections the beam pipes are being closed for commissioning with a first stored ion beam. Detailed mechanical and thermal tests of the cryogenic structure have been performed in one of the corner sections. In these tests, the CSR design [1] was proven by achieving 2 K at the cryogenic pumping units and less than 10 K for the overall temperature of the cryogenic vacuum chambers (clad by thin copper sheet for thermal equalization) and ion optics elements (Fig. 2). In addition, the positions of the cryogenic electrodes were surveyed during the cooling cycle. The deviations from their expected positions, caused by the thermal shrinking of chambers, support structures and the electrodes themselves, were found to remain within the limits for closed orbit shifts of less than 0.1 mm, which perfectly corresponds to the specifications.

On the basis of these results, at times also using the opportunity to fine tune the design from the experience gained, all electrodes were manufactured from an aluminium alloy, adding a thin gold plating on all surfaces facing the beam. Moreover, orders were placed for the bulk of the stainless steel cryogenic vacuum chambers. After their delivery and placing the copper cladding, the chambers were installed and the electrode assemblies aligned by laser tracking methods. Detachable vacuum seals were mostly realized with metallic o-rings, which significantly released the demands on the material thickness and hardness of stainless steel flanges. The seals performed reliably in the thermal cycling of the test quadrant. Around the ring they were installed under careful leak testing; less expectedly, also in-house quality control of the commercially supplied gaskets became necessary.

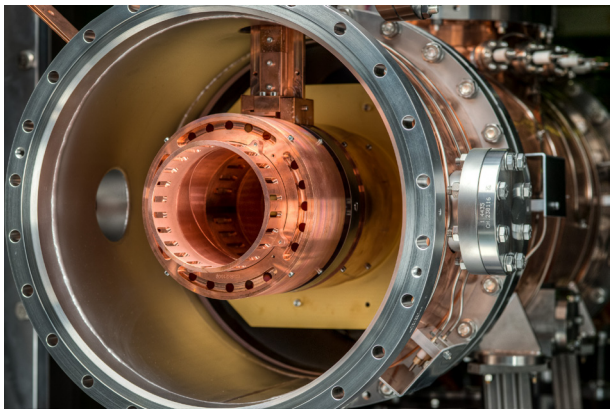

Fig. 3: (cut from right) Electronic pickup unit for non-destructive detection of the stored ion beam in CSR, installed near a quadrupole unit.

The high voltage performance of all components for beam deflection and focusing was carefully fine tuned in laboratory experiments and after final installation in the test quadrant. Applicability of the system for ±25 kV electrode voltages at the bending electrodes (thus exceeding the stored beam energy of 300 keV per ion charge unit) was confirmed in these tests. The infrastructure for controlling the system's high voltages, temperature sensors, vacuum and ion beam diagnostic elements (see Fig. 3) has been largely installed and cabled. Commissioning with a first stored ion beam at room-temperature is scheduled for spring 2014 and will also include the first operation of electronic pick-up devices and particle detectors. The second phase of commissioning will follow a few months later at cryogenic temperature near 10 K and is planned to include a first laser fragmentation experiment sensitive to the rotational quantum levels of molecular ions.

Robert von Hahn, Florian Fellenberger, Andreas Wolf, Klaus Blaum

The Ion Source Area

An important component of the CSR facility is the ion source area, whose main component is a 5 × 5 m² floating ion-source laboratory space, forming the terminal of a high-voltage acceleration column that can be biased to up to 300 kV. This floating laboratory will act as a link of CSR to advanced ion preparation techniques of current ion chemical research. While projects at CSR will make use of its unique capabilities – fast beam collision fragment detection, long-time ion beam storage, beam cooling, internal quantum state control and sensitive electronic detection – suitable ionic compounds will be obtained from specialized ion sources (such as, among many others, electrospray ionization), mass spectrometric filtering and possibly pre-trapping techniques.

The infrastructure of the 300 kV floating laboratory (Fig. 4) has been completely set up and offers all necessary supplies of power, cooling water, pressurized air and fast control links. It is placed in an environmentally controlled Faraday shielding hall with easy access by large doors and overhead cranes. Temperature, humidity, dust and air quality are monitored and automatically controlled to enable operation at positive or negative high voltage, independent of climate conditions. High voltage operation has been proven up to 270 kV in tests limited by the power supply. This was followed by installation of the acceleration column

and successful first ion beam tests used to verify the performance of detectors for CSR. Also the beam line from the platform to the CSR injection has been largely set up. It is combined with installations for overlapping fast beams of neutral atoms with the stored CSR beam for reaction studies.

Fig. 4: Ion source platform.

Fast Merged Electron and Ion Beams

Cold electron beams from a cryogenic photocathode have been proven for phase space cooling of molecular ion beams (up to mass ~40 amu) and for low-energy collision studies with merged electron and ion beams already at the ion storage ring TSR. The TSR, the photocathode electron target and the fragment detectors there have been vital for recent results on laboratory astrophysics and on atomic and molecular collisions. For electron cooling and collision experiments with much improved control over the internal quantum states and with heavier molecular ions, the CSR will continue to employ the cryogenic photocathode source. With this source and a cryogenic merged electron beam device, the CSR will be the first electrostatic ion storage ring to utilize phase space compression of the stored ion beam by electron cooling. The CSR electron cooling system (Fig. 5) is under construction in parallel to the finalization of CSR itself. Many components of the setup have been built, and non-standard components of the cryogenic system, in particular coils using high-temperature superconductor wire for the magnetic guiding field, are being assembled after successful tests. This way, it can be expected that the merged beams system will far advance during 2014. In parallel with this work, detectors for collision fragments released by the fast stored beam in CSR have been built and tested and will be included already for the first CSR commissioning phase in 2014.

Claude Krantz, Manfred Grieser, Andreas Wolf

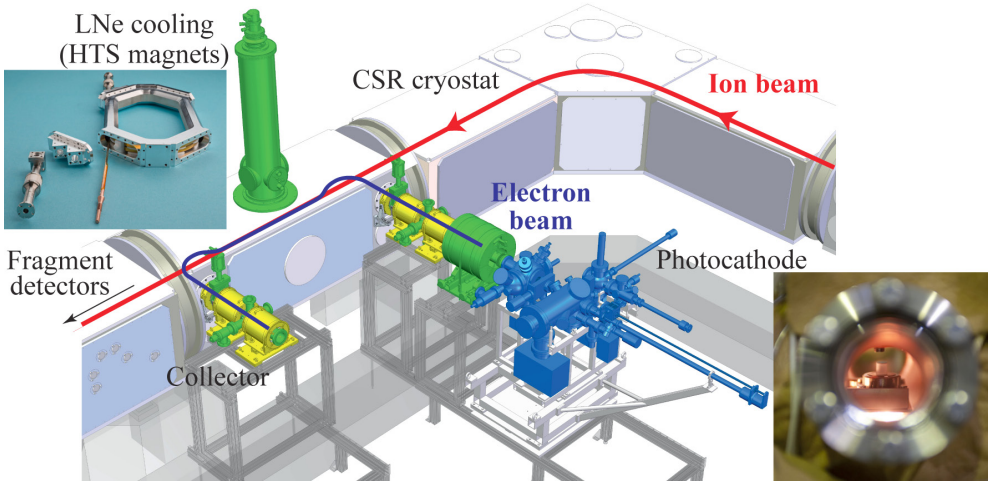

Fig. 5: Layout of the CSR electron cooling device under construction. A low-energy magnetically guided electron beam is merged with the circulating ions. It is obtained from a GaAs photocathode shown in its preparation chamber for cesium coating of the emitting surface. High-temperature superconducting (HTS) coils were developed for creating the magnetic field in the cryogenic region.

Reference:

[1] R. von Hahn, F. Berg, K. Blaum, J. R. Crespo Lopez-Urrutia, F. Fellenberger, M. Froese, M. Grieser, C. Krantz, K.-U. Kühnel, M. Lange, S. Menk, F. Laux, D. A. Orlov, R. Repnow, C. D. Schröter, A. Shornikov, T. Sieber, J. Ullrich, A. Wolf, M. Rappaport, and D. Zajfman, Nucl. Instrum. Methods Phys. Res. B 269 (2011) 2871.

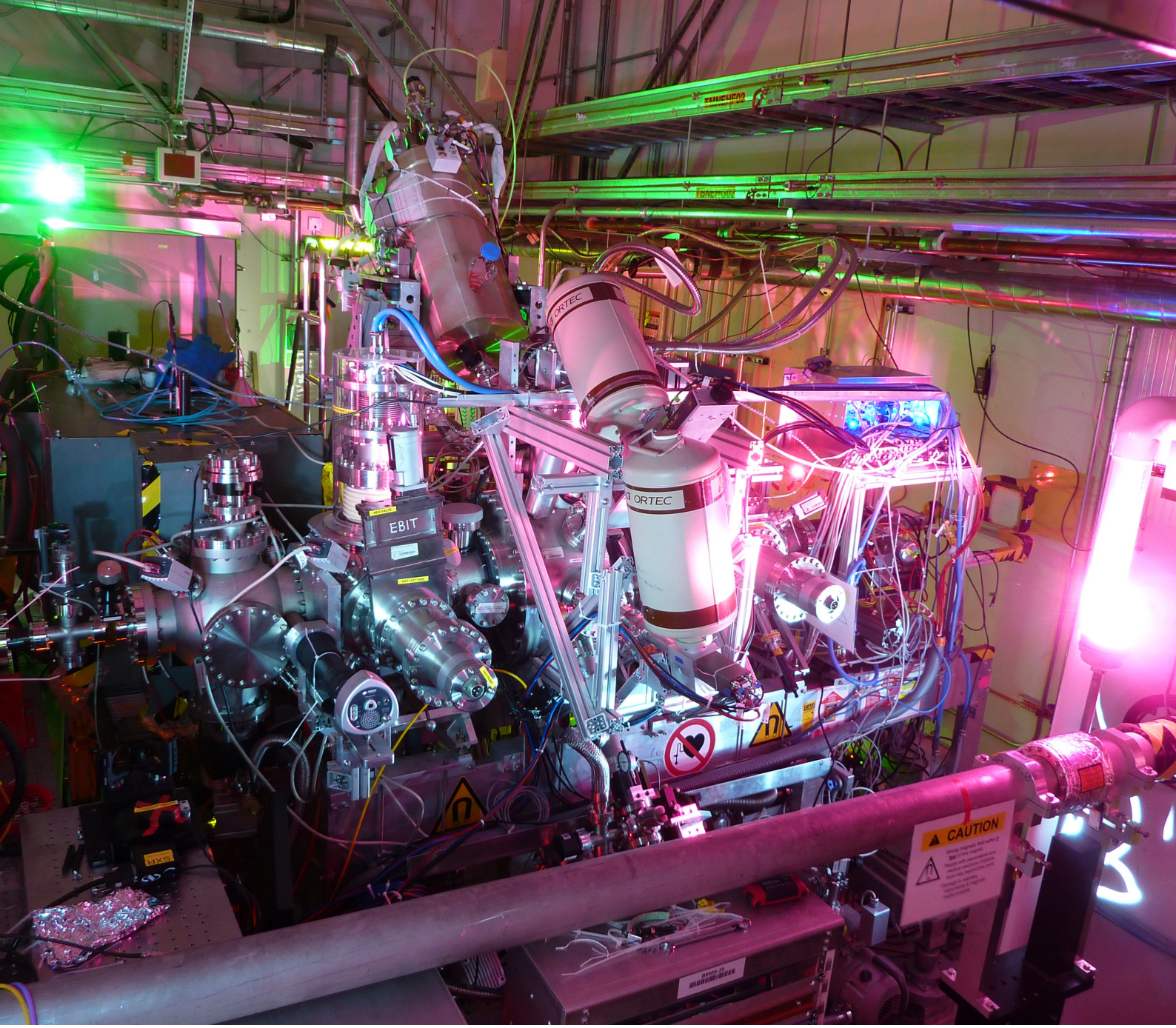

2.4 Astrophysics with Ions and Strong Light Fields

FLASH-EBIT setup at the X-ray free-electron laser LCLS (SLAC, Stanford). The X-ray laser beam enters FLASH-EBIT from the left, and excites the HCI trapped within. Fluorescence resulting from resonant transitions is collected with several detectors including a NASA X-ray microcalorimeter, which are arranged around the device.

Introduction

Interdisciplinary atomic and molecular quantum dynamics laboratories offer access to processes under a variety of conditions which can be observed only passively in astrophysics. In this discipline, the scientific picture is based on observations brought together in a model description. The young field of laboratory astrophysics seeks investigating the basic physical mechanisms in controlled and reproducible ways. At the MPIK laboratories, the range of conditions which can be realized stretches from the lowest values of both temperature and density to very high ones, also including intense fields of electromagnetic radiation.

In large regions of the universe, matter is extremely dilute and cold. Yet, the formation of molecules, up to complex compounds, influences, and is intricately linked with, the formation of stars, the abundance of isotopes, and the composition of planetary objects. At cryogenic temperatures, reactions of molecular ions play a key role for driving formation of more complex molecules. In experiments with stored ion beams or trapped ions, data on the decisive reaction steps could be obtained.

Around, and inside stars as well as massive astrophysical objects, as the temperature rises more and more, atomic ions in high charge states become dominant. We study them in electron beam ion traps with the help of optical lasers, X-ray lasers, and synchrotron radiation. At even higher temperatures during violent astrophysical events, the energy density can by far exceed that at the core of a hot star. Ultrarelativistic jets emerging from violent astrophysical events generate and carry large quantities of positrons; by employing extremely short and intense laser pulses, we can recreate comparable conditions in the laboratory.

Understanding the Engine of Interstellar Chemistry: the Triatomic Hydrogen Ion H_3^+

The triatomic hydrogen ion is the simplest polyatomic molecule, and as such it has attracted a lot of attention as a benchmark system for theory. Moreover, H_3^+ is the most crucial ingredient for the formation of larger molecules in interstellar space. As a universal proton donor, it facilitates the build-up of molecular complexity even at extremely low temperatures and low densities.

However, lacking electronically excited states, spectroscopic studies of H_3^+ are restricted to ro-vibrational transitions. While the fundamental bands are well-understood, the situation changes drastically for level energies above 10 000 cm^{-1}. Here experimental investigations become increasingly challenging due to the weakness of the transitions, and theoretical calculations have to cope with very floppy vibrational modes that cover a vast configuration space. Nevertheless, spectroscopic data between 10 000 cm^{-1} and the dissociation limit at ≈ 35 000 cm^{-1} are highly desirable, firstly to guide theory, and secondly to understand dynamical processes and reactions that sample higher-lying areas of the potential.

To address this need, we have developed a chemical probing scheme combined with cryogenic trapping techniques. To this end H_3^+ ions are stored in a 22-pole ion trap at a nominal temperature of 55 K in the presence of He and Ar gas at densities of 10^{14} cm^{-3} and 10^{12} cm^{-3}, respectively. The He serves to cool the ions in buffer-gas collisions, the Ar is

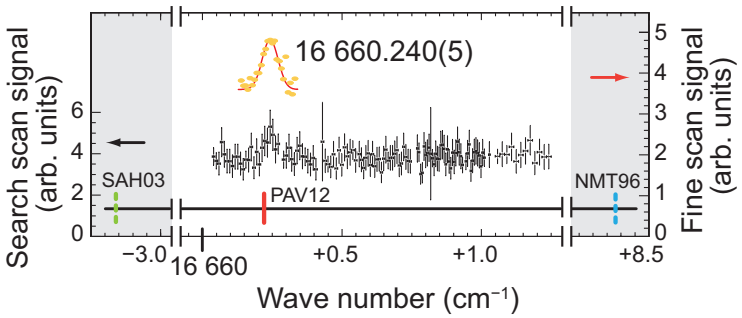

Fig. 1: The weakest and highest energy vibrational transition of H_3^+ ever observed, seen in the MPIK measurements. Unusually high for vibrational transitions, the wave number of the transition corresponds to visible light of orange color. The labels denote previous predictions and the new high-accuracy result (PAV12) triggered by the MPIK experiment.

used as a probe gas. For this scheme we utilize the reaction $Ar + H_3^+ \rightarrow ArH^+ + H_2$, that is endothermic and thus blocked for ground state H_3^+. Irradiation of the stored ions with laser light leads to excitation of H_3^+ above the reaction barrier and thus triggers the formation of ArH^+. The ArH^+ ions are extracted from the trap, mass-selected and detected with a highly-sensitive single particle detector. This detection scheme is many orders of magnitude more sensitive than direct absorption methods and has allowed us to measure the weakest transitions ever observed for molecular ions [1].

For this key species of interstellar chemistry, reactions between H_3^+ and electrons, atoms or molecules receive special attention in the astronomical community. The electron recombination process ($H_3^+ + e^- \rightarrow H_2 + H / H + H + H$) has a long history of controversy that is still not fully resolved [2]. The most detailed measurements, allowing for comprehensive comparison to theory, were carried out utilizing the cold electron target of the TSR storage ring at MPIK.

Currently, the nuclear spin temperature of H_3^+ and H_2 in space are under close scrutiny. Similar to H_2, H_3^+ exists in two different nuclear spin modifications, with para-H_3^+ being 30 K lower in energy than ortho-H_3^+ (for H_2, the difference between para and ortho is 170 K). Initially, it was assumed that the nuclear spins of H_3^+ and H_2 would come to thermal equilibrium with the kinetic gas temperature of the interstellar medium through frequent proton exchange in collisions with one another (the $H_3^+ + H_2$ collision process is the most frequent bi-molecular reaction in the Universe). However, recent observations of H_3^+ and H_2 in the same lines of sight are not lying anywhere near the expected thermal curve (Fig. 2). It turns out that the excitation temperature of H_3^+ is much lower (around 30 K) than the cloud temperature, which agrees with the excitation temperature of H_2 (≈ 70 K). This mystery is, as-of-today, unresolved.

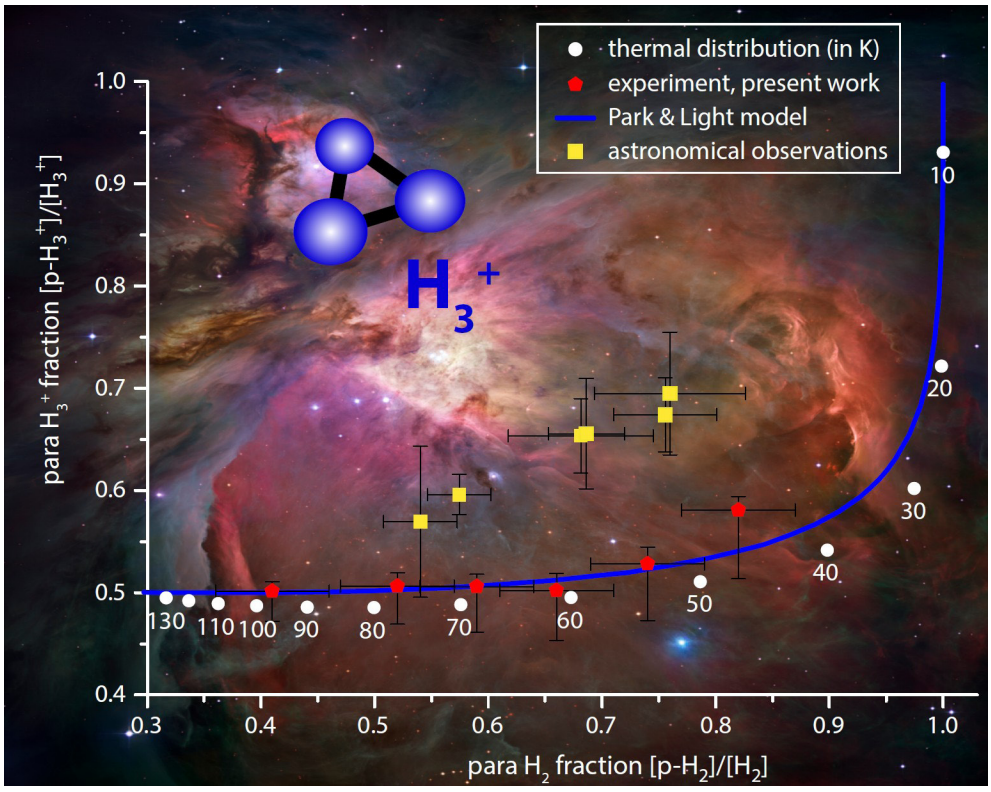

Fig. 2: Nuclear spin fractions of H_3^+ and H_2. Plotted are the respective para-fractions. The yellow squares show interstellar observations which reveal an excess of para-H_3^+, deviating from the thermal expectation (white dots, blue line). The red pentagons show our ion-trap measurements under steady-state interstellar conditions. The discrepancy between the thermal curve (confirmed by our experiments) and the interstellar observations is unresolved as-of-today. (Credit background image: NASA/ESA Hubble Space Telescope).

In a first step, we have measured the steady-state nuclear spin populations of H_3^+ at interstellar temperatures from 40–100 K, exposing the ions to thermal H_2 of varying nuclear para-H_2 fractions from 0.4–0.9. For these challenging measurements we used the same chemical probing spectroscopy technique, as described above. But in addition we prepared sample H_2 gas with defined para-H_2 fractions, using a home-built para hydrogen generator and Raman spectroscopy for diagnostics. Our experimental measurements (Fig. 2) show that the steady-state H_3^+ populations in collisions with H_2 indeed lie close to the expected thermal curve [3]. This comes as a relief, as a non-thermal outcome for one of the most basic molecular reactions would not bode well for the predictive power of interstellar models.

However, the discrepancy between interstellar models and observations remains. Very recent comprehensive studies carried out in collaboration with the MPI for Astronomy reveal that the electron recombination reaction of H_3^+ is the key process for the nuclear spin temperature. Therefore, renewed efforts to measure the nuclear-spin dependence of the H_3^+ electron recombination rates at low collision energies are foreseen, once the new Cryogenic Storage Ring (CSR) at MPIK is fully operational. Further studies at the neutral collision beamline at the CSR, which is currently under development, will include merged beams experiments to study reactions of H_3^+ with neutral atoms like O, C and D. These collision processes are experimentally unconstrained, and they are at the heart of major problems of astrochemistry, like the synthesis of organic molecules in space, the formation of interstellar water and deuterium enrichment, which can give us important hints on the origin of our own water on Earth.

Holger Kreckel, Andreas Wolf

Breakup of Polyatomic Molecules in Cold Electron Collisions

In the dilute interstellar medium, complex molecules can be efficiently built up by ion-neutral reactions. Heavy neutral atoms (C, O) can react with H_3^+ as a proton donor, and these larger molecular ions continue to bind further protons in reactions with H_2. In a final step, when further proton binding is not possible, the reaction with free electrons then leads to the formation of stable neutral compounds. The cold collision environment is modeled by using co-moving electron and ion beams. Up to 2012, the heavy ion storage ring TSR was used for these experiments. Together with a merged electron beam from a cold photocathode source, established at TSR, further experiments will be performed at the new cryogenic storage ring CSR.

Spectral lines serve astronomers to identify molecules in space. In spite of the low interstellar temperatures, the molecules are sometimes found in isomeric states, where the atoms have exchanged their positions in the compound. This requires high energy, usually available in high-temperature regions only. Experiments with cold merged electron and ion beams at the MPIK have shown that in the reaction of a protonated molecule with cold electrons such energetic isomers can be produced.

This was shown for cyanide (HCN) and its isomeric species iso-cyanide (HNC) which are found in molecular spectra to be both similarly abundant in several interstellar molecular clouds. In its formation, the protonated precursor ion $HCNH^+$ reacts with cold electrons. The relative fraction at which both isomers are formed in this reaction was never measured. At MPIK, $DCND^+$ molecules were used in the TSR storage ring. In merged ion and electron beams, they recombined with electrons at only ≈ 10 K thermal energy. On a multistrip surface barrier detector that could record the masses of the fragments and their relative velocities, those dissociative recombination events were filtered out that lead to a DNC or a DCN fragment together with a deuteron (D). From these results [4] the fragment kinetic energy release (i. e., the energy given to them by the reaction) was determined (Fig. 3).

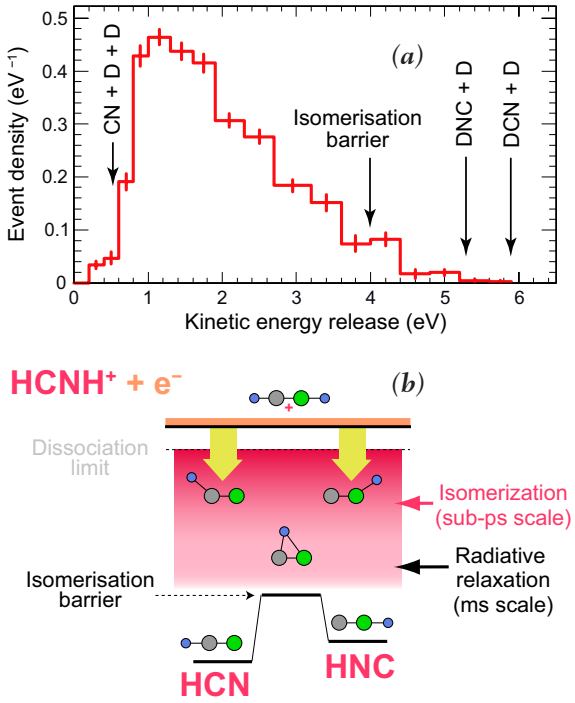

Fig. 3: (a) The kinetic energy release of the two-product dissociation DCN/DNC + D triggered by recombination of cold (≈ 10 K) electrons with $DCND^+$ ions. A stored beam of $DCND^+$ ions was merged with a cold electron beam. (b) For the equivalent reaction $HCNH^+ + e^-$ in space, one concludes that the internal energy of its molecular product is mostly high enough for a rapid place change of the H atom, so that none of the isomers HCN or HNC is produced directly.

Ground-state DCN or DNC fragments would lead to a high kinetic energy release, but any internal excitation of the molecular fragments will reduce it. This way the measurement showed that the DCN/DNC compound in this cold reaction is produced with extremely high internal excitation, corresponding to thousands of K if expressed by equivalent temperature. The excitation energy is much higher than the barrier separating the isomers DCN and DNC; the three atoms already form a bound molecule, but can freely interchange their isomeric forms. Hence, the dissociative recombination reaction is proven as an efficient pathway to both isomers. Measurements at the MPIK are finding similarly high internal excitation in molecular products from dissociative recombination also for other cases.

Dissociative Recombination Rates for Molecular Ion Reaction Networks

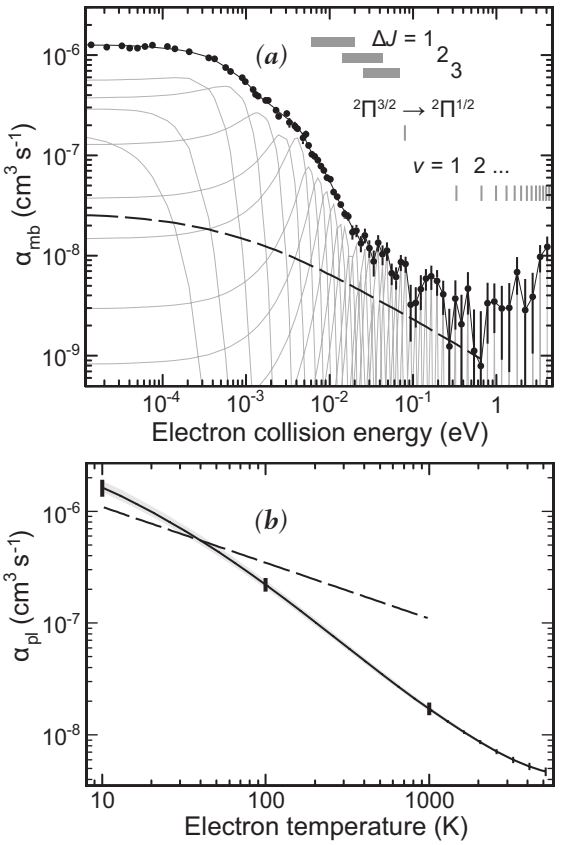

Fig. 4: (a) Dissociative recombination rate of HCl^+ ions measured with merged electron and ion beams in the TSR as a function of the electron collision energy. Excitation thresholds of HCl^+ ions and cross section contributions used in the fit of the data are marked. (b) Deduced plasma rate coefficient for the process and its variation with the electron temperature; dashed line: values previously assumed in astrophysical models.

The much improved observations of molecular spectra in interstellar and circumstellar environments, becoming possible by new observatories, motivate world wide activities also for modeling the reaction networks that lead to molecular compounds in the interstellar medium. Dissociative recombination of molecular ions with electrons is an important, often rate limiting step in these networks. In the cold photocathode electron target of the TSR, rate measurements for this process were performed at variable collision energies between ≈ 10 K and several 10 000 K (1 meV to > 10 eV). The measurements were extended to ions important for the initial steps of nitrogen, chlorine and sulfur chemistry. New methods were developed for the determination of absolute recombination rates from these merged-beams measurements, as illustrated by the results for HCl^+ (Fig. 4) [5]. Increasing merged-beams collision energy probes the decrease of the HCl^+ recombination rate as the colliding electrons become faster. This reflects the microscopic cross section and sensitively depends on the quantum processes (predissociation and autoionization) undergone by excited neutral molecular states in the vicinity of the HCl ionization limit. Contributions to the cross section are determined with high energy resolution by fitting the merged-beams experimental signal. In a second step the cross section results are used to predict the dissociative recombination rates under interstellar conditions, where they are described by the plasma rate coefficient α_{pl} as a function of the temperature assigned to the electrons in this medium. For the case of HCl^+ a surprisingly sharp drop in the dissociative recombination rate coefficient is found as the electron temperature increases to a few hundred Kelvin. Since the TSR with its room-temperature ion beam enclosure is used in these measurements, the HCl^+ ions themselves still have ≈ 300 K rotational temperature; dissociative recombination measurements excluding this rotational excitation in the laboratory will only become possible with the cryogenic storage ring CSR.

Claude Krantz, Oldřich Novotný, Andreas Wolf

Laboratory Astrophysics with Highly Charged Ions

Astrophysics aims at giving a coherent description of the plethora of astronomical observations made with an ever growing number of methods and instruments, from imaging to spectroscopy, and with messengers as diverse as neutrinos, cosmic rays, and photons. The most comprehensive body of data is derived from the latter. Visible baryonic matter, by definition, emits electromagnetic radiation. Most of this radiation arises from very hot large mass agglomerations, be they point-like, such as stars or active galactic nuclei, or diffuse, such as galactic halos or intergalactic hot gas. These sources draw their radiative power from gravitational accretion and from nuclear fusion. A common feature of all these objects is the presence of highly charged ions (HCI), which can be detected by virtue of their spectral

features. Although the underlying physical theory of spectra, quantum electrodynamics, enjoys the privilege of being the most exactly predictive of all theories for simple systems, its realizations in complex ions and atoms are limited in accuracy by the approximations needed to cope with many-body interactions. While the astrophysical data quality improves and their quantity keeps growing with every new space mission or terrestrial observatory, the means for theory tests in the laboratory are still limited. Difficulties in the production of HCI, in their storage, and diagnostics have to be dealt with, and only a few laboratories are equipped with the required instrumentation. The MPIK is worldwide leading in the field, with three operational electron beam ion traps (EBITs) and a variety of diagnostic apparatus from own developments. A particular emphasis lies in X-ray astrophysics with HCI, since this is a field with a fast growth in the number of missions, and where theory still encounters serious challenges. The scientific harvest from observations is thus reduced, and the guidance by precise experiments is crucial for further developments. At the same time, a strong theoretical research program within the MPIK in close collaboration with the experimentalists ensures the best possible mutual sharing of scientific findings, with all its advantages.

X-ray laser spectroscopy: understanding stellar microphysics: In the field of X-ray laboratory astrophysics, our activities focused on improving the resolution of photon-HCI interaction studies using free-electron lasers (FEL) and synchrotrons, as well as on investigating both the photoionization of HCI and its time reversal, photorecombination. These two processes determine radiation transport in stars and in the photoionized plasmas surrounding compact objects such as black holes and neutron stars. We have introduced a method enabling these investigations at hitherto inaccessible photon energies. The MPIK electron beam ion trap FLASH-EBIT, in combination with the novel FEL LCLS (at SLAC) and the synchrotrons PETRA-III (at DESY) and BESSY-II (Berlin), enabled expanding the energy range of laser spectroscopy by three orders of magnitude deep into the X-ray region. The FLASH-EBIT setup at LCLS shown in the title figure overlaps the strongly collimated, extremely intense X-ray beam emitted by the FEL with the thin cloud of highly charged ions trapped at the center of the EBIT. By varying the FEL photon energy, electronic transitions can be resonantly excited. Since this process occurs only at narrowly defined values, accurate determinations of the level structure and of the related cross sections become possible. And the enormous X-ray fluxes provided by LCLS allows one to bring for the first time to the laboratory the conditions found in astrophysical objects which are dominated by X-ray excitation and ionization, like accretion disks of active galactic nuclei, and X-ray binaries.

With the novel method of resonant excitation of X-ray transitions in HCI, their energies and line widths can be determined more accurately than before, and systematic uncertainties are largely suppressed. Fig. 5 displays the fluorescence of the strongest soft X-ray transitions found in most astrophysical X-ray sources as realized in the laboratory under well-defined photonic excitation conditions. The timing of the fluorescence is thereby coincident with the LCLS pulses, and only at the right energy the excitation of a certain charge state of the iron ions takes place. FLASH-EBIT can be loaded with ions in any charge state, and line blends from other ionic species, an old hindrance of spectroscopy, can be in this way avoided. Our studies have solved a long-standing astrophysical controversy concerning these, the strongest transitions observed in the soft X-ray spectrum of stars at around 800 V [6]. Here it was shown that the quality of the wave functions used to describe Fe XVII, a 10-electron system with a closed $n=2$ shell, and its excited states, is insufficient to yield an accurate transition probability. Other possible explanations had been brought forward in the last forty years. In essence, those postulated either an inadequate modelling of the collisional excitation process or of the plasma effects, but in view of the experimental results the primary problem sits already at the beginning, in the imperfections of the atomic physics description of the system. This conclusion was reached by comparing the experimental spectra to our large-scale atomic structure calculations, and also to other state-of-the-art theoretical results.

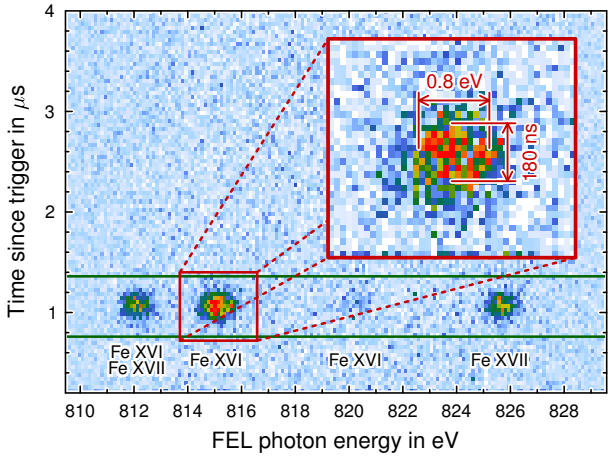

Fig. 5: Time-resolved fluorescence from different iron HCI acquired as a function of the exciting photon beam energy obtained at LCLS [6]. The purely photonic excitation mechanism allows theoreticians to exclude uncertainties which are inherent to calculations of collisional excitations.

Moreover, for the first time, the K-shell ground state transitions of iron HCI, which are the strongest contributors to opacity inside radiatively dominated stellar cores, could be systematically measured [7]. Here, a K-shell electron is transferred to the L shell by photon absorption using highly monochromatic synchrotron radiation. Fig. 6 shows the X-ray fluorescence of iron HCI as a function of the excitation photon energy. Since the photon beam delivered by the synchrotron undulator is horizontally polarized, the pattern of fluorescence emission depends on the angle at which the X-ray detectors are mounted. Thus, information on the total orbital momentum change resulting from the photon absorption and emission is obtained. However, the major advantage is that not only the positions and relative strengths of the associated lines, but also their radiative widths could be directly determined. These electronic transitions had until now always been studied under conditions of collisional excitation, which are not representative of the radiation-dominated interior of stellar cores, and at a lower spectral resolution. Our data deliver accurate energy determinations for core-hole excitations for the isoelectronic sequences from heliumlike to carbonlike iron ions. While the heliumlike transitions can be predicted with very good accuracy, the other ones have far larger theoretical uncertainties. This trend does not hold for the experimental data. Even for the heliumlike system, the larger uncertainties of earlier experimental work have recently led to claims of an atomic-number dependent deviation from advanced QED predictions. These claims are not supported by our experimental results, which confirm the most sophisticated heliumlike calculations within far reduced error bars.

QED, relativistic, and correlation effects in highly charged ions: We carried

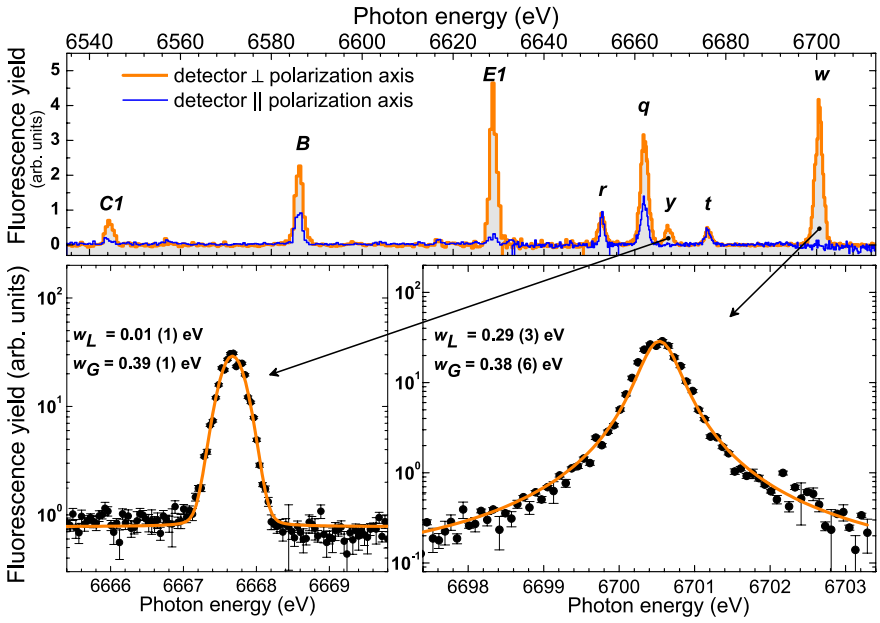

Fig. 6: Resonantly excited fluorescence of iron HCI in the heliumlike (transitions w, y), lithiumlike (transitions r, q, t), and other charge states were recorded at low (upper panel) and high resolution (lower panel) using the FLASH-EBIT at PETRAIII [7]. These K_α transitions of iron are extremely strong absorbers of X rays within the solar radiative zone.

out further spectroscopic studies of QED, photorecombination, and electronic structure in HCI with experiments in house. Thereby, we found strong contributions from hitherto neglected high-order interelectronic correlations, where two or more electrons are simultaneously excited. These recombination processes are illustrated on Fig. 7 and can be even stronger than first-order processes for some HCI with large abundances in the solar radiative zone. Such contributions change the energy-dependent photabsorption as well as photorecombination cross sections significantly, and future quantitative stellar models will have to include them in order to improve the quality of their predictions. The question arises, whether these effects and the corresponding changes in mean opacities could be responsible for the present discrepancy between the elemental abundances believed to be needed for the current Solar Model, and their spectroscopically measured counterparts.

Typically, interpreting the spectra obtained in EBIT experiments is completed by a thorough theoretical modeling. The strong nuclear field pushes the dynamics of the bound electrons into the relativistic domain, which requires a description based on Dirac's equation. Correlation effects, i.e. the intricate way how the mutual interactions between the

shell electrons shape their wave functions are tackled by large-scale numerical computations. The picture of underlying physical effects also includes contributions from quantum electrodynamics: vacuum fluctuations strongly influence the electronic wave function and thus all observable properties of the HCI. Besides the prediction of transition energies from the optical up to the X-ray range, we calculate transition probabilities and cross sections for the excitation and recombination processes mentioned above.

Optical laser spectroscopy and cooling of highly charged ions: In the optical range, the main spectral realm of astrophysical information, we carried out the first demonstrations of laser spectroscopy on forbidden transitions in trapped HCIs. Their long-lived states will be a particularly interesting object of study in the context of time variation of fundamental constants. The "oldest" known HCI transition, the "green coronal line" of Fe XIV at 530 nm - first observed in the total eclipse of 1869, and not yet fully understood regarding its excitation mechanism - was accurately measured in the laboratory for the first time [8]. For this purpose, we introduced the setup depicted in Fig. 8. In it, a tunable optical laser is used to excite the forbidden lines, and a photomultiplier detects their relatively slow decay after each excitation pulse. Given that the forbidden lines are indeed five orders of magnitude more difficult to excite with photons than allowed transitions, careful work is needed to reduce the background of stray light due to the laser to a level amenable for detection of the weak fluorescence signal. Equipped with our measured value, which is one of the most accurately determined wavelengths ever for an HCI, Doppler-shift-based velocity determinations with an error bar of only 0.24 km/s are possible. Since coronal plasmas reach bulk velocities of several hundred km/s, having wavelength data with a small error bar is essential. Moreover, since Fe XIV is present in a large variety of astrophysical objects, our results can lead to a better diagnostics of stellar coronae, of stellar winds and outflows, and of their dynamics.

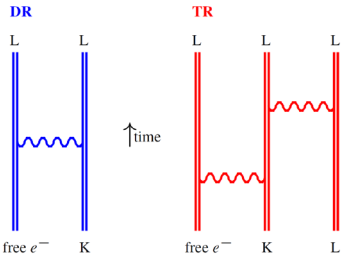

Fig. 7: Feynman diagrams representing the dielectronic (DR, left) and trielectronic (TR, right) recombination processes. The double lines stand for the actively involved electrons moving in the nuclear Coulomb field, while wave lines represent the virtual photons exchanged between them. K and L stand for the electronic shells involved.

At present, all experiments using HCI still suffer from the high translational temperature of the trapped ions (in the order of 10^5 K and more), which results from the production through electron impact ionization inside of a deep trapping potential. Overcoming this serious obstacle has been a long term goal of several research groups. We have developed a cryogenically cooled Paul trap (CryPTEx) for sympathetic laser cooling of HCI and molecular ions. As shown in Fig. 9, a set of radio-frequency electrodes holds in its center a submillimeter-sized ensemble of singly charged ions of Mg or Be. These ions are then cooled by a red-detuned laser acting on their fast resonance transitions. This efficient cooling induces a phase transition in which the trapped ions order themselves in a so-called ion crystal, a stable structure levitating in the center of the trap. The ions stay at distances in the order of micrometers from each other, thus enabling imaging of each trapped ion even at moderate resolutions of the viewing microscope. The achievable translational temperatures go down below 1 K, and can reach values of a few mK. This implies a reduction of Doppler broadening by more than 4 orders of magnitude, a decisive step in the way to ultrahigh accuracy measurements with HCI. The insets in Fig. 9 show a Be ion crystal and also a Be four ion chain as well as an ion pair.

During commissioning experiments, performed with the Ion Trap Group at Aarhus University, we have obtained excellent results for slow electromagnetic transitions of molecular ions, obtaining the decay rate of the lowest vibrationally excited state in MgH^+, and thus its absorption strength [9]. Accurate knowledge of such absorption strengths of basic molecular ions is particularly important for the determination of their abundances in the interstellar medium. Using CryPTEx we have also reached the lowest measured internal temperature in a molecular ion (accepted for publication in Nature). These studies hold great promise for research on astrophysically ubiquitous molecular ions at low temperatures, as our methods can readily be extended to other molecules of particular astrophysical relevance. CryPTEx has proven to be a versatile device capable of preparation of molecular ion targets of diverse

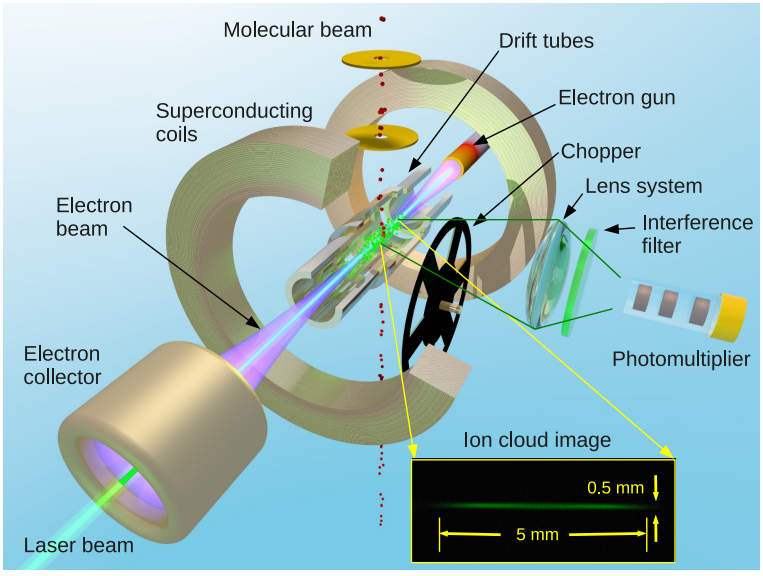

Fig. 8: Optical lasers are used at the Heidelberg EBIT facility to excite forbidden (M1 type) electronic transitions with lifetimes of several milliseconds. The HCI investigated, Ar XIV and Fe XIV [8], have long-known coronal lines, and were chosen for demonstration of the novel technique.

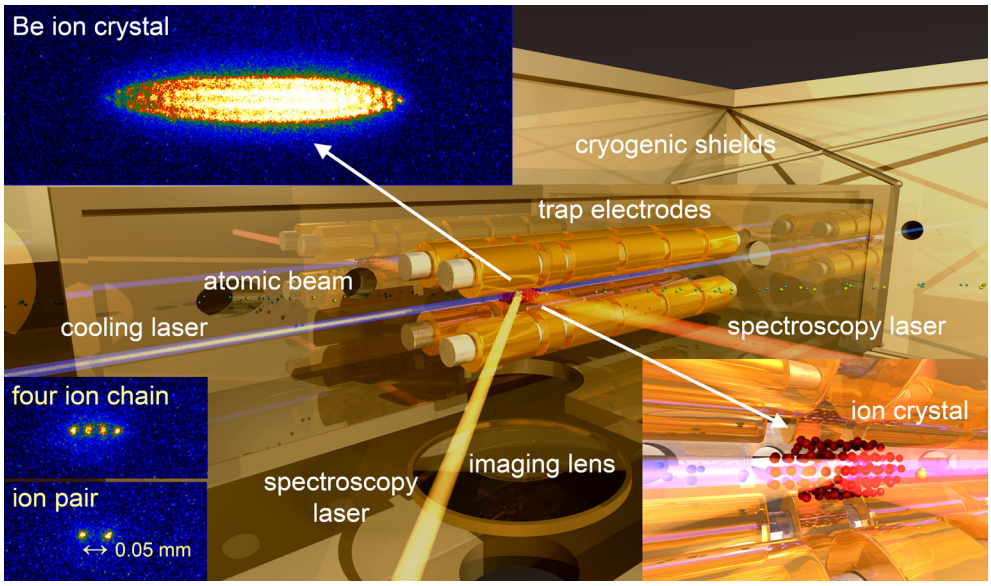

Fig. 9: Principle of sympathetic cooling of ions using CryPTEx, the Cryogenic Paul Trap Experiment developed at MPIK in collaboration with Aarhus University. Molecular ions (MgH^+) were used for commissioning runs, reaching the lowest measured internal temperatures for molecular ions. Planned applications are studies of possible drifts of fundamental constants using HCI [9] and molecular ions, by using Be^+ ion crystals as shown above.

species, with an unprecedented degree of control of both internal and external temperatures, reaching even the single-state stage of sample preparation. Currently, the apparatus is used at MPIK to produce and cool crystals of laser-cooled Be^+ ions, and first tests of the implantation of HCI into those crystals are being carried out.

José R. Crespo López-Urrutia, Zoltán Harman

Intense Laser Astrophysics: Laser-Produced Ultra-Relativistic Leptonic Jets

In addition to high-frequency free-electron lasers also intense low-frequency lasers have turned out to be usual devices in exploring astrophysical scenarios on earth. Such laser facilities have shown to be suitable to accelerate particles to the GeV regime allowing for the controlled investigation of numerous nuclear and high-energy processes [10]. In fact, it has been recently realized that ultra-intense laser-matter interaction can create in terrestrial laboratories analogous physical conditions as those in violent astrophysical events like supernova explosions.

Laboratory astrophysics is thus one of the youngest branches of astrophysics and possibly one of the most promising, as it allows to investigate in a controlled and repeatable way extreme processes, which otherwise could be studied only indirectly. In particular, the possibility of generating high-energy lepton beams in laboratory is of central importance for astrophysics, due to their similarity to jets of long gamma-ray bursts.

In [11], in a joint effort with external groups we have investigated both theoretically and experimentally the possibility of generating ultra-relativistic, highly-collimated positron and electron-positron beams with a table-top laser facility. So far, such experiments have been performed only by employing large-scale electron accelerators. The electron beams produced by the accelerator collided with a high-Z solid target (typically gold or lead), generating on the rear side electron-positron bunches.

By generating the incoming monoenergetic electron beam via laser wake-field acceleration, our collaboration with experimental colleagues from Belfast and Michigan succeeded in producing for the first time positron beams of short (≈ 30 fs) duration, with ultra-relativistic energies (> 100 MeV), and with a narrow angular distribution (≈ 3 mrad) in a table-top setup. By means of analytical fittings of the dependence of the positron yield Ne^+ on the solid-target thickness l (see Fig. 10a) and on the ratio Z^2/A (see Fig. 10b), with Z (A) being the charge (nucleon) number of the solid target, we have established that the main mechanism responsible of the positron-production process is the emission of photons via bremsstrahlung by the incoming electrons deflected by the ions in the solid target and the

consequent transformation of the bremsstrahlung photons into electron-positron pairs when still in the target. Thus, leptonic bunches containing both electrons and positrons are originally produced in such an experiment. However, pure electron and positron jets have been then also obtained, by installing a strong magnet at the rear side of the solid target and able to separate the oppositely charged components of the original mixed bunch.

There are clear prospects for this work for understanding the yet far from fully clarified dynamics of ultra-relativistic astrophysical jets. By means of varying, e.g., the thickness of the target, one may modify and control the ratio between the number of electrons and that of positrons in the jets. In addition, the bunch energy may be adapted up to the 100 GeV regime with facilities currently under investigation and in earth laboratories the environment may be comparably well controlled. On the theory side, particle in cell codes including QED processes are also under development, such that there are clear reasons for confidence that more understanding in the complex dynamics of astrophysical jets may be gained with intense lasers in the not too remote future.

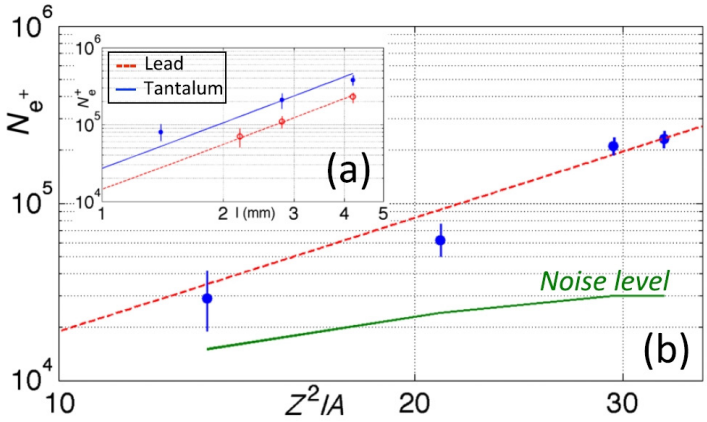

Fig. 10: (a) Measured positron yield, in the positron energy range 90 MeV < E_p < 120 MeV for Ta (blue full circles) and Pb (red empty circles) for different target thicknesses l. Lines give the theoretical best quadratic fits. (b) Measured positron yield, in the same positron energy range for different materials but constant areal density nl, with n being the target density, as a function of Z^2/A. The dashed line represents the theoretical best quadratic fit.

Antonino Di Piazza, Christoph H. Keitel

References

[1] M. Pavanello, L. Adamowicz, A. Alijah, N. F. Zobov, I. I. Mizus, O. L. Polyansky, J. Tennyson, T. Szidarovszky, A. G. Császár, M. Berg, A. Petrignani and A. Wolf, Phys. Rev. Lett. 108 (2012) 023002.

[2] H. Kreckel, A. Petrignani, O. Novotný, K. Crabtree, H. Buhr, B. J. McCall and A. Wolf, Phil. Trans. R. Soc. 370 (2012) 5088.

[3] F. Grussie, M. H. Berg, K. Crabtree, S. Gärtner, B. McCall, S. Schlemmer, A. Wolf, H. Kreckel, Astrophys. J., 759 (2012) 21.

[4] M. B. Mendes et al., Astrophys. J. Lett. 746 (2012) L8.

[5] O. Novotný et al., Astrophys. J. 777 (2013) 54.

[6] S. Bernitt et al., Nature 492 (2012) 225.

[7] J. K. Rudolph et al., Phys. Rev. Lett. 111 (2013) 103002.

[8] K. Schnorr, V. Mäckel, N. S. Oreshkina, S. Augustin, F. Brunner, Z. Harman, C. H. Keitel, J. Ullrich and J. R. Crespo López-Urrutia, Astrophys. J. 776 (2013) 121.

[9] O. O. Versolato, M. Schwarz, A. K. Hansen, A. D. Gingell, A. Windberger, L. Kłosowski, J. Ullrich, F. Jensen, J. R. Crespo López-Urrutia and M. Drewsen, Phys. Rev. Lett. 111 (2013) 053002.

[10] A. Di Piazza, C. Müller, K. Z. Hatsagortsyan, and C. H. Keitel, Rev. Mod. Phys. 84 (2012) 1177.

[11] G. Sarri, W. Schumaker, A. Di Piazza, M. Vargas, B. Dromey, M. E. Dieckmann, V. Chvykov, A. Maksimchuk, V. Yanovsky, Z. H. He, B. X. Hou, J. A. Nees, A. G. R. Thomas, C. H. Keitel, M. Zepf and K. Krushelnick, Phys. Rev. Lett. 110 (2013) 255002.

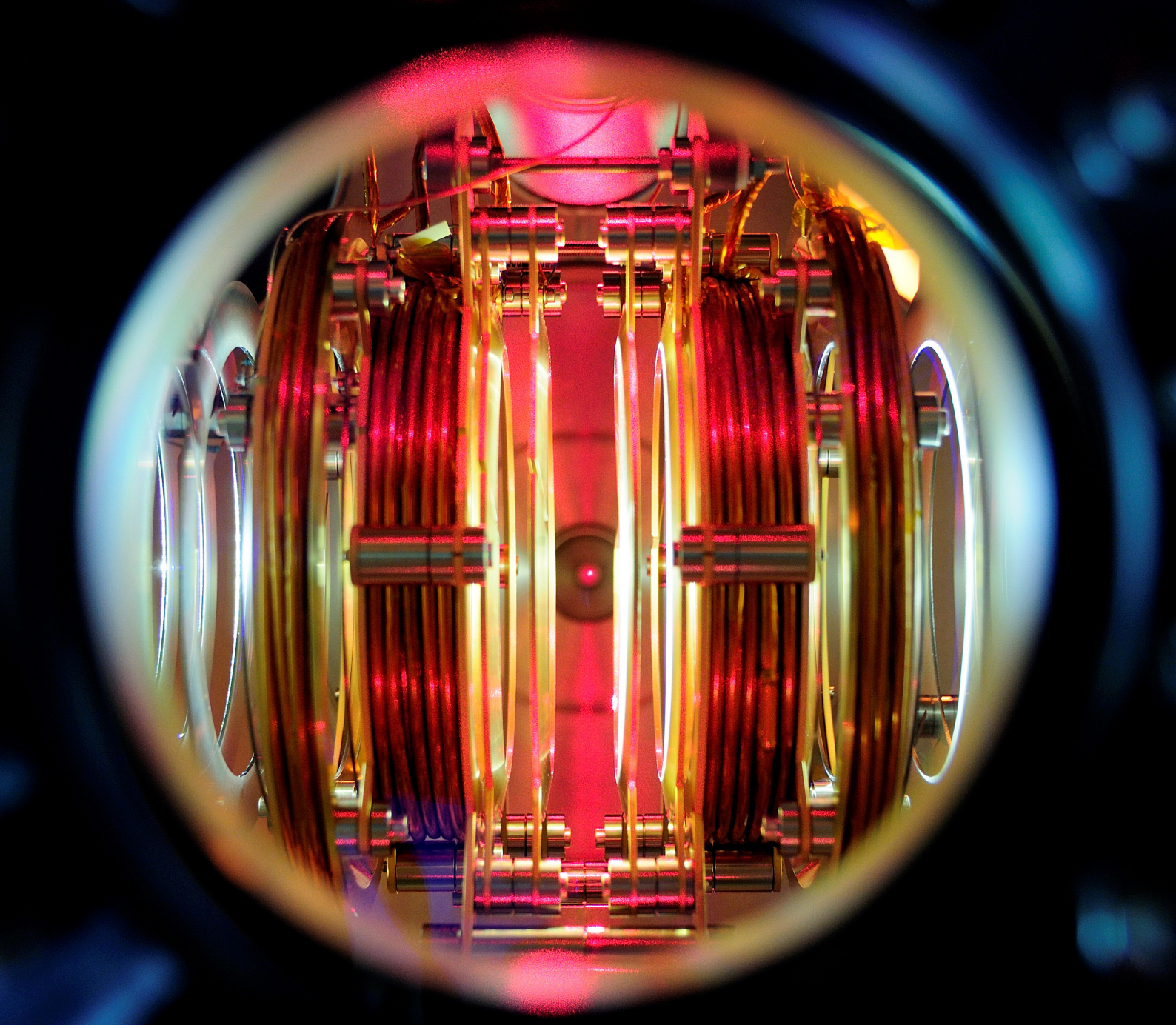

2.5 Atomic and Molecular Collisions

A cloud of laser-cooled lithium atoms glowing in red in a magneto-optical trap. Its decay dynamics induced by ion impact is imaged with a reaction microscope.

Introduction

Experiments on collisions with atomic and molecular targets are perfectly suited to investigate the correlated quantum-dynamics of few electrons and nuclei under the action of external, time-dependent perturbations on atto- and femtosecond time scales. New milestone experiments are enabled by world leading in-house experimental developments. Some examples presented in the following are based on many-particle detection techniques (reaction microscopes), new target preparation techniques as laser trapping and cooling of target atoms and the foil-induced Coulomb explosion technique for molecular structure imaging.

Ion-Atom Collisions

The study of ion-atom collisions has a long tradition in atomic physics. Nevertheless, our understanding of the collision dynamics is still limited. For electron impact, the simplest collision systems can nowadays be calculated numerically with tremendous precision. However, for ion collisions one might conclude that new and more detailed experimental observations just reveal more shortcomings of our modeling.

In in the last years the dynamics of one of the most fundamental inelastic processes in ion atom collisions, the single ionization of the target, has been studied in experiments in the test storage ring TSR with the focus mainly on two aspects: First, possible effects due to a property of ion beams – the ion coherence length – was investigated which is presently not accounted for in any theoretical model. The new experiments give indications that decoherence of the projectile, indeed, might affect the cross sections and even explain earlier observed discrepancies between experimental data and theoretical predictions. Second, the influence of the target initial state was studied. In earlier experiments the interest focused mainly on the ionization of helium, because it was the only atom that could be prepared at sufficiently low temperatures as target for kinematically complete experiments. This experimental obstacle has been overcome by the development of the MOTReMi which is a combination of a magneto-optical trap (MOT) and a momentum imaging spectrometer (reaction microscope, ReMi).

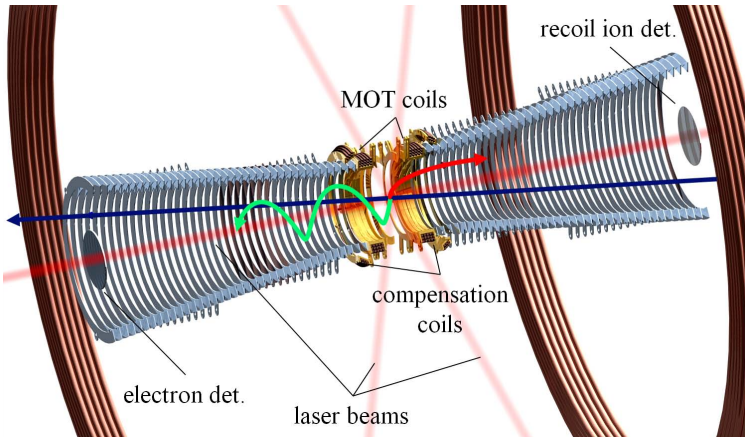

Fig. 1: Schematic view of the MOTREMI.

Projectile coherence effects: In all available fully quantum-mechanical descriptions of charged particle scattering the projectiles are considered being a wave of infinite (or very large) coherence length. In general, the coherence length is defined to be the maximum distance between two points in space for which the relative phase of the impinging wave does not fluctuate more than π during the collision time. The relation of coherence length Δx and momentum spread Δp is closely connected to the Heisenberg uncertainty principle, and it is (for a given point in space) $\Delta x \cdot \Delta p = h$. Using this equation it can be shown easily

that the assumption of a large (compared to the target size) projectile coherence length is generally valid for the impact of electrons. However, due to their much higher mass, the coherence length of ions is substantially smaller and in many cases only reaching a fraction of the size of an atom. Recently, the finite coherence length was proposed to resolve long-standing and puzzling discrepancies between experimental results and theoretical descriptions [1,2] observed in an earlier experiment on single ionization of helium by 100 MeV/amu C^{6+} ion impact. There, a substantial emission of electrons in an angular range has been observed, where the intensity should strongly be suppressed due to dipole selection rules.

This interpretation has been tested in two experiments: In the first one, a coherent beam ($\Delta x \approx 4$ a. u.) of 3 MeV protons has been prepared in the TSR exploiting electron cooling and was used to ionize the He target [1]. Due to the very similar charge to velocity ratio, this projectile is directly comparable to the C^{6+}-beam in the earlier experiment, and the theoretical cross sections are almost identical for these two collision systems. However, strong differences have been observed between the two data sets and the new data with the coherent beam are in much better accord with the theoretical results. In a second experiment [2], two different reaction channels, the single ionization and the transfer ionization, where one electron of the target is promoted to the continuum and the other one is captured by the projectile, were investigated simultaneously. The impact parameters contributing to single ionization are about an order of magnitude larger than those for the transfer ionization. As the projectile properties are identical in both experiments, possible decoherence effects are expected to be much stronger for the single ionization. Indeed, also here the data suggest that such effects exist and that they are weaker for the transfer ionization channel.

Though to date there is no fully quantum-mechanical calculation available that accounts for the limited projectile coherence length, the present experimental observations strongly suggest that the projectile coherence properties have an influence on the collision dynamics. If this interpretation proves to be true the cross sections are not independent of the beam "quality" which could have far-reaching implications potentially on many ion-atom collision studies.

Initial state dependence in ion-atom collision dynamics: Most of the earlier kinematically complete experiments studying the dynamics of ion-atom collisions were focused on the ionization of helium. This concentration on the helium target was mainly motivated by two reasons: First, helium has a relatively simple structure facilitating the theoretical modeling. Second, it is the only atomic target that can be prepared with the required very low temperatures (<1 K) by supersonic expansion in gasjets in order to allow for the extraction of fully differential cross sections. The experimental obstacles of preparing other targets only have been overcome by the development of the MOTReMi [3].

The MOTReMi is a novel and world-wide unique experimental apparatus which has been developed and used [4] at the MPIK. It is a combination of a laser-cooled and magneto-optically trapped (MOT) target with a Reaction Microscope (ReMi). All earlier attempts to realize this combination failed due to the incompatibility of magnetic fields required for the MOT and the Reaction Microscope. The temperatures achievable by laser cooling are at least two orders of magnitude lower than the temperatures in gasjets which results in a drastically improved momentum resolution. Moreover, lithium becomes available as target for multiple differential collision experiments. Lithium is particularly appealing, because it is the simplest atom with an optically active electron. Therefore, the initial target state can easily be prepared with lasers allowing for excited and polarized target atoms. This provides unique possibilities to study the dependence of the dynamics on the initial target state or target orientation effects.

In a first study, we investigated fully differential cross sections (FDCS) of 2s, 2p, and 1s ionization of lithium by 1.5 MeV/amu O^{8+} ($\eta = 1.03$) impact [4]. Here, distinct features were observed that were traced back to the characteristics of the initial state wave functions. In the case of 2s ionization, a three-peak structure occurs in the electron emission pattern that does not appear for the 2p ionization nor for He ground state ionization. This feature is the signature of the nodal structure of the initial state 2s wave function. For the 2p ionization an asymmetry of the FDCS with respect to the scattering plane (i.e. the plane spanned by the incoming and outgoing projectile momentum vectors) was found. This fundamental symmetry breaking cannot occur for isotropic initial states. However, in the experiment the target is polarized and the resulting symmetry breaking – in the literature referred to as 'magnetic dichroism' – has been observed for ion collisions for the first time.

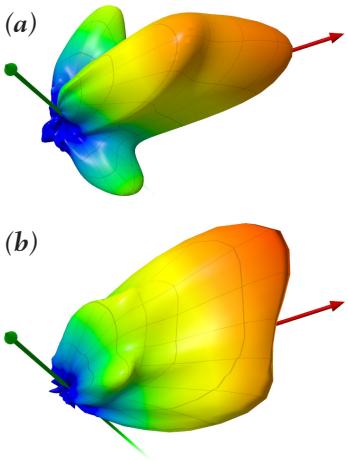

Fig. 2: Three-dimensional, fully differential angular distributions of electrons ejected from the (a) 2s and (b) 2p state of Li by 24MeV O^{8+} impact. The electron energy is fixed at 1.5 eV and q at 1.0 a.u. for the 2s state and at 0.3 a.u. for the 2p state. The green and red arrows denote the projectile beam and momentum transfer directions, respectively.

Daniel Fischer

Electron Collision Dynamics for Atoms, Molecules and Clusters

Electron collisions are relevant in natural environments as in the upper atmosphere and interstellar space but also in technical plasmas and, e.g., in radiation biology. Here, a large part of damage to living cells is caused by slow secondary electrons produced along the track of the energetic primary particle. In addition, the study of slow electron collisions enables detailed insight into the correlated dynamics of fundamental few-body quantum systems. An illustrative example is the knock-out of one electron in molecular hydrogen H_2 consisting of just two protons bound together by two electrons. In literature, it is a hotly debated topic if for electron impact single ionization the spatial alignment of the molecular axis is relevant and if the reaction involves electron-nucleus scattering. Respective experiments in which the molecular alignment is determined were unfeasible with conventional techniques.

At MPIK, a reaction microscope was developed in the recent years to address this reaction and to perform a number of more unprecedented experiments on atomic, molecular and cluster targets: a pulsed electron beam with an energy down to 10 eV is guided and focused by means of electric and magnetic fields into a gas jet target. The same fields collect all charged fragments, ions and electrons produced in a collision and guide them onto two large area detectors. As result fully differential cross sections for single (so-called (e,2e) experiments) and multiple ionization covering the full solid angle are recorded. In addition molecular ionic fragments give information on the fragmentation channel, the kinetic energy release and the molecular alignment.

For ionization of H_2 the cross section pattern was observed to be strongly dependent on the molecular alignment in case of large projectile scattering angle where the projectile penetrates deep into the electronic cloud [5]. Then the ejected electron is preferentially emitted along the molecular axis in particular for low ejection energies (Fig. 3). For this collision system the time-dependent close coupling (TDCC) theory achieves a rather good agreement with our experimental data. This model is one of several recently developed theories describing the projectile-target interaction non-perturbatively - a mandatory approach at low collision energies. While initially only the simplest systems like atomic hydrogen or helium could be handled now more complex systems come into reach. We have performed a benchmark test of the BSR model, a theoretical approach developed at Drake University (Des Moines, USA). 3-dimensional cross sections for 3p-ionisation of the atomic neon target were recorded covering a large range of kinematics at 100 eV impact energy [6]. The BSR results show an unprecedented degree of agreement not only in shape but also in relative magnitude of the fully differential cross section (Fig. 4). More critical is the handling of even larger atoms as argon where larger discrepancies persist.

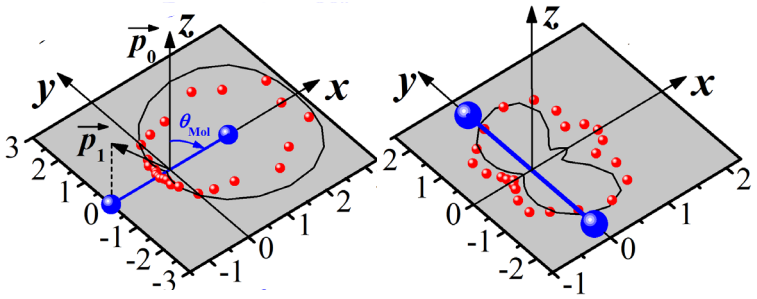

Fig. 3: Ionisation cross section for 54 eV electron impact on H_2. The projectile is coming in from below (p_0) and is scattered to the left (p_1). Two H_2 alignment angles are shown as indicated by the blue dumbbells. Red dots: exp. cross section. Solid line: TDCC theory.

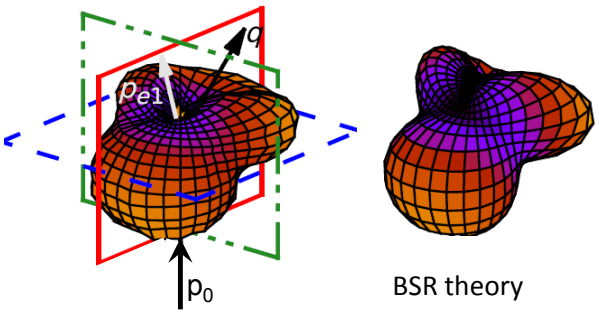

Fig. 4: Fully differential ionization cross section of the neon 2p-orbital at 100 eV impact energy. The projectile is coming in from below (p_0) and is scattered to the left (p_{el}). The emission pattern of an electron with 8 eV energy is displayed as 3d-surface. Left: experiment. Right: BSR theory.

Interesting new collision phenomena are to be expected for targets where several noble gas atoms are joined to form small clusters. Using a cold supersonic jet target of argon containing a fraction of clusters we have performed the first (e,2e) experiments on noble gas clusters [7]. The detection of the recoil ion in addition to the two outgoing electrons in a triple-coincidence allowed distinguishing collisions involving atoms, dimers and small clusters. For ionization of dimers a modified electron emission pattern was observed which could be attributed to elastic scattering on the partner atom. For clusters multiple-collisions could be identified where the projectile ionizes one constituent and excites a second one. As result the electrons' angular emission pattern is completely modified compared to the atomic or dimer case. This is illustrated in Fig. 5 where fully differential ionization cross sections are shown for 100 eV electron impact on small argon clusters. As indicated the projectile p_0 is coming in from below and scattered to the left. For ionization of a 3p-electron atoms (bottom) and clusters (centre) exhibit electron emission patterns which are peaked roughly along the momentum transfer direction q (the binary peak) and also in the opposite direction

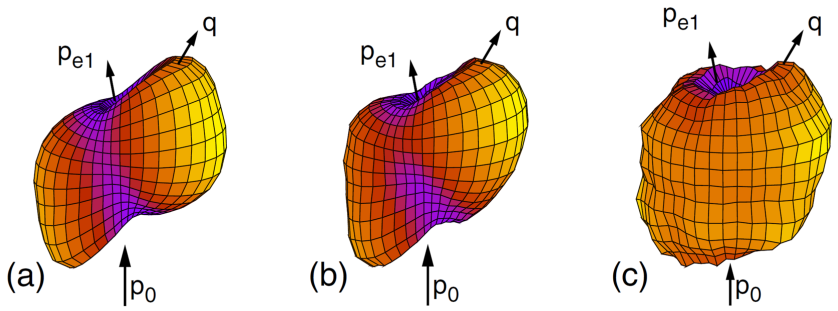

Fig. 5: 3-dimensional electron emission patterns for 100 eV electron impact ionization [7] of Ar atoms (a), of Ar-clusters (b, mean number of atoms: 25) and clusters involving additional excitation of another cluster atom (c). p_0: incoming projectile momentum. q: momentum transferred in the collision.

(the recoil peak). Both emission patterns show subtle differences, e. g. in the shapes of the binary peaks. A completely different pattern is seen in the top diagram for collisions where in addition to 3p-ionization a 3p→4s transition of another cluster atom is excited. Due to this double scattering reaction the relation of the ionized electrons' emission pattern and the total momentum transfer direction q is essentially lost. So far for these rather complex collision systems no theories are available.

Electron collisions with molecules of biological relevance are subject of a collaboration of our group with the department 6.6 *Fundamentals of Dosimetry* at the Physikalisch-Technische Bundesanstalt (PTB) in Braunschweig. Goals are the establishment of a new method to study the fragmentation of biomolecules after electron impact ionization using reaction microscopes. The plan is to record differential ionization and dissociation cross sections and to obtain insight in the reactions giving rise, e. g. to DNA strand breaks and successive cell death by the action of slow secondary electrons. Pilot studies demonstrating the capabilities of the reaction microscope have been done for the rather simple CH_4 molecule [8]. Here we could show that the molecular fragment species and their kinetic energies correlate with the ionization of particular molecular orbitals. In future, these studies will be extended to biologically relevant molecules as the DNA building blocks. Furthermore a new dedicated reaction microscope is build up with improved energy resolution resulting from a fast photoemission electron gun and an optimized field configuration for the charged particle extraction.

Alexander Dorn

Direct Imaging of Chiral Molecules

Some of the most fundamental problems in molecular physics defy the established spectroscopic techniques and have to be tackled with a more direct approach, preferably on a single-molecule basis. We have used the powerful foil-induced Coulomb explosion imaging (CEI) technique to record the first direct snapshots of chiral molecules in the gas phase.

In chemistry and biology, chirality refers to molecules that exist in two different spatial configurations which are incongruent mirror images of one another. Chirality is a fundamental property of nature, and the interactions of chiral molecules are an active field of stereochemical and pharmaceutical research. The determination of the microscopic atomic structure of chiral molecules, referred to as their absolute configuration, has proven to be a formidable challenge. Although in recent years anomalous X-ray diffraction (XRD) and Raman optical activity (ROA) have become established techniques to determine absolute configurations, both methods rely on theoretical input and cannot be applied to small gas phase molecules. To address this challenge, we have performed direct imaging experiments with small epoxide molecules in the gas phase. In a collaboration with organic chemists from Heidelberg University, the sense of chirality of a derivative of tartaric acid was transferred to oxirane (C_2OH_4) molecules by double-deuteration, yielding chiral $C_2OH_2D_2$. For the CEI experiments at MPIK we ionized these molecules in a discharge source, accelerated them to 2 MeV, and directed them at an ultra-thin diamond foil (Fig. 1). Upon impact on the foil the binding electrons are stripped off within less than a femtosecond, during which the nuclei can be considered frozen. Behind the foil the mutual Coulomb energy of the

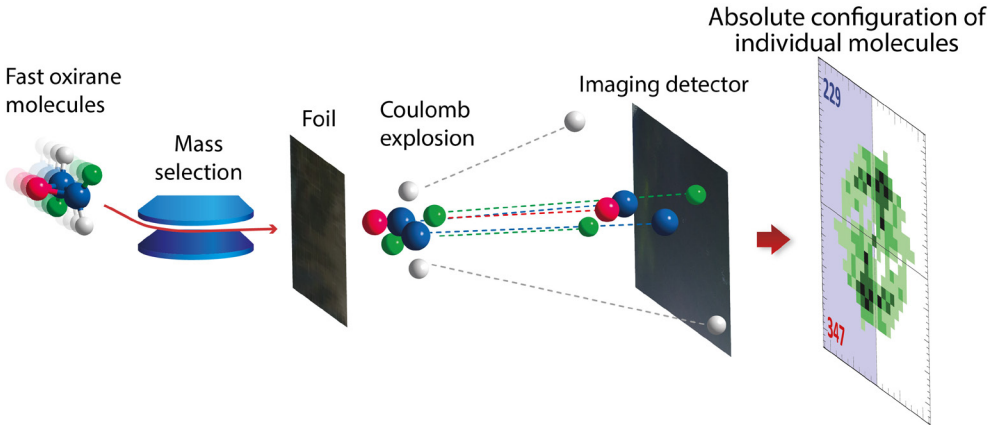

Fig. 6. Sketch of the Coulomb Explosion Imaging experiment with chiral dideuterooxirane molecules. Fast molecular ions are directed at an ultrathin diamond foil where they lose all of their binding electrons within less than a femtosecond. The remaining positively charged atoms repel each other, and after a flight distance of a few meters an enlarged image of the molecular configuration (under conservation of the original handedness) is recorded by a time-and-position-sensitive detector system, counting D^+, O^{2+} and two C^{2+} ions.

positive fragments is rapidly converted to kinetic energy. After a flight distance of ≈3 m, the atoms have gained distances of a few centimeters which are recorded by a time-and-position sensitive detector. Since the purely repulsive Coulomb force preserves the handedness, the relative detector positions identify the sense of chirality of the molecules prior to the Coulomb explosion process [9].

In contrast to established spectroscopic and crystallographic methods, our technique can potentially be applied to very small samples of chiral molecular ions (as demonstrated here), as well as neutral and radical species. Combined with mass spectrometry and ion storage techniques, this paves the path for promising concepts of chiral sequencing of reaction products and molecular fragments. Furthermore, our approach has the added intellectual merit of providing the first direct visualization of chirality on a molecular level.

The Most Fundamental Negative Molecular Ions: Metastable H_2^- and D_2^-

We have also used the CEI technique to investigate an altogether different mystery in molecular physics, namely the structure of the elusive negative hydrogen molecules H_2^- and D_2^-. Since the early 1950s, the fact that H_2^- is not a stable molecule has been established theoretically. Calculated lifetimes with respect to autoionization were shorter than 10^{-16} s. Nevertheless, observations of molecular hydrogen anions have repeatedly appeared in the literature. The theoretical explanation for these long-lived ions predicts a stabilization mechanism through a rotational barrier that keeps the ions from reaching the autoionization zone at short internuclear distances. Consequently, metastable H_2^- ions are supposed to be heavily rotating ($J = 26-27$) and very large ($R = 6$ a.u.). To verify the calculations, we have performed CEI measurements with metastable H_2^- [10] and D_2^- ions [11]. The H_2^- ions were produced in a sputter ion source (using a TiH target), accelerated and guided into the CEI beamline. As only very small amounts of H_2^- are formed in this process, the vast majority of the beam consisted of D^- ions owing to natural deuterium contamination. Behind the CEI foil, a magnetic separation field discriminated the D^+ particles and directed only the H^+, stemming from the Coulomb explosion of H_2^-, onto a 3D imaging detector. The observed internuclear distance distribution reflects the square of the initial molecular wave function. Our results confirmed the calculated wave functions as well as the high angular momentum of $J = 25 \pm 2$ for metastable H_2^- [15]. Our experiments also set an independent limit for the lifetime of these longlived states of 5±2 µs, in fair

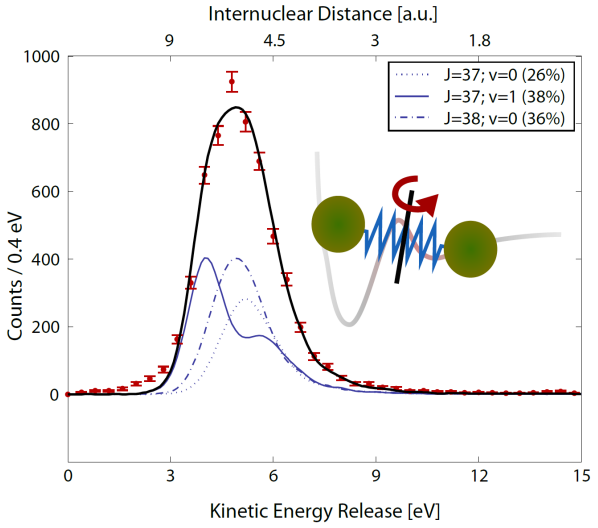

Fig. 7: Kinetic energy release distribution measured by Coulomb Explosion Imaging of metastable D_2^- ions. The dots with error bars denote the experimental results. The blue solid, dotted and dash-dotted lines show three individual metastable states and the solid black line shows the best fit (details given in the inset). For reference, a rough conversion to internuclear distances in atomic units is given at the upper abscissa.

agreement with calculations. Hence theory and experiment were found to be in accord for essentially all properties of this most fundamental molecular ion. However, a discrepancy appeared to remain for the deuterated D_2^- ion, where significantly lower angular momenta than predicted by theory had been inferred from photofragmentation studies at Aarhus University. To resolve this puzzle, we carried out CEI measurements with metastable D_2^- [11]. The measured kinetic energy release distribution is shown in Fig. 7. Similar to the H_2^- case, the results were found to be in good agreement with calculated wave functions for the predicted metastable states, which in the case of D_2^- possess angular momenta of $J = 37$–38. A rough conversion to internuclear distance (neglecting charge exchange and scattering effects inside the stripping foil) is also given in the plot, for illustrative purposes. It shows that the equilibrium distance for D_2^- is about 4 times larger than for neutral D_2 (≈ 1.4 a.u.). Furthermore, our analysis revealed that the discrepancy with the previous photofragmentation studies can be settled when all possible dissociation channels are considered [11]. In summary, together with the theoretical progress, it is clear that after decades of speculation, a good understanding of the most fundamental molecular anions H_2^- and D_2^- has been reached.

Holger Kreckel, Dirk Schwalm, Andreas Wolf

Vibrational Autodetachment of the Sulfur Hexafluoride Anion

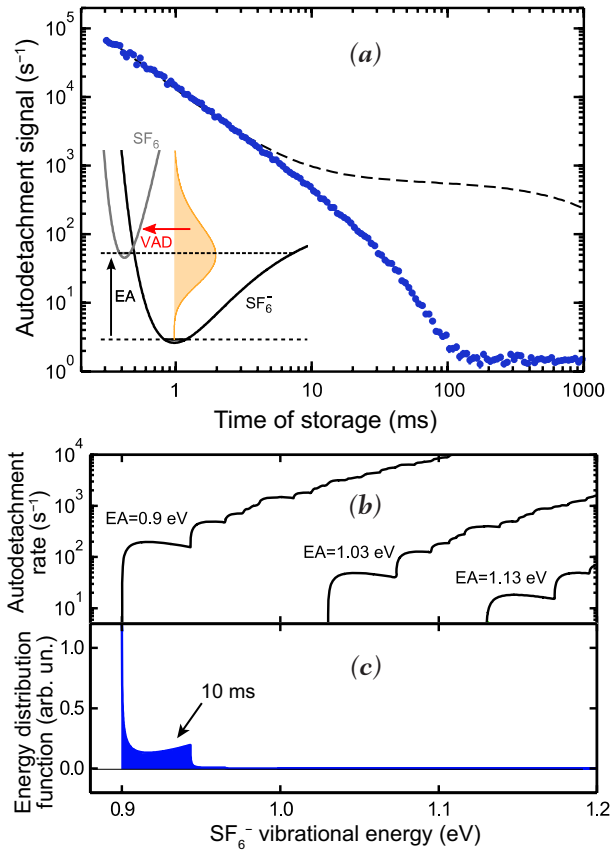

Fig. 8: Vibrational autodetachment (VAD) of SF_6^- at the CTF. (a) Signal as a function of storage time (blue dots) and typical previous results (dashed). The inset illustrates the relevant potential curves and the VAD process. (b) Simulated autodetachment rate as function of SF_6^- internal excitation for different SF_6 electron affinities EA; the irregular increase indicates the opening of new SF_6 final vibrational states. (c) Simulated SF_6^- internal energy distribution at energies > EA after 10 ms storage time and for EA = 0.9 eV.

At high vibrational excitation, the negative ions of molecules and clusters can spontaneously "evaporate" the bound excess electron by the transfer of vibrational to electronic energy. Since vibrational-electronic coupling is weak, these vibrational autodetachment rates can become very small, leading to emission delays up to a fraction of a second. To measure the small rates at the long-lifetime limit, the anions must be stored in an essentially perturbation free environment. This has become possible in the cryogenic trap for fast ion beams (CTF) built at MPIK as a prototype of the cryogenic storage ring CSR. Beams of sulfur hexafluoride anions (SF_6^-) at ≈ 6 keV, becoming highly excited by their production in the ion source, were stored in the extremely good cryogenic vacuum of the CTF, at temperatures below 15 K. The fast neutral SF_6 molecules produced by vibrational autodetachment (VAD) from the stored beam could be observed up to the storage times when this process became very slow (Fig. 8). In this long time limit, the only excited SF_6^- molecules still left in the stored beam have internal energies that only barely exceed the SF_6 electron affinity (EA); hence, the neutral SF_6 can be produced only in its vibrational ground-state, in contrast to the many highly excited SF_6 states that are produced at earlier times. The vibrational autodetachment rates then sensitively probe the vibrational level density of SF_6^- in a small, well defined excitation energy window. The high-statistics data of the CTF experiment were found to support a recently predicted, quasi-Jahn-Teller distorted geometry of the SF_6^- anion and to exclude the more symmetric geometries predicted for it previously. Moreover, the SF_6^- vibrational level density represented by the measured small decay rates could be used to infer a value for the electron affinity of SF_6, EA = (0.91±0.07) eV. Under the low-background conditions in the CTF the anions could be stored for average times up to more than 10 min before being neutralized in unwanted collisions with residual gas molecules in the trap. The small delayed vibrational autodetachment rates becoming measurable under these conditions offer a new tool to extract essential molecular properties difficult to determine by other methods.

Michael Lange, Sebastian George, Dirk Schwalm, Andreas Wolf

Transfer-ionization in Collisions with a Fast Highly Charged Ion

In a collision between a bare ion and an atom with two or more electrons one of them can be captured by the ion whereas another one be emitted. Such a process is called transfer ionization. It involves two active electrons and is very difficult to describe *ab initio*. Therefore, it is often analyzed in terms of different reaction mechanisms characterized by distinct features in the electron emission pattern. Depending on whether the electron-electron interaction plays in them a crucial role, these mechanisms can be termed "correlated" or "uncorrelated".

Two (dynamical) correlated mechanisms – the electron-electron Thomas (EET) and electron-electron Auger (EEA) – were proposed for describing transfer ionization in collisions between a light atom and a low charged ion which moves with a velocity v much higher than the typical velocities of the electron(s) in their initial and final bound states: $v \gg Z_a e^2/\hbar$ and $v \gg Z_i e^2/\hbar$, where $Z_a e$ and $Z_i e$ are the charges of the nuclei of the atom and ion, respectively. Recently transfer ionization was considered [12] for fast collisions between a light atom and a highly charged ion when the charge $Z_i e$ of the ion is so large that $Z_i \sim \hbar v/e^2$. It was shown there that, compared to transfer ionization in collisions with low charged ions, new and interesting features can arise in this process when the ion has a high charge.

Fig. 1 shows the momentum spectrum of electrons emitted in transfer ionization in collisions of 22.5 MeV/u Ca^{20+} ($v = 30$ a.u.) with helium atoms when capture occurs into the K and L shells. The spectrum is given in the laboratory frame (in which the target is at rest and the ion moves with a velocity $\mathbf{v}$) as a function of the longitudinal, k_{lg} and transverse, k_{tr}, parts of the momentum $\mathbf{k}$ of the emitted electron. The maximum at small momenta has its origin in the so called independent transfer ionization whereas the maxima at much larger momenta arise due to the correlated mechanisms. The outer ridge at large k arises due to the transfer ionization with electron capture into the ground state of the highly charged ion while the inner ridge originates from capture into the L-shell. Each of them has two distinct maxima. The maxima at $k_{tr} \approx 0$ appear due to the EEA mechanism. The other maxima, which were recently predicted in [12], appear due to the action of the field of the highly charged ion on both electrons and are, therefore, a signature of a new reaction mechanism qualitatively different from the EET which proceeds via the interaction between the incident ion and only one of the atomic electrons.

Thus, the strong field of the highly charged ion has a profound effect on the correlated transfer ionization. Compared to the weak-field regime realized in collisions with low charged ions the strong field weakens (in relative terms) the EEA and eliminates the EET. Instead, a new reaction mechanism appears whose intensity increases with the field strength [12].

Alexander B. Voitkiv

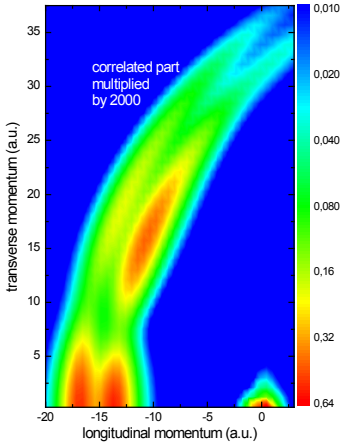

Fig. 9: Momentum spectrum (in $b/(a.u.)^3$) of electrons emitted in the reactions 22.5 MeV/u $Ca^{20+} + He(1s^2) \rightarrow \Sigma_{n=1}^{2}\, Ca^{19+}(n) + He^{2+} + e^-$ (v = 30 a.u.). The contribution of the correlated channels is multiplied by 2000.

References

[1] X. Wang, K. Schneider, A. LaForge, A. Kelkar, M. Grieser, R. Moshammer, J. Ullrich, M. Schulz, D. Fischer, J. Phys. B (FTC) 45 (2012) 211001.

[2] K. Schneider, M. Schulz, X. Wang, A. Kelkar, M. Grieser, C. Krantz, J. Ullrich, R. Moshammer, D. Fischer, Phys. Rev. Lett. 110 (2013) 113201.

[3] D. Fischer et al., Phys. Rev. Lett. 109 (2012) 113202.

[4] R. Hubele et al., Phys. Rev. Lett. 110 (2013) 133201.

[5] X. Ren, T. Pflüger, S. Xu, J. Colgan, M. S. Pindzola, A. Senftleben, J. Ullrich, and A. Dorn., Phys. Rev. Lett. 109 (2012) 123202.

[6] T. Pflüger, O. Zatsarinny, K. Bartschat, A. Senftleben, X. Ren, J. Ullrich and A. Dorn, Phys. Rev. Lett. 110 (2013) 153202.

[7] T. Pflüger, A. Senftleben, X. Ren, A. Dorn, and J. Ullrich, Phys. Rev. Lett. 107 (2011) 223201.

[8] S. Xu , X. Ma, X. Ren, A. Senftleben, Th. Pflüger, Sh. Yan, P. Zhang, J. Yang, J. Ullrich, and A. Dorn, J. Chem. Phys. 138 (2013) 134307.

[9] P. Herwig et al., Science 342 (2013) 1084.

[10] B. Jordon-Thaden et al., Phys. Rev. Lett. 107 (2011) 193003.

[11] P. Herwig, D. Schwalm, M. Cizek, R. Golser, M. Grieser, O. Heber, R. Repnow, A. Wolf and H. Kreckel, Phys. Rev. A 87 (2013) 062513.

[12] A. B. Voitkiv, Phys. Rev. Lett. 111 (2013) 04320.

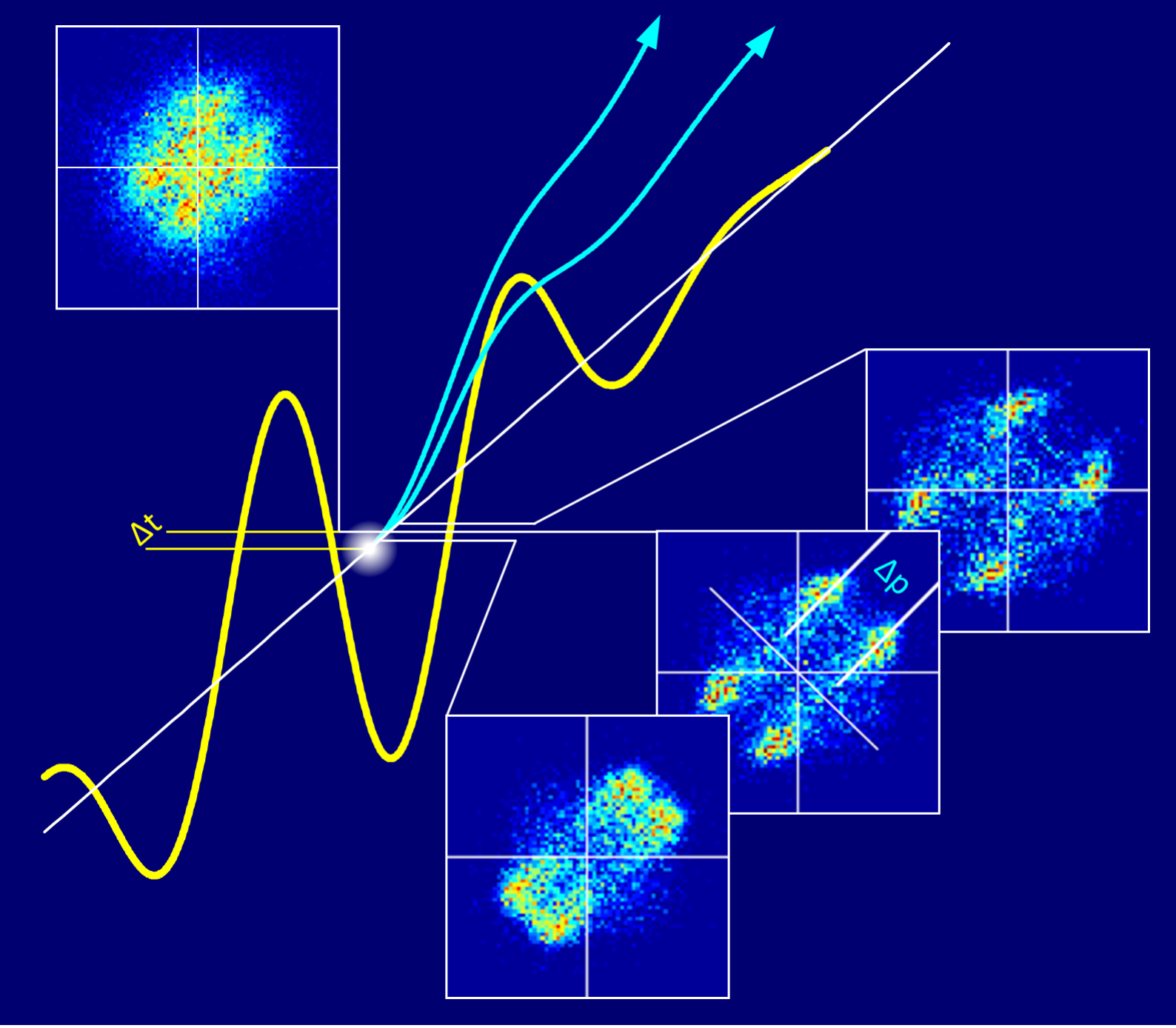

2.6 Time-Resolved Phenomena

Strong-field emission of two electrons from a doubly excited atomic state in Ar. The ionization time difference Δt translates into a (longitudinal) momentum difference Δp in the correlated two-electron spectra (attosecond streaking): experiment (top left) and model calculations for a Δt of 100 as (bottom), 200 as (middle) and 300 as (right).

Introduction

How does a quantum system evolve in time, and can we visualize or even control the underlying correlated quantum dynamics on its natural length- and time-scale? These and similar questions are in the very focus of modern atomic, molecular and optical physics, and they inevitably move into the field of view of other research areas as well, ranging from solid-state physics over materials science to quantum chemistry and molecular biology.

At MPIK, we explore the quantum dynamics experimentally at its most fundamental level, considering systems with a very limited number of interacting particles in atoms and molecules, or small conglomerations of those like finite-size clusters. The corresponding time scales are ten to hundreds of femtoseconds (10^{-15} s) for the motion of nuclei in molecules or in chemical reactions while attoseconds (10^{-18} s) are characteristic for the action of electrons bound in atoms or during the formation or cleavage of a molecular bond. Only recently, due to the revolutionary advances in IR laser-technology and in the generation of intense XUV and X-ray radiation, this whole time-range down to several attoseconds became accessible in experiments with ultra-short laser pulses.

In our laboratories, laser-generated attosecond XUV as well as sub-10 fs IR pulses with intensities of more than 10^{16} W/cm^2 are routinely available. In combination with many-particle imaging spectrometers, high-resolution spectral analyzers, pump-probe techniques as well as carrier-envelope-offset (CEO) phase control methods they open new avenues for the visualization and control of ultra-fast quantum dynamics.

Exploiting intense femtosecond XUV or even X-ray pulses provided by the most advanced 4th generation light sources, the free-electron lasers (FEL), we extend these studies towards most fundamental two- and few-photon processes in atoms as well as time-resolved observations of fragmentation, rearrangement and isomerization reactions in molecules. A small selection of recent results will be highlighted here.

Electron Wave-Packet Interference in Strong-Field Driven Neon

When atoms and molecules are exposed to strong laser fields, ionization occurs. Rather than just losing an electron at one instant in time, the quantum-mechanical wave function of one electron is emitted coherently over a range of times. Each maximum of the absolute electric field strength of the laser wave, the electron emission probability peaks. Interference of the resulting coherent bursts of electrons gives rise to discrete equidistant peaks in the observed spectrum of electrons, or the recombination light they produce.

The time-domain picture of these processes has been found of paramount importance for attosecond-pulse generation, as the bursts of electrons, recolliding with their parent ions, result in sub-femtosecond emission spikes of vacuum-ultraviolet (VUV) or extreme-ultraviolet (XUV) light that is used in time-resolved spectroscopy. The exact generation dynamics of these light pulses, especially in few-cycle driving fields is, however, still a subject of intense research.

We successfully addressed this long-standing question by a unique time-domain strong-field spectroscopy concept which involves the carrier–envelope phase (CEP), i. e. the phase of the carrier wave at the peak of a laser pulse. The second technological key is the use

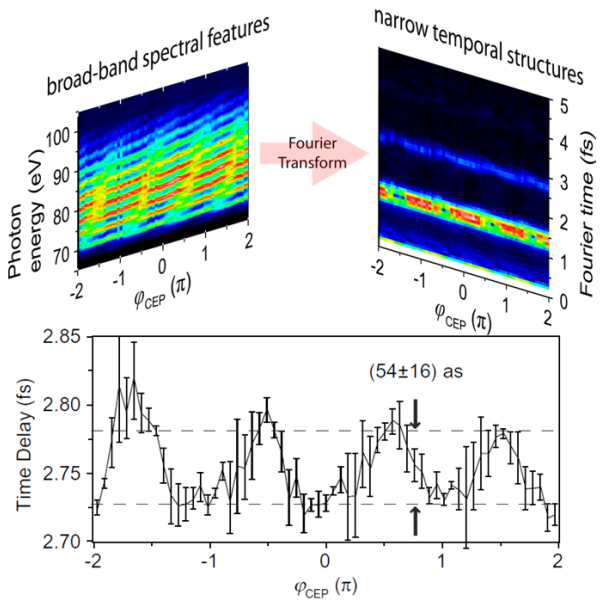

Fig. 1: Top: Fourier transformation of CEP-resolved HHG spectra that map spectral interference information into the time domain, where localized temporal structures rather than broad-band interference features can be extracted and analyzed. Bottom: Reconstruction of the group delay between two attosecond pulses as a function of the CEP.

of an interferometry concept termed spectral interferometry. The combination of CEP control and spectral interferometry (CEPSI) allows the measurement of temporal strong-field dynamics as a function of the CEP [1]. The temporal information is obtained by a Fourier transformation of the high-harmonic (HHG) spectrum.

The resulting CEPSI representation is thus a two-dimensional map of light intensity vs. time and CEP. It encodes the temporal interference of the coherently emitted electron bursts, which would have been buried if only a CEP-averaged, one-dimensional spectrum would have been acquired. We were not only able to measure and understand the CEP dependence of the attosecond-pulse phases in the few-cycle (non-adiabatic) HHG limit, but additionally to quantify the group-delay variations of two produced attosecond pulses as a function of the CEP with a precision of 16 attoseconds (see Fig. 1).

The methodology is fully general and expected to create a major impact for strong-field dynamics research. We have taken the first step to prove this by applying CEPSI to the coherent emission of laser-field-ionized electron wave packets emitted from nanoscale metal tips. Here, we were able to use the method as a sensitive test of theory used to explain the experimentally observed spectra. For example, it was found that the strong-field approximation breaks down at surfaces, pointing to the importance of fundamental effects such as surface polarization during strong-field photoemission.

Christian Ott, Thomas Pfeifer

Probing and Controlling Wave-Packet Dynamics of Two Excited Electrons in Helium Atoms

A key vision in ultrafast science is the measurement and control of the motion of correlated electrons in atoms and molecules. The prototype system for correlated electrons – at its most fundamental level – is the helium atom with its two electrons. While past research has focused on the static spectroscopy of electronic double-excitation to infer information on electronic correlation, we took on the challenge to explore the time-resolved quantum motion in doubly-excited states.

The measurement was enabled by utilizing broadband attosecond-pulsed XUV and femtosecond near-visible (VIS) laser pulses to outrun the autoionization lifetimes ranging between 10 and 100s of femtoseconds for some of the low-lying doubly-excited states. The experimental key was to obtain temporal resolution on the order of tens of attoseconds in combination with high spectral resolution (20 meV) in the XUV (near 60 eV) to access the characteristic spectral (Fano) line shapes.

The application of multidimensional time-resolved XUV/near-visible spectroscopy – based on VIS-perturbed XUV transmission through a gaseous helium sample – enabled the measurement of a correlated two-electron wave packet as a function of time (Fig. 2). The shape of this wave packet could be reconstructed in a theory cooperation with Javier Madroñero who provided the static He eigenstates. This reconstructed wave packet was compared to an *ab-initio* quantum-dynamics simulation of Luca Argenti and Fernando Martín. The good agreement at weak probing laser fields tested our understanding of the two-electron dynamics in the weak-field regime and validated the experimental spectroscopy and wave-packet-reconstruction technique.

At stronger VIS field strength, the relative phase of the states constituting the wave packet could be controlled. Again a recons-

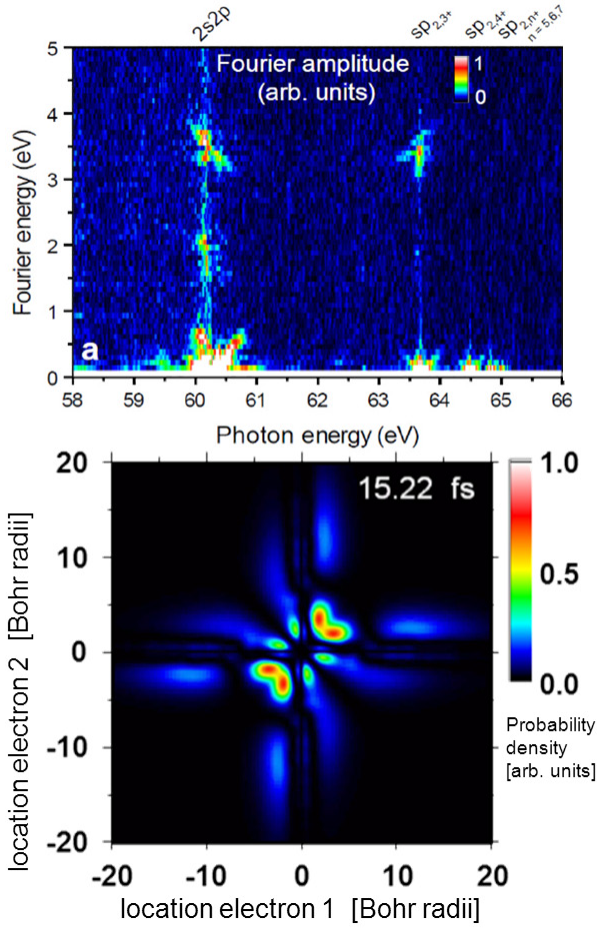

Fig. 2: Top: Two-dimensional spectrum of doubly-excited state dynamics measured in Helium. Bottom: Reconstructed shape of a correlated two-electron wave packet at a specific time after its creation by an XUV attosecond pulse.

truction of the shape of the wave packet at different times was carried out and demonstrated that laser fields are effective tools to direct two correlated electrons in space and time near a binding nucleus. In the future, this level of control will be necessary to fully control the course of chemical reactions with shaped laser fields, as molecular bonds are typically occupied by two or more electrons. Laser control methods as the one introduced here may allow the selective synthesis of molecular structures or states that would not be achievable by traditional thermodynamic means.

Christian Ott, Andreas Kaldun, Thomas Pfeifer

Electron Correlation in Double Ionization of Atoms

How are two electrons released from an atom when it is exposed to an ultra-short and very strong laser field? This question is subject of intense research since many years. In contrast to the trivial case of a sequential or step-wise electron removal, which is valid only at very high intensities, the so called non-sequential ionization at intermediate intensities is a highly correlated two-electron process. Here, one electron is set free by field- or tunnel-ionization and afterwards driven back and forth in the laser electric field. For linear polarization the electron may recollide with its parent ion thereby transferring sufficient energy to knock out another electron. Supported by numerous theoretical and experimental studies this scenario is considered as being the basic mechanism behind non-sequential double ionization. A prerequisite is a sufficiently high laser-intensity such that the electron recollision energy is larger than the ionization threshold. What happens at lower intensities when the collision energy is too small for further ionization? Still, double ionization occurs, but what is the mechanism under these special conditions? This question, with a particular focus on the time-sequencing in non-sequential double ionization of atoms was studied experimentally with ultra-short laser pulses comprising only a few optical cycles. We could demonstrate that intermediate doubly excited states play an important role. These states get populated in a first stage of the interaction with the laser field via electron recollision and electron-electron interaction. In the second step the electrons are set free, one after the other, within a very short time interval of less than a femtosecond.

The measurements were carried out with Argon atoms in 6 fs laser pulses at a central wavelength around 800 nm and intensities slightly below 10^{14} W/cm^2 [2]. A quantum mechanical description of this problem is extremely challenging and until now it is out of reach even if only the two active electrons and the ionic core are taken into account. Surprisingly, however, semi-classical models have been demonstrated to be very successful in the description of non-sequential double ionization. There, tunnelling is treated quantum mechanically whereas the motion of all three particles (the two electrons and the ion) as well as electron recollision is mimicked by solving the classical equations of motion. The process of double ionization is illustrated in Fig. 3 for the specific case of low intensity. Shown are the two electrons inside the ionic potential well in the presence of the laser field, which can be represented by an oscillating inclined plane. The temporal evolution of the electric field (Fig. 3, upper right) is indicated by yellow lines, respectively.

In the first step (Fig. 3a) an electron tunnels through the potential well and is accelerated by the laser field before it is driven back to its parent ion causing a recollision. At the given intensity the collision energy is too low to lift another electron out of the atomic potential. Instead, the recolliding electron may relax into an excited state thereby transferring its energy to another one which gets also promoted into an excited state (Fig. 3b). Though the doubly excited states created by this dielectronic recombination are only weakly bound, the release of both electrons into the continuum is more difficult than expected because of the mutual Coulomb interaction. Very often one electron falls back into a deeply bound state while the second one is ejected in an auto-ionization event. This would lead to single ionization. The situation is somewhat different here because the external laser field supports the escape of both electrons by suppression of the potential barrier such that they can freely propagate out of the atom (Fig. 3c). We like to note that on the basis of semi-classical model calculations the creation of highly excited two-electron states was proposed already some time ago (see [2]), but it took until now to unambiguously verify this mechanism by experiment.

A reaction microscope was used to determine the momenta of both emitted electrons. The electron momentum difference allows us to estimate the time delay between the

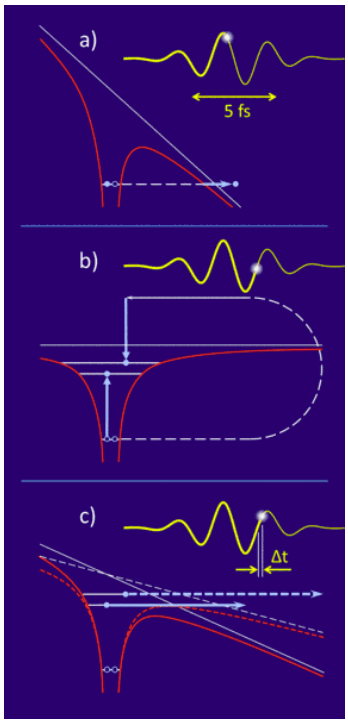

Fig. 3: Non-sequential double ionization of argon in a strong laser field. (a) Tunneling of the first electron. (b) Recollision and production of a bound doubly-excited state. (c) Decay of the highly excited intermediate state by above-the-barrier field-ionization.

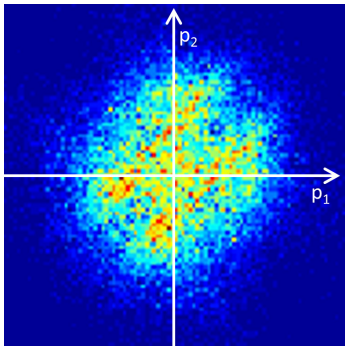

Fig. 4: Experimental two-electron momentum distribution for non-sequential double ionization of argon atoms.

emission of the first and second electron out of the doubly excites states. In order to achieve this we rely on the fact that the velocity of each electron, after acceleration in the laser field, depends on the actual field strength at the moment of ionization. This works best for very short laser pulses, a condition that is well fulfilled here with a pulse-duration of 6 fs, where the ionization process is confined to within one optical cycle. The measured momenta of both electrons can be presented in a diagram where the distance from the diagonal reflects their momentum difference (Fig. 4). This in turn can be used to determine the time difference: the larger the distance of an event from the diagonal the larger is the time delay between the release of electron one and two out of the doubly excited state.

The comparison with semi-classical model calculations (as shown in the title figure), which are expected to be adequate in particular for the description of highly excited states, yields best agreement with the experiment for an ionization time difference of about 200 attoseconds [2].

Nicolas Camus, Thomas Pfeifer, Robert Moshammer

Directed Proton Emission in Molecular Photoionization

Molecular hydrogen (H_2) is the most simple molecule in which electron correlation is of high importance. This is reflected by the occurrence of double-excited electronic states above the single-electron binding energy. These states may decay by emission of an electron leaving the molecular ion either in a bound or dissociating state. In contrast to the decay of doubly-excited sates in He, where auto-ionization gives rise to characteristic Fano-type resonances in the photon absorption cross-section, an additional parameter has to be taken into account in the case of H_2, namely the internuclear distance. With an auto-ionization time being comparable to the dissociation time this parameter is of particular importance. Moreover, it is the highly correlated interplay of electronic and nuclear degrees of motion on a very short time scale that makes auto-ionization of H_2 a benchmark system for theory.

By means of a kinematically complete experiment we investigated the break-up of molecular hydrogen into a proton and a neutral H-atom after photoionization with broadband attosecond-pulsed XUV radiation in the energy range between 25 and 35 eV [3]. Two possible pathways may lead to the same final state with three free particles: a continuum electron, a proton and a neutral H-atom (see Fig. 5). (i) The photoelectron can be emitted directly in the photoabsorption process leaving the H_2^+ system in an excited dissociating state with 'ungerade' symmetry. This means that the wave-function of the bound electron has opposite sign at the positions of either proton. (ii) The photon promotes the system into a doubly excited state that afterwards decays via auto-ionization (and emission of an electron) into the ground state of H_2^+. The ground state has 'gerade' symmetry, meaning that the spatial electronic wave-function has the same sign at both protons.

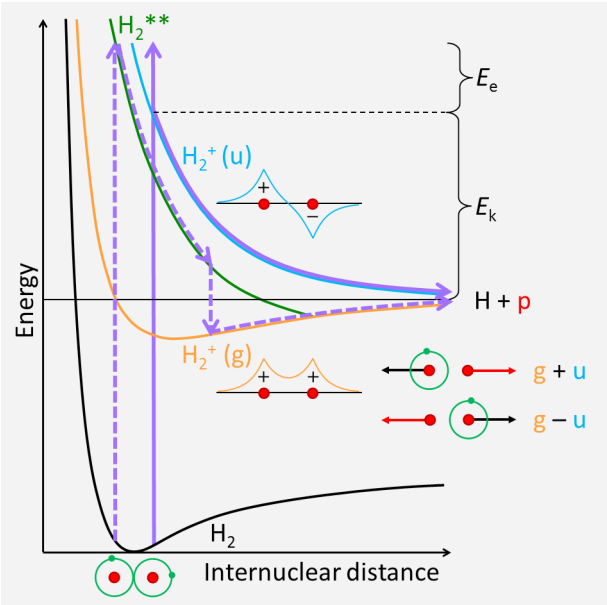

Fig. 5: The relevant molecular potential energy curves of H_2. Photoionization leads to dissociation into a neutral H-atom and a proton. Violet arrows – solid: direct ionization; dashed: auto-ionisation of doubly-excited H_2^{**}. The emission direction of the proton is encoded in the superposition of states with 'gerade' (g) und 'ungerade' (u) symmetry of H_2^+.

The two pathways are indistinguishable if both, the emitted electron and the dissociating fragments (proton and H-atom) exhibit identical energies. In this case the system as a whole needs to be treated as a superposition of the above mentioned 'gerade' (g) and 'ungerade' (u) states, reflecting direct ionization and auto-ionization, respectively (Fig. 5). Depending on how this superposition is formed the bound electron is localized either on one or the other nucleus – initially the electron oscillates back and forth between the two nuclei. The proton at which it stays bound eventually for infinitely large distances between the fragments depends on the molecular break-up dynamics. It leads to an asymmetry in the relative emission direction of the photo-electron and the proton.

All particles in the molecule are quantum mechanically entangled: after the absorption of the photon the system as a whole must obey 'ungerade' symmetry. Thus, if the H_2^+ is in the (u) state the emitted electron has 'gerade' symmetry, and vice versa. The localization of the bound electron determines the emission direction of the proton or, in other words, the bound electron "remembers" to some extend what the emitted electron is doing.

Depending on how the system evolves electron and proton are emitted preferentially either into the same direction, or opposite to each other (Fig. 6). The choice of the bound electron, and therewith the electron localization or the directional asymmetry, is strongly dependent on the kinetic energy of both the photoelectron and the proton. Thus, for a given energy sharing between them the asymmetry maximizes in one or the other way.

The observations can be explained within a semi-classical model which explicitly takes the superposition of the two quantum paths into account. It allows a rather comprehensive modelling of both, the fragmentation dynamics and the electron-proton asymmetry. A quantitative description of the measured asymmetry, however, requires a full ab-initio quantum calculation which was performed by the group of F. Martín. The comparison with experiment is shown in Fig. 6.

Andreas Fischer, Thomas Pfeifer, Robert Moshammer

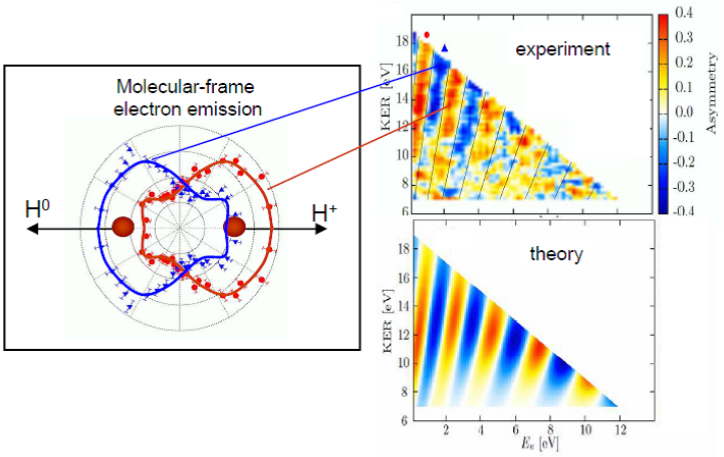

Fig. 6: Right: Asymmetry in the relative emission direction of electron and proton as a function of the kinetic energy of the electron (E_e) and the heavy particles (KER= 2 times the proton energy). Areas in red: preferred emission into the same direction; blue: preferentially opposite emission. Left: Electron angular distribution for fixed molecular orientation (as indicated), and given energy sharing.

'Noisy' Laser Pulses Enhance Temporal Resolution of Molecular Dynamics

It is commonly accepted understanding that short events are required for the measurement of dynamics on short time scales. For example: a short pump and probe laser pulse sets off and measures, respectively, the coherent dynamics of a molecular vibrational wave packet, but only as long as the pulse duration is shorter than the vibrational period. A major result of our recent research [4] was the finding that such short pulses are not really necessary for probing time-resolved coherent quantum dynamics. Instead, the key quantity for access to short time-scale dynamics is the temporal correlation function between a pump and a probe pulse, and sufficiently fast temporal variation (sufficient spectral bandwidth) within the pulse. The latter can be achieved by a short laser pulse, but it turns out to be sufficient to have a long, but temporally sub-structured pulse to achieve time resolution on the scale of the sub-structures. The measurement principle still operates for the case where the pulse shape statistically varies from shot to shot and when averaging over many such pulses occurs, as long as pump and probe pulse always are two identical replicas.

The physical picture we developed to explain this statistical probing mechanism entails important consequences for time-resolved sequential-excitation probing in general: The observed measurement signal can be decomposed into a matrix product of an autocorrelation matrix, specifying the nature of the pulse shapes (e.g. fully coherent or statistical) and a system matrix, determined by the system-specific response after its evolution for a given time. This formalism was successfully applied to the interpretation of a recent experiment carried out at the free-electron laser (FEL) FLASH. It allowed solving the puzzle why with (statistically varying) FEL pulses of ≈30 fs average duration it was still possible to experimentally observe the coherent wave-packet motion of ≈20 fs in D_2^+ molecular ions (Fig. 7).

Robert Moshammer, Thomas Pfeifer

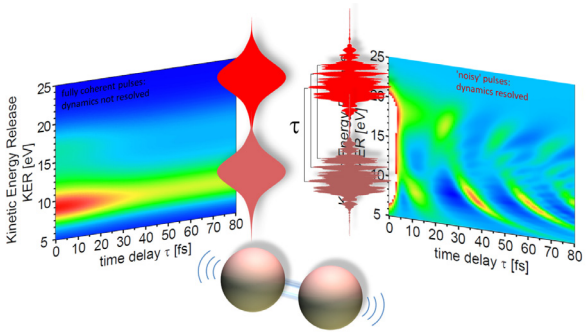

Fig. 7: Enhancement of temporal resolution in pump–probe measurements by using statistically varying, noisy pulse shapes with time-delay-τ correlated substructures instead of fully coherent pulses.

Radiationless Energy Transfer Between Atoms

Efficient energy transport within or between molecules plays a crucial role in many chemical and biochemical processes. The redistribution of energy that is deposited in a system at a certain point by absorption of a photon may lead to an internal movement and eventually to the breakage of a chemical bond at another point. In many cases, the energy is transferred

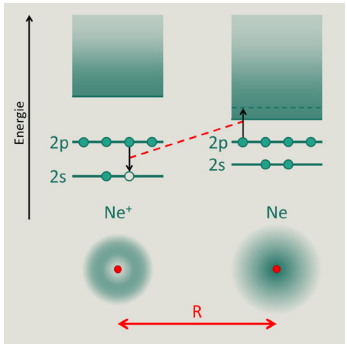

Fig. 8: Illustration of Interatomic Coulombic Decay (ICD) in a loosely bound Ne-dimer.

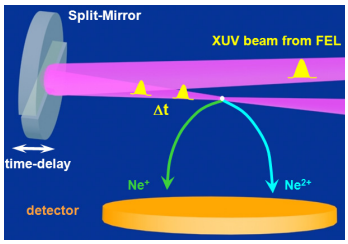

Fig. 9: Schematic drawing of the XUV pump-probe setup at FLASH. The incoming beam is split geometrically into two parts that are focused onto the same spot with adjustable time delay. The charged particles created in a gas-target are detected with a reaction microscope.

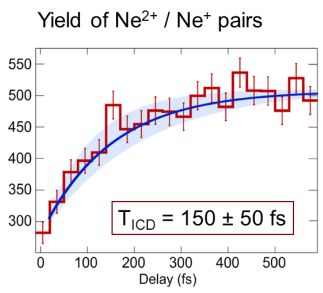

Fig. 10: Yield of coincident $Ne^+ + Ne^{2+}$ ions as a function of the time delay (red histogram). Blue line: exponential fit resulting in an ICD lifetime of (150±50) fs. The experimental uncertainty is indicated by the blue area.

by moving electrons or a rearrangement of charges, but very often the electric force between electrons alone is sufficient for an efficient energy transfer – even over long distances (on the atomic scale).

Interatomic or intermolecular Coulombic decay (ICD) is a prime example for such a process. It is an extremely efficient relaxation mechanism that comes into play whenever excited atoms (or molecules) are embedded in a weakly interacting environment. In particular, isolated excited ions that have relaxation times on the order of pico- or nanoseconds after the removal of an inner-valence electron can relax much faster via ICD by transferring their excess energy to a neighboring atom and thereby ionizing it. After its first theoretical prediction in 1997, ICD has by now been observed in several systems: in van-der-Waals bound rare-gas clusters of various sizes as well as hydrogen-bonded water clusters (see e. g. references in [5]). Hydrogen bonds are essential for holding large bio-molecules together giving them their characteristic shapes. Once ICD has occurred in such a system the ejected low energetic ICD electron can effectively interact with the environment itself, destroying chemical bonds for instance in DNA, which makes the ICD process also relevant for radiation therapy.

The ICD decay-time of Van-der-Waals bonded neon dimers (Ne_2) was measured at the free-electron laser (FEL) in Hamburg (FLASH) exploiting a XUV pump-probe scheme [5]. While an isolated excited Ne^{+*} ion with one of its 2s electrons removed needs almost 1 ns to decay into its ground state by emission of a photon we found that the relaxation is about 10 000 times faster when a second Ne atom is placed in the vicinity of the first one, as realized in neon-dimers (Ne_2) with an internuclear distance of about 6 atomic radii. Then, the excitation energy is transferred non-radiatively from the excited Ne^{+*} to its neutral neighbour, thereby ionizing it (Fig. 8). Different theoretical calculations predicted ICD in Ne^2 to occur on a time-scale between some ten to hundred femtoseconds, which is within the range of our experimental value.

In our experiment at FLASH we used a Reaction Microscope (REMI) equipped with an on-axis back-reflection split-mirror setup [5] for focusing and FEL pulse-pair creation as schematically depicted in Fig. 9. The REMI enables the coincident and momentum-resolved detection of ionic fragments that emerge from the dissociation or Coulomb-explosion of single molecules (or clusters) which are provided by means of a localized and intrinsically cold supersonic gas-jet. The split-mirror consists of a spherical multi-layer mirror (1 inch Mo/Si mirror, 50 cm focal length, 20 µm focus diameter) that is cut into two identical "half-mirrors". While one of them is mounted at a fixed position, the other one is movable along the FEL beam axis by means of a high precision piezo-stage. This results in an adjustable time delay between the two reflected parts of the incoming pulse. The incoming FEL beam (58.2 eV photon energy) with a pulse-duration of approximately 60 fs and an intensity of 10^{12} W/cm^2 is focused onto a beam of Ne-dimers. The REMI is used to unambiguously identify those fragment pairs that emerge from the same dimer.

The XUV pump-probe measurement is done in the following way. The first pulse initiates the process of ICD in Ne_2 by the removal of a 2s inner-shell electron from one of the two Ne atoms, as illustrated in Fig. 8. The time it takes for the excited Ne^{+*}-ion to relax by transferring its energy to the neighboring Ne atom, and thereby ionizing it, is referred to as ICD decay time. Hence, the system remains in the excited state until it decays into $Ne^+ + Ne^+$ via ICD, and we need a method that allows us to determine at what time (with respect to the excitation) this happens. This is done by testing the dimer's charge-state with the probe pulse which further ionizes one of the Ne fragments after an adjustable time delay. Only if ICD has happened before the arrival of the probe-pulse an effectively triply ionized dimer ($Ne^+ + Ne^{2+}$) can be formed. Hence, the increase of the yield of coincident $Ne^+ + Ne^{2+}$ ions for larger delays reflects the ICD decay time. Fig. 10 shows the recorded ion yield together with an exponential fit resulting in a decay time of (150±50) fs [5].

The obtained ICD lifetime is in good agreement with theoretical predictions, but only with those that take the nuclear motion into account: The removal of the first electron causes a change of the binding force between the two neon nuclei which leads to a time-dependent inter-nuclear distance. Because the ICD lifetime is predicted to be strongly dependent on this distance, the nuclear dynamics plays a crucial role for the decay process. This dependence shall be investigates in future experiments.

Kirsten Schnorr, Thomas Pfeifer, Robert Moshammer

Structural Changes in Acetylene (C_2H_2): Time-Resolved and in 3D

Being at the heart of photo-chemistry and biology, light-induced isomerization drives many fundamentally important reactions, e.g. in photosynthesis, in eye vision, and even in immunity and viral infection. In all of these reactions it is the migration of individual atoms within a molecule that results in a change of the geometrical structure and thus leads to a product with sometimes drastically different properties and functionalities. For example, while one isomer of the essential oil carvon is responsible for the aroma of mint, the other one smells like caraway. During the course of isomerization often a sequence of transient species is involved, which, as intermediate states with various geometrical structures, control the details of the reactant-to-product process. In general, the system evolves along multi-dimensional electronic potential energy surfaces, it may pass through conical intersections, and typically several vibrational modes are involved whose energies are redistributed to achieve a stable product state [6]. Even small molecules comprising only a few atoms may undergo isomerization. With typical rearrangement times from ten to few hundreds of femtoseconds they serve as prototype systems to advance our understanding of larger molecules that are more relevant for applications. The acetylene cation, for example, has been studied extensively in particularly for low-lying excited states, which are known to decay unexpectedly fast via non-radiative mechanisms.

The ultrafast dynamics of geometrical rearrangements in photo-excited acetylene molecules $(HCCH)^+$ leading to the formation of vinylidene cations $(CCH_2)^+$ has been traced in an XUV-pump/XUV-probe experiment with FEL pulses at FLASH (see Fig. 9). FLASH-pulses with an average pulse duration of ≈40 fs, peak intensities of $I \approx 1\times10^{13}$ W/cm^2, and a photon energy of 38 eV were employed for the measurements. Recording the yield of characteristic $C^+ + CH_2^+$ fragment-pairs that emerge from the dissociation of the product molecule (CCH_2) as a function of the pump-probe time delay allowed us to directly access the mean isomerization time of (52±15) fs, thus measuring the time it takes for one of the hydrogen atoms to migrate from one side of the molecule to the other (see Fig. 11). It is anticipated that this first temporally resolved observation of isomerization on a femtosecond time-scale will pave the way to visualize or even control molecular reactions in real time.

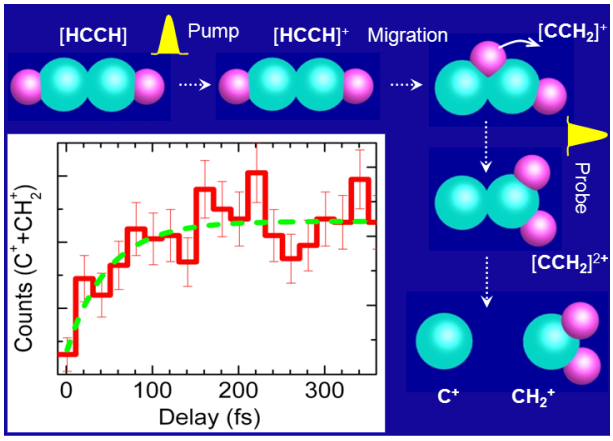

Fig. 11: Sketch of Isomerization in C_2H_2 and delay-dependent fragmentation rate.

The absorption of one photon from the pump pulse leads to the formation of an acetylene cation $(HCCH)^+$ in a low-lying excited state. This serves as a trigger for the migration of a hydrogen atom from one end (breaking of CH bond) to the other end of the C=C core (making of CH bonds) since there are almost no potential barriers for isomerization into the $(CCH_2)^+$ vinylidene configuration. During its course of isomerization the molecular cation is ionized further by absorption of an additional photon, now from the probe-pulse, and then, depending on the delay-time, it dissociates into the $C^+ + CH_2^+$ channel, which is considered to be a unique signature for the H-transfer. Hence, the probe-pulse "clocks" the hydrogen migration in real time at various positions along the isomerization reaction coordinate like "a femtosecond XUV stopwatch" by measuring the fragment-pairs that are characteristic for the vinylidene product state. A mean isomerization time of (52±15) fs was extracted. Confirmed by recent calculations (see discussion in [6]), our findings provide first evidence that isomerization is responsible for the ultrafast non-radiative relaxation dynamics ending a long lasting controversial debate. Due to the perturbative nature of the XUV pump-probe scheme, essentially not imposing any field-induced modifications of the potential surfaces, a wealth of chemical reactions as well as molecular dynamics can be explored on the few-femtosecond time scale under unprecedented clean conditions in the future.

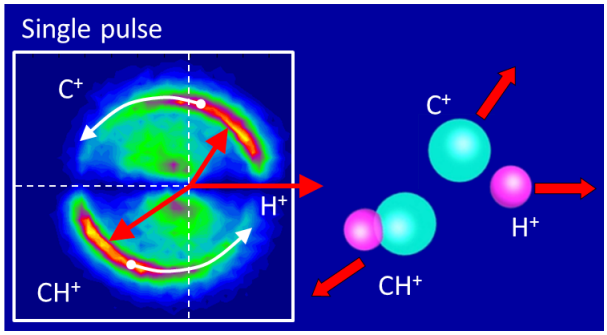

Fig. 12: Left: Newton-plot representation for the three-particle Coulomb explosion of Acetylene. The white arrows indicate the expected changes in the course of isomerization. Right: The corresponding geometrical molecular structure at the moment of explosion.

Beside the measurement of isomerization times it is a long standing dream of scientists to capture the ultra-fast dynamics in real time and to "make a molecular movie". With free-electron lasers delivering extreme ultraviolet (XUV) light at unprecedented intensities it is now possible to visualize structural changes on the femtosecond time scale in photo-excited molecules. Very recently

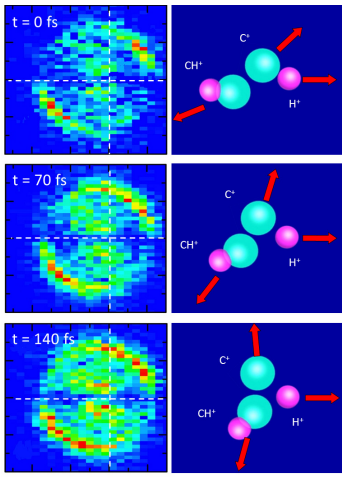

Fig. 13: Time-dependent Newton-plots of Coulomb explosion fragments for isomerization of acetylene.

we succeeded for the first time to "film" such a reaction in acetylene by resolving the motion of the proton along the carbon backbone [6].

This was achieved in an XUV pump-probe experiment where the first pulse initiates the isomerization reaction and a very intense probe pulse causes Coulomb-explosion into three charged fragments (H^+, C^+, CH^+). This allows us to infer the geometrical structure of the molecule, as a function of the time delay, from the correlated three-particle momenta analyzing in particular the fragments' relative emission angles. We use the fact that the break-up into three ionic fragments is always planar, and to resolve the geometric structure we plot the correlated momenta in a two-dimensional representation, so-called Newton-plots, by selecting only those events where the proton momentum only has a non-zero component in the positive x-direction. This means that the proton is always emitted to the right (see Fig 12). What is plotted in the diagrams are the momentum distributions of the two heavy fragments in the common (paper-) plane where the y momentum components of the CH^+ ions are restricted to positive values (upper half) and that of the C+ fragments to negative values (lower half). The experimentally obtained Newton-plots for the three time intervals of ≈ 60 fs, ≈ 100 fs and ≈ 140 fs are displayed in the left column of Fig. 13. For small molecules, as is the case here, the geometrical structure at the moment of Coulomb-explosion is very well reflected in the relative emission angles of the fragments which can be read form the Newton-plots. This is indicated by sketching the corresponding molecular structure in the right column of Fig. 13. As the time delay increases (indicated in Fig. 13) the centre of both the C^+ and the CH^+ momentum distributions move anti-clockwise. This shows that we actually image the migration of the hydrogen atom. At time delays larger than 140 fs (not shown), no further changes in the Newton-plots are found. Overall, the delay-dependent changes in the Newton-plots are less pronounced than expected on the basis of generally assumed classical particles moving along molecular potential surfaces. However, the nuclear motion within the molecule must be treated quantum mechanically in the framework of wave-packets that evolve in time. Correspondingly, the measured Newton-plots are in very good agreement with first quantum-mechanical model calculations.

Arne Senftleben, Robert Moshammer

Preparing and Probing Wave Packets in Laser-Excited Lithium Atoms

An electronic wave packet is a coherent superposition of several nondegenerate eigenstates and, therefore, is a nonstationary state evolving in time. The creation, control, and measurement of wave packets are central topics in a broad range of research areas. Specially designed wave packets have been proposed to control key processes in atomic, molecular, and solid-state systems.

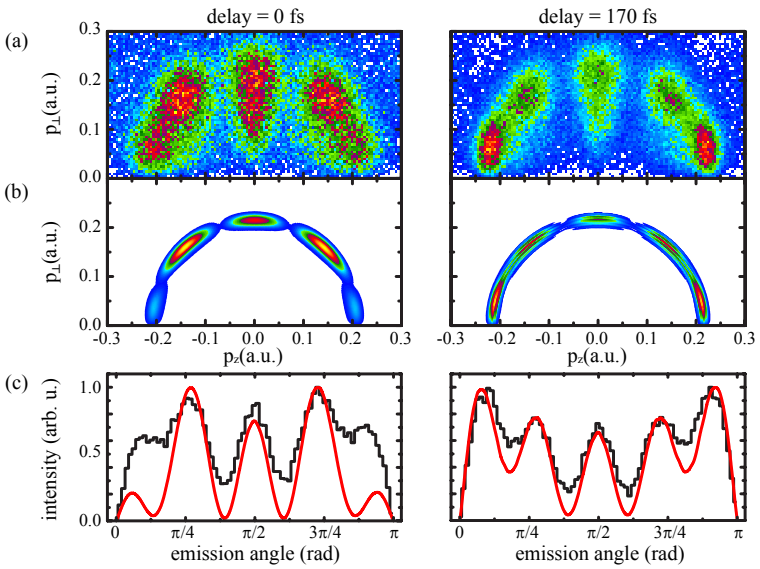

Fig. 14: Left: Experimental (a) and theoretical (b) photo-electron momentum distributions along (p_z) and perpendicular ($p_\perp$) to the light polarization axis for overlapping pump and probe pulses (delay = 0 fs). (c): Photo-electron intensity as function of the emission angle. Black line: experiment. Red line: theory. Right: pump-probe pulse delay of 170 fs.

We have performed a joint experimental and theoretical study of the time-resolved photoionization of a superposition of two angular-momentum eigenstates in the quasi-one-electron lithium atom. A 30 fs laser pulse transfers part of the 2s ground state population to the 4p and 4f excited states via a three-photon transition. The coherent superposition of both states with different orbital angular momenta is allowed to evolve for a certain time and is then probed by a second identical laser pulse, ionizing the system. The resulting photoelectron angular distribution (PAD) is characteristic for angular momenta of the intermediate excited states and for their relative phases. As a consequence of the relative phase evolution, the observed PAD oscillates with the frequency corresponding to the energy difference between the excited 4p and 4f states.

The experiment was realized by combining many-particle momentum spectroscopy techniques (reaction microscope: REMI) with a magneto-optical trap (MOT) which provides an ultra-cold and dense lithium gas target [7]. Fig. 14a shows on

the left the experimentally observed momentum distribution of the emitted photo-electrons [8]. Here the excitation and ionization pulses overlap and the wave packet is not allowed to evolve in time but ionized in a single pulse. The excess energy of the four photons absorbed leads to an electron momentum of 0.22 a.u. According to the total angular momentum transferred five maxima are observed in the emission pattern. In Fig. 14b predictions from ab initio calculations that numerically solve the time-dependent Schrödinger equation (TDSE) are shown. In comparison the radial width of the experimental peaks is larger which indicates the finite momentum resolution of the spectrometer. The relative peak intensities are compared in Fig. 1c showing qualitative agreement except for the outermost peaks which are too small in magnitude in theory. The PAD at pump-probe delay time of 170 fs is displayed on the right side of Fig. 14. Here the relative peak intensities are different compared to the case of overlapping laser pulses with the outermost peaks being strongest. In this case theory and experiment are in good agreement (see Fig. 14c).

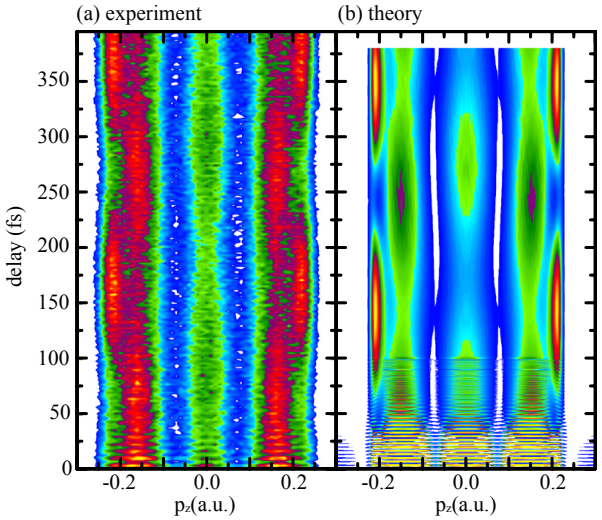

Fig. 15: Photo-electron momentum projected onto light polarization direction (horizontal axis) as function of the pump-probe delay time (vertical axis). Experiment (a) and theory (b).

The evolution of the peak intensities as function of the pump-probe delay is illustrated in Fig. 15. The horizontal axis shows the longitudinal electron momentum allowing the distinction the individual peaks in the PAD. On the vertical axis the probe pulse delay is plotted in the range from 0 to 300 fs. Clearly a periodic evolution of the peak intensities is observed with a period of roughly 200 fs corresponding to the energy difference of the excited 4p and 4f states. Theory in Fig. 2b qualitatively reproduces this pattern except a delay offset of 40 fs which can be caused by AC stark shift of the populated states during the initial laser pulse. Furthermore the delay time has to be scaled due to a deviation of the calculated 4p–4f energy difference [8].

Interestingly the calculation indicates that an outgoing electron wave is produced already from the pump pulse and interferes with the wave from the probe pulse. If this is considered fully in the theoretical model the calculation becomes time-consuming and elaborate even for this basic one-electron system.

In conclusion, this study demonstrates how the combination of optical target trapping and cooling techniques with particle momentum spectroscopy is used to study a fundamental one-electron model system. Theory is challenged but can qualitatively reproduce the dynamics such that more complex systems can be addressed in future.

Michael Schuricke, Alexander Dorn

References

[1] C. Ott et al, New J. Phys 15 (2013) 073031.
[2] N. Camus et al, Phys. Rev. Lett. 108 (2012) 073003.
[3] A. Fischer et al, Phys. Rev. Lett. 110 (2013) 213002.
[4] K. Meyer, C. Ott, P. Raith, A. Kaldun, Y. Jiang, A. Senftleben, M. Kurka, R. Moshammer, J. Ullrich and T. Pfeifer, Phys. Rev. Lett. 108 (2012) 098302.
[5] K. Schnorr et al, Phys. Rev. Lett. 111 (2013) 093402.
[6] Y. Jiang et al, J. Phys. B: At. Mol. Opt. Phys. 46 (2013) 164027.
[7] M. Schuricke, G. Zhu, J. Steinmann, K. Simeonidis, I. Ivanov, A. Kheifets, A. N. Grum-Grzhimailo, K. Bartschat, A. Dorn and J. Ullrich, Phys. Rev. A 83 (2011) 023413.
[8] M. Schuricke, K. Bartschat, A. N. Grum-Grzhimailo, G. Zhu, J. Steinmann, R. Moshammer, J. Ullrich and A. Dorn., Phys. Rev. A 88 (2013) 023427.

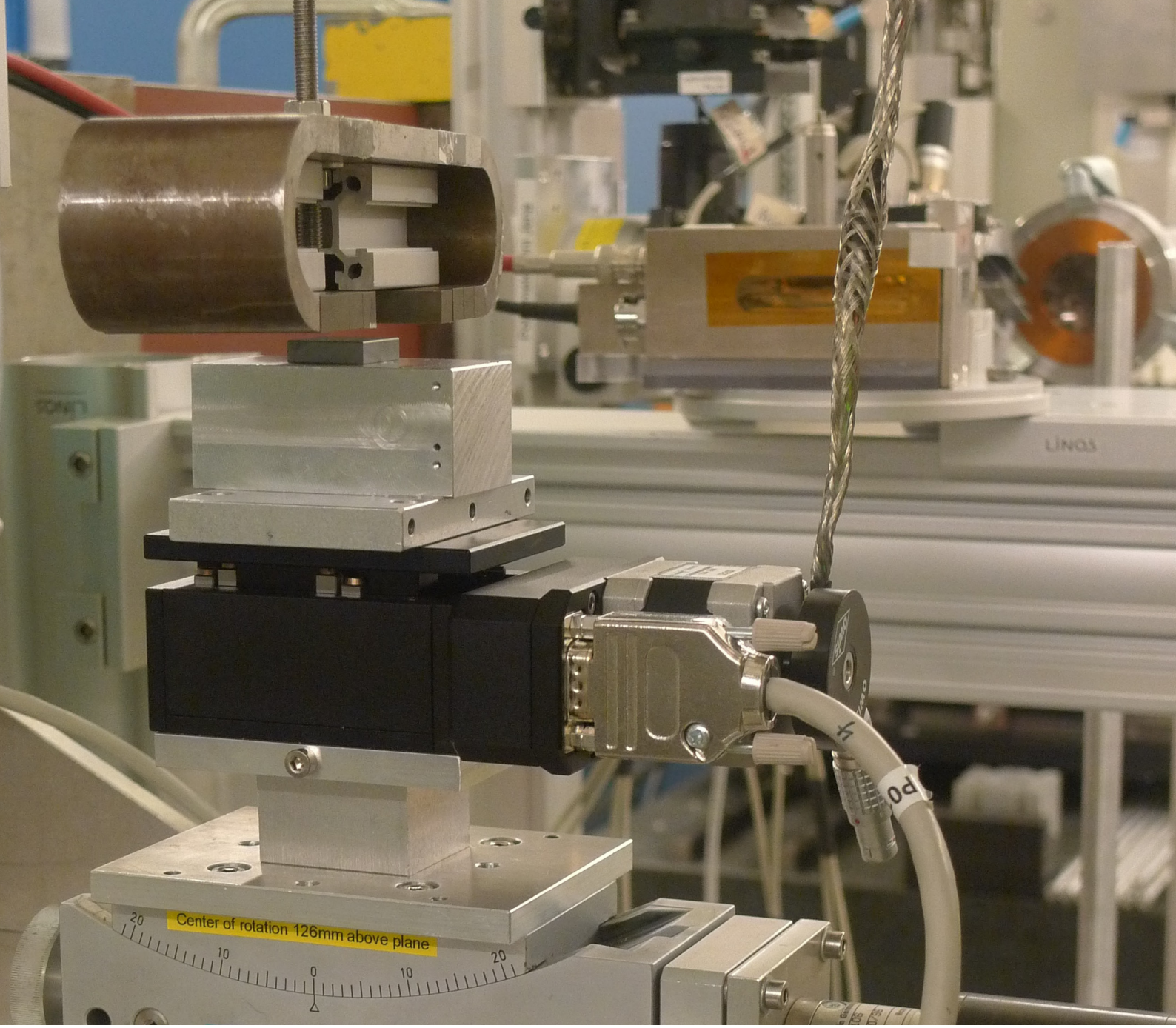

2.7 Laser Control of Atoms and Nuclei

Experiment on nuclear quantum optics with synchrotron radiation: A sample with iron atoms embedded (grey cuboid on top of the positioning stage) is irradiated with X-ray light from a flat angle (beamline in the background), and the reflected light is measured. The magnet (top left) provides an external field for control of the nuclear level structure.

Introduction

Traditionally, the interaction of matter with light is exploited to gain a detailed understanding of the quantum mechanical foundations of atomic, molecular, ionic and nuclear systems. While in particular at the most fundamental level this continues to be a challenge, by now it is nevertheless possible both in theory and in experiment to deliberately control the quantum dynamics of many systems of interest. This on the one hand opens perspectives for a multitude of fascinating applications. On the other hand, it provides a handle to probe the validity range of theoretical models and intuitive interpretations, and to explore systems far away from their equilibrium properties.

In this overview, we outline some of our recent approaches towards the active control of quantum dynamics and material properties. The target systems range from visible frequencies with atoms near their ground state up to the hard X-ray domain of nuclear excitations. Interestingly, the fundamental mechanisms based on coherence, non-linear interactions and quantum effects underlying the control of the dynamics are often shared across the different platforms. In this sense, the various approaches complement each other, which together with the fruitful interplay of theory and experiment enable us to extract the fundamental principles of laser control.

Fano Control of Light-Matter Interaction

Spectroscopy is a primary tool to investigate structure and dynamics of physical systems. The archetype spectroscopic signature is a symmetric Lorentzian line shape, which is observed if the probing radiation is near-resonant to an isolated bound-state resonance in the system. In contrast, excitation of a continuum of resonances leads to a structure-less spectral response. More generally, a broad class of asymmetric line shapes arises, if an isolated resonance couples to a continuum of resonances. These Fano line shapes were first characterized by Ugo Fano to theoretically model the ionization of Helium by electron impact, which can either proceed directly into a continuum of final states, or via an auto-ionizing isolated bound-state resonance, that subsequently decays to the same final state. Fano resonances, the consequence of a fundamental coupling process, play an important role in a multitude of quantum processes and applications across the natural sciences.

In a joint collaboration of experimental and theoretical teams at the institute [1], we have developed a new interpretation of Fano resonance absorption in the time domain, which opens a direct route to the external manipulation of the spectral response. In this picture, the detected signal arises from the interference between the incident probing radiation, and the radiation emitted by the sample's time-dependent oscillating dipole moment excited by the probing field. A spectral continuum translates into a short peak in the temporal response, while an isolated resonance leads to a slower exponential decay of the oscillating dipole moment. The key result of the new interpretation is the observation that the coupling between continuum and isolated bound state resonance responsible for the asymmetric Fano line shapes leads to a relative phase shift between the dipole response and the incident radiation. This phase shift changes the interference between the two contributions, and thereby modifies the observed line shape. In particular, an intuitive analytic one-to-one

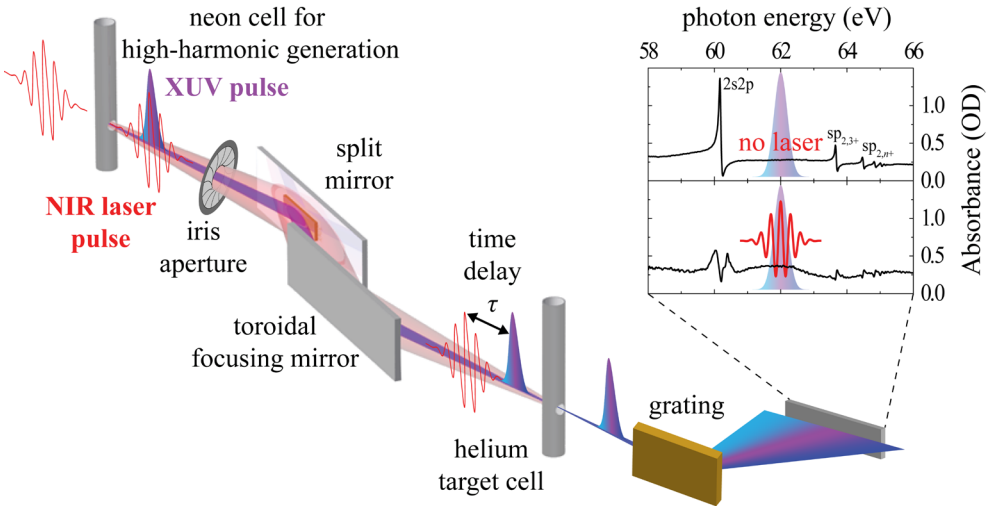

Fig. 1. Schematic experimental setup used for time-domain Fano line shape control in helium.

mapping between this phase shift and the q-parameter that determines the asymmetric Fano line shapes could be developed. The significance for applications arises from the generalization that any physical mechanism which shifts the phase between the dipole response and the incident field can be used to manipulate the spectral response of the system.

This line shape control was experimentally demonstrated in the photoionization of helium by broadband attosecond pulsed extreme ultraviolet (XUV) light (see Fig. 1). An intense femtosecond near-infrared (NIR) laser field is focused into a neon cell to generate the attosecond XUV probe pulse via high-harmonic generation. Behind the neon cell, a split mirror is used to impose a variable delay between the generated XUV pulse and the transmitted remainder of the NIR pulse. The sequence of these two pulses is then sent through the helium target cell. Finally, the helium absorption spectrum is recorded using a flat-field grating spectrometer with high spectral resolution developed in house. While the XUV pulse is used for the actual spectroscopy, the NIR pulse sent through the helium target with a short time delay causes a transient energy-level shift (Stark shift) on the observed doubly-excited states. Throughout this level shift, a phase is accumulated, which can be approximated as an instantaneous shift since the dipole oscillations excited by the XUV pulse decay slowly compared to the NIR pulse duration. The magnitude of the phase shift can be tuned by the intensity of the NIR pulse.

As a result of this phase control, the experiment clearly demonstrated the conversion of asymmetric Fano line shapes naturally occurring in doubly-excited helium into symmetric Lorentzian line shapes (see Fig. 2) and beyond to inverted Fano shapes. In the same way, Lorentzian line shapes naturally observed in singly-excited helium were converted into asymmetric Fano line shapes. Finally, the experiment confirmed the possibility to transform absorption into gain, by inducing a phase shift of π.

The broader impact of these results also includes a complementary interpretation of related phenomena such as electromagnetically induced transparency or lasing without inversion. Future experiments could exploit that the change in absorption is directly linked to the phase shift. This gives access to phase information, which together with the possibility to manipulate the coupling between different quantum mechanical states provides a handle to control and interpret correlations and dynamics in more complicated settings. Since the time-domain analysis and the phase-control of Fano line shapes are fundamental concepts, the developed methods can be generalized to other target systems and spectral regions, including the hard X-ray or gamma-ray domain.

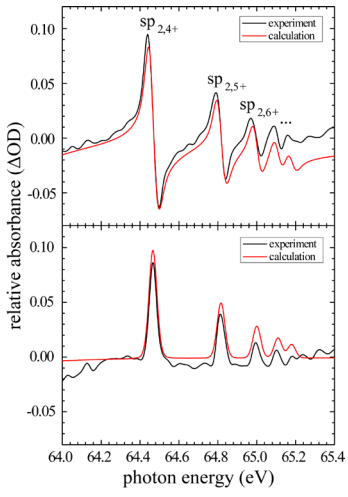

Fig. 2: XUV absorption spectra of helium without (upper panel) and with (lower panel) NIR control field.

Thomas Pfeifer, Christian Ott, Jörg Evers, Christoph H. Keitel

Control of Cooperative Dynamics in Atoms and Nuclei

The success story of optical lasers is founded on coherence, non-linearities and quantum effects. Recent advances in existing and upcoming light sources provide access to laser-like light in the X-ray and gamma-ray frequency domain, with a multitude of novel applications across all the natural sciences. However, it remains a challenge to exploit quantum optical

phenomena in the X-ray domain, which will be required to unleash the full potential of the new light sources. Motivated by this, we develop quantum optical methods in the hard X-ray domain. A particularly promising platform is X-ray cavity quantum electrodynamics (QED) with Mössbauer nuclei embedded in thin-film cavities probed by near-resonant X-ray light, as used in a number of recent experiments. We developed a quantum optical framework for the description of this setting. It allows identifying and separating all physical processes contributing to the recorded signal, and encompasses nonlinear and quantum effects. Based on this model, the light polarization and an external magnetic field can be used to control the nuclear level structure.

An important step towards X-ray quantum optics is the generation of coherent superpositions of quantum states. These were crucial in the development of quantum mechanics, as exemplified by the famous thought experiment about the fate of Schrödinger's cat. Nowadays, such coherent superpositions are key resources for quantum technologies. But in experiments, usually inevitable decoherence destroys the superposition states, restricting many applications. An important source of decoherence is spontaneous emission, induced by the interaction with the surrounding vacuum field. We have developed a method to manipulate the interaction with the vacuum in such a way that it produces the desired superpositions instead of destroying them [2]. These spontaneously generated coherences (SGC) are realized based on two mechanisms. First, the cooperative acceleration of the nuclear dynamics is exploited. Second, the cavity vacuum field experienced by the nuclei is tailored suitably via the external magnetic field.

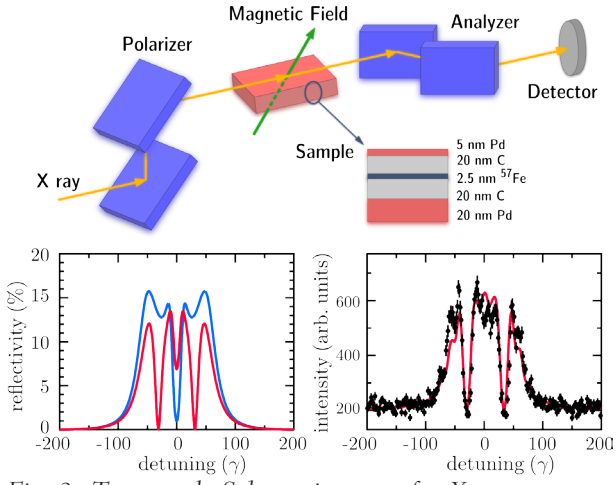

Fig. 3: Top panel: Schematic setup for X-ray quantum optics with nuclei in cavities. The inset shows the structure of the nanoscale cavity with embedded ^{57}Fe nuclei. Lower left panel: Theoretical predictions with (red) and without (blue) SGC show a clear signature of the SGC. Lower right panel: The experimental data confirm the presence of SGC.

The theoretical predictions were subsequently verified in collaboration with an experimental team around R. Röhlsberger at the PETRA III Dynamics Beamline P01 (DESY, Hamburg). In the experiment, X-rays are reflected in grazing incidence from the cavity with embedded nuclei, and subsequently detected (see title figure). To fully exploit the additional degrees of freedom of the X-ray photon polarization and the sample magnetization, an X-ray polarimeter developed by the group around G. G. Paulus (University and Helmholtz Institute Jena) was used in the experiment. The experimental results obtained are in good agreement with our quantum optical theory (see Fig. 3). The method opens up a variety of possibilities for future studies because it enables the realization of undisturbed and highly configurable quantum optical model systems for applications with hard X-rays from synchrotron radiation and X-ray laser sources. Moreover, our approach is not restricted to the X-ray range but also works with visible light. This offers the chance to realize the applications based on SGC theoretically proposed previously by other groups reaching from novel laser mechanisms to the efficiency increase of solar cells.

An essential feature of the setups we study in nuclear quantum optics is the collective dynamics of a large ensemble of nuclei. We are thus interested in generic properties of collective dynamics. An alternative approach to the study of collective and strongly correlated dynamics are highly excited Rydberg atoms, which in addition to the cooperativity already present with nuclei feature a controllable long-range interaction between excited atoms. A primary motivation is to achieve strong interactions between photons, enabled by interfacing them with interacting states of matter. This also provides an interesting link to other activities in the theory division, which aim at photon-photon interactions in the absence of matter, due to vacuum non-linearities induced by strong laser fields. We have developed numerical techniques to characterize large ensembles of such Rydberg atoms in experimentally relevant settings. As one application, we have modeled recent experiments in the group of M. Weidemüller (University of Heidelberg) on light propagation through Rydberg atoms in an electromagnetically induced transparency configuration [3]. In this system, an additional coupling laser field is used to control the propagation of a weak probe field, and the atom interactions lead to large optical nonlinearities and to non-classical atom excitation statistics.

The laser control of material properties becomes particularly interesting if the matter is structured at length scales compatible with the probing wavelength. This is possible, e.g., using standing wave control laser fields. These can periodically modulate the refractive index of an ensemble of atoms such that it acts like a photonic crystal. In particular, a band

gap is formed, and certain frequencies cannot propagate through the medium. In collaboration with the group around S. Y. Zhu (Beijing Computational Science Research Center, China), we showed that a detuning of the two light fields forming the standing wave leads to a motion of the light-induced photonic crystal-like structure [4]. Due to the Doppler shift, light propagating along this movement or in reverse direction through the atoms experience different optical properties. This breaks the time reversal symmetry, such that light is emitted from one side to the other, but not in reverse direction. This optical diode was demonstrated in a proof-of-principle experiment in the group of J.-X. Zhang (State Key Laboratory of Quantum Optics and Quantum Optics Devices, Taiyuan, China).

Jörg Evers

Phase Control in High-Frequency Nonlinear Optics

The control of matter by phase-shaped electromagnetic radiation is now routinely achieved from radio frequencies up into the visible domain, enabling access to quantum dynamics from nuclear spins via rotations of large and small molecules to vibrational dynamics of individual molecular bonds and some electronic states. However, to control matter on a fundamental and comprehensive level — involving all electrons in low-lying bound states or excitations within atomic nuclei — high-frequency radiation needs to be shaped in amplitude and phase.

In our experiments, we study the elementary building blocks of phase control in high-frequency light. We focus on the highly-nonlinear optical process of high-harmonic generation converting visible laser light and its coherence properties into the extreme ultraviolet (XUV) region. One experimental challenge is the stabilization of the driving visible laser field to enable complete transfer of the phase coherence from the femtosecond driver pulse through the strongly-nonlinear recollision process into the spectral phase of the produced high-order attosecond-pulsed harmonic light.

The phase of the XUV harmonic light depends on the exact shape of the driver field, which creates essentially two experimentally accessible ‚control knobs': The phase between spectral components of the driver pulse (the relative spectral phase), and the phase of the carrier wave with respect to the pulse envelope (the ‚absolute' or carrier–envelope phase, CEP) [5]. To focus on the most fundamental spectral-phase control operation, we divided the driver spectrum in just two parts and introduced the relative phase between them by a time delay operation realized by a piezo-driven split mirror (see Fig. 4), while the CEP of the laser pulse was globally stabilized and controlled by traditional technology.

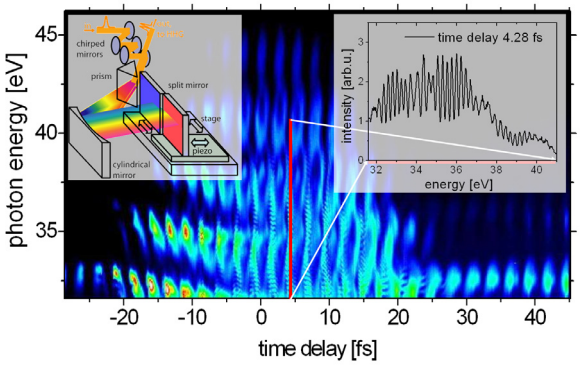

Fig. 4: Two-color phase control of high-order harmonic generation. A sub-harmonic comb-like modulation (inset right) is obtained at certain time delays (created by a split-mirror pulse shaper, inset left) by interference of attosecond pulse trains.

Qualitatively different shapes of coherent high-harmonic XUV spectra were measured as a function of the two (time-delay and CEP) control operations. For specific ranges of time delays, the traditional odd-order high harmonics (spaced by ~3 eV photon energy in our case) were tuned in their photon energy, and were explained by a modulation of the instantaneous frequency at the peak of the driver pulse by time-domain interference of the two-color field [6].

For another set of time delays, the traditional 3 eV odd-harmonic modulation vanished and was replaced by a much faster spectral modulation structure of ~0.2 eV (see Fig. 4), corresponding to the mean frequency difference of the two spectral components separated by the split mirror. An intuitive time-domain interpretation was found for this phenomenon: The time-domain beating of the two-color subfields resulted in a double pulse with a temporal spacing given by the inverse frequency difference of the subfields. Spectral interference between the corresponding two temporally separated attosecond pulse trains resulted in the sub-harmonic modulation.

Controlling the CEP from 0 to π allowed us to fully spectrally tune the sub-harmonic modulation from peak to peak. This provides evidence of spectral phase control between two attosecond pulse trains all the way from 0 to 2π, thus achieving a substantial goal of attosecond high-frequency (XUV) control of coherent light.

Philipp Raith, Thomas Pfeifer

Storing and Manipulating X-ray Photons

Optical lasers have been at the heart of quantum physics for the last decades. The commissioning of the first X-ray free electron lasers and the developments of X-ray optics elements bring into play higher photon frequencies and promote the emerging field of X-ray quantum optics. Compared to optical photons, X-rays are not plagued by the diffraction limit and can be much better focused. Thus, forwarding optics and quantum information to shorter wavelengths in the X-ray region has the potential of shrinking computing elements in future photonic devices using photons as the information carriers.

Prior to the realization of short-wavelength quantum photonic circuits, mastery of X-ray optics and powerful control tools of single-photon wave packet amplitude, frequency, polarization and phase are required. In particular, efficient phase-sensitive photon storage and phase modulation, preferably even for single-photon wave packets, are desirable but so far very challenging. A first successful scheme using nuclei as the „cage" to store single X-ray photons was designed theoretically in Ref. [7] exploiting a nuclear forward scattering setup. Employing nuclei to tame X-rays has here a two-fold advantage. First, due to their suitable transition frequencies, nuclei rise as promising candidates for X-ray quantum optics studies. Second, when using a solid-state sample with Mössbauer nuclei, the delocalized nature of the excitation leads to cooperative effects. These in turn open the possibility to control the re-emission of the single photon by external magnetic fields responsible for the nuclear hyperfine splitting.

The typical nuclear forward scattering setup involves a solid-state target containing ^{57}Fe Mössbauer nuclei. A synchrotron radiation pulse tuned on the 14.4 keV nuclear transition from the ground state to the first excited state shines perpendicular to the nuclear sample (see Fig. 5). Typically, given the small coupling constant, at most one nucleus is excited per pulse. In coherent scattering, the absence of nuclear recoil or spin flip does not allow identification of this nucleus, leading to a delocalized excitation often denoted as nuclear exciton. The key to control the excitonic decay relies on an externally applied magnetic field inducing hyperfine splitting of the nuclear states. Due to the broadband nature of the incident pulse, several nuclear transitions are addressed simultaneously. The scattering process and correspondingly the involved single X-ray photon can be controlled by means of interference effects between these transitions. Switching off the hyperfine magnetic field at specific times will render the transition currents interfere destructively, strongly suppressing the nuclear decay and leading to coherent storage of the excitation for time intervals of 10-100 ns. Switching on the magnetic field will release the stored single photon and by using a releasing hyperfine magnetic field oriented in the opposite direction to the initial one, a phase modulation of π can be achieved for the X-ray [7]. With coherent storage and phase modulation as powerful means to control single X-ray photons, an important missing link between nuclei, photonic devices and photon qubits is established.

Adriana Pálffy, Wen-Te Liao, Christoph H. Keitel

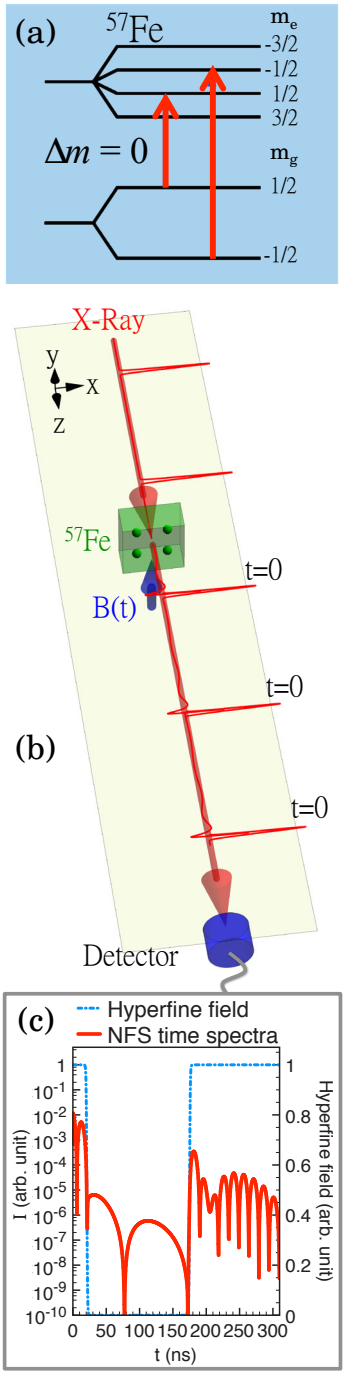

Fig. 5: (a) Relevant energy level scheme of ^{57}Fe. (b) Schematic illustration of the nuclear forward scattering setup. (c) The calculated spectrum shows the storage and release induced by the hyperfine magnetic field switchings.

References

[1] C. Ott, A. Kaldun, P. Raith, K. Meyer, M. Laux, J. Evers, C. H. Keitel, C. H. Greene and T. Pfeifer, Science 340 (2013) 716.

[2] K. P. Heeg, H.-C. Wille, K. Schlage, T. Guryeva, D. Schumacher, I. Uschmann, K. S. Schulze, B. Marx, T. Kämpfer, G. G. Paulus, R. Röhlsberger and J. Evers, Phys. Rev. Lett. 111 (2013) 073601.

[3] C. S. Hofmann, G. Günter, H. Schempp, M. Robert-de-Saint-Vincent, M. Gärttner, J. Evers, S. Whitlock and M. Weidemüller, Phys. Rev. Lett. 110(2013) 203601.

[4] D.-W. Wang, H.-T. Zhou, M.-J. Guo, J.-X. Zhang, J. Evers and S.-Y. Zhu, Phys. Rev. Lett. 110 (2013) 093901.

[5] P. Raith, C. Ott and T. Pfeifer, Opt. Lett. 36 (2011) 283.

[6] P. Raith, C. Ott, C. P. Anderson, A. Kaldun, K. Meyer, M. Laux, Y. Zhang and T. Pfeifer, Appl. Phys. Lett. 100 (2012) 121104.

[7] W.-T. Liao, A. Pálffy and C. H. Keitel, Phys. Rev. Lett. 109 (2012) 197403.

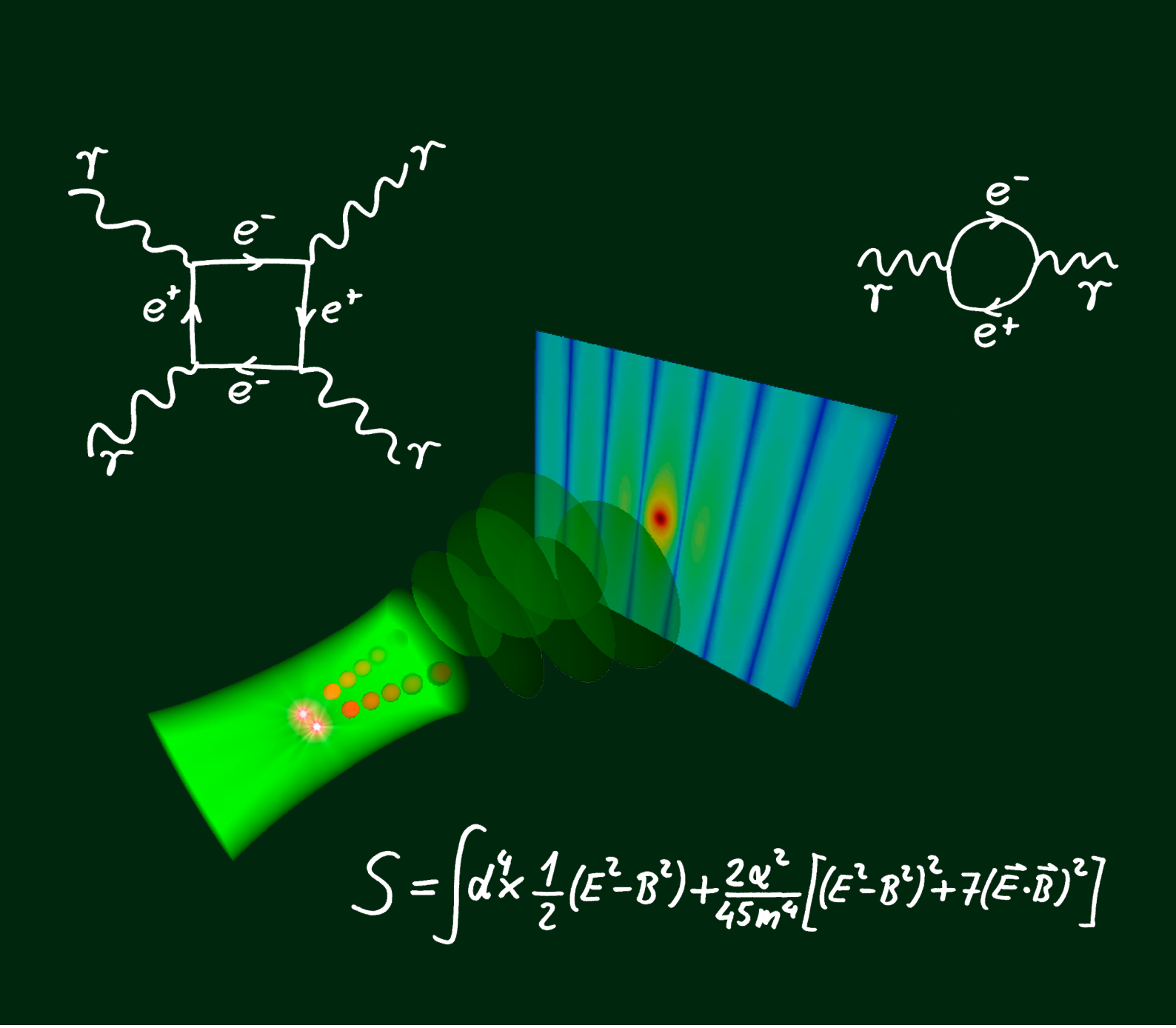

2.8 Matter in Extremely Intense Laser Pulses

A matterless double slit: light is scattered by light via the modified vacuum fluctuations in ultra-intense laser fields.

Introduction

In the past, research on intense laser-matter interaction generally has been focussing on dynamical aspects of the interplay of atoms, molecules, and plasmas with external light waves. Recent technological progress such as the construction of the Extreme Light Infrastructure is now opening up the possibility of employing intense laser radiation to trigger or substantially influence physical processes well beyond atomic-physics energy scales. Optical laser intensities exceeding 10^{22} W/cm^2 can explore the fundamental light-electron interaction in the extreme limit where radiation-reaction effects dominate the electron dynamics, allow to shed light on the structure of the quantum vacuum, and may trigger the creation of particles such as electrons, muons, and pions and their corresponding anti-particles [1]. Also, novel sources of intense coherent high-energy photons and laser-based particle colliders can pave the way to nuclear quantum optics and may even allow for the potential discovery of new particles beyond the standard model. Various topics in this section are devoted to recent investigations on high-energy processes within the realm of relativistic quantum dynamics, quantum electrodynamics and nuclear physics, occurring in extremely intense laser fields.

Relativistic Quantum Dynamics in Intense Laser Pulses

Various quantum effects such as wave packet spreading, interference, vacuum fluctuations, spin oscillations and tunneling may be relevant when extremely intense laser pulses are impinging on atomic systems. In particular a quantum tunneling barrier is shaping temporarily around an atomic nucleus due to the interplay of attractive Coulomb forces and counteracting forces of the laser pulse. For highly charged hydrogen-like ions, i.e., an atomic core with a single electron, ultra-strong lasers with intensities of the order of 10^{18} W/cm^2 and above are required to achieve measurable ionization probabilities. Such ultra-strong lasers can no longer be treated as pure electric fields and the laser's magnetic field component has to be taken into account, too. Magnetic fields, however, do not fit into the conventional picture of a tunneling barrier. Therefore, it has been argued that the whole tunneling concept may break down in the presence of magnetic fields. In [2] it was shown however that the notion of a tunneling barrier can also be applied in the presence of magnetic fields of ultra-strong lasers via reshaping the potential barrier, see Fig. 1.

A question that has caused many controversial discussions among physicists and remains unsolved till today is how long an electron needs to tunnel through a barrier. Direct measurements of tunneling times are hampered by experimental as well as conceptual difficulties. While extending the tunneling picture into the regime of ultra-strong lasers, we demonstrated that tunnel ionization of hydrogen-like ions via ultra-strong lasers features two time scales which may be measured indirectly. In particular, a small shift of the point of exit where the electron leaves the tunneling barrier is caused by the presence of the laser magnetic field. This shift is proportional to the so-called Eisenbud-Wigner-Smith tunneling time. Furthermore, the magnetic field changes the velocity distribution of the ionized electrons. Ionized electrons escape with a non-zero velocity along the propagation direction of the laser that is proportional to the so-called Keldysh tunneling time. Thus,

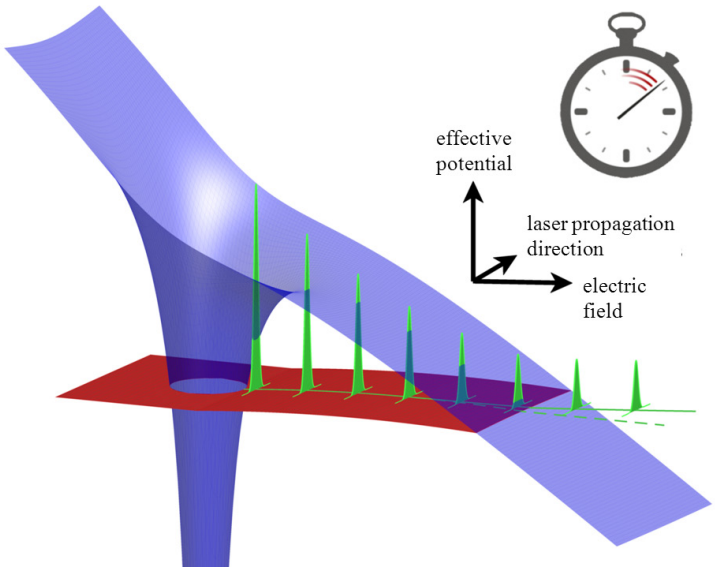

Fig. 1: Schematic description of tunnel ionization of highly charged ions at relativistic laser intensities. The superposition of the Coulomb potential of the atomic core and the electric field of the laser forms a potential barrier (in blue) that the electronic wave packet (in green) may tunnel through into the direction of the laser's electric component. Unlike in nonrelativistic tunneling the ionization potential (in red) becomes position-dependent as a consequence of the laser's magnetic field. Furthermore, while tunneling the wave packet is shifted under the influence of 'light pressure' into the propagation direction fields (solid green line).

one can relate these two tunneling times to quantities that are accessible to direct measurements in laboratory experiments. For tunnel ionization of hydrogen-like ions with small atomic numbers lasers of moderate intensities and, therefore, weak magnetic components are sufficient and the consequences of the two tunneling time scales become small. This may explain why experimentalists have not been able so far to measure non-zero tunneling times in tunneling through high barriers. By increasing the laser's intensity the height of the tunneling barrier decreases and the shape of the barrier changes qualitatively. Recent calculations have shown that in this regime the tunneling times become relevant again and may be determined experimentally.

Furthermore, the role of the spin may become essential in intense laser-matter interaction. For example the electron spin dynamics in scattering from a standing laser wave of high frequency and high intensity has been studied in [3] where a fully relativistic quantum theory of the laser-driven electron motion based on the time-dependent Dirac equation has been developed. Distinct spin dynamics, with Rabi oscillations and complete spin-flip transitions, were demonstrated for this so-called Kapitza-Dirac scattering involving two and three photons in a parameter regime accessible to near-future high-power x-ray laser sources. In a different study also effects of the quantum nature of the driving laser field have been demonstrated in laser-driven electrons.

Christoph H. Keitel, Karen Z. Hatsagortsyan, Heiko Bauke

Nuclear Reactions in Extremely Intense Laser Fields

With increasing intensity and frequency of coherent laser pulses, all constituents of matter can eventually be brought into frenzy. While strong-field phenomena in atoms have been the object of numerous investigations in the past decades, it is only recently that laser fields have become or hold promise to become strong enough to also considerably affect nuclei. Bound by the strong force, nuclei typically do not show any response even to extremely intense optical fields. This is because the first excited state in a nucleus has a typical excitation energy of approximately 100 keV, about four orders of magnitude larger than the energy carried by each optical photon. Such a state is not accessible even by multi-photon transitions. Intense optical fields can only induce nuclear reactions indirectly, as they are very efficient in transferring kinetic energy to charged particles. Laser-driven nuclear accelerators using intense optical fields are thus one candidate for nuclear physics experiments with strong external fields, one step beyond the traditional setups using heavy ion accelerators.

Laser-driven recollisions have come to play a crucial role in atomic strong-field physics, due to their role in the development of attoscience. The nuclear conterpart of such processes is investigated theoretically, aiming at developing new probes of nuclear decay processes on very short time scales. A promising candidate are laser-driven recollisions of alpha particles immediately following alpha decay. A charged heavy particle bound by the strong force, the alpha particle is set free after tunneling through the nuclear and Coulomb barriers. Because of the strong force, the tunneling process is not disturbed by electromagnetic effects. However, under the action of an intense laser field, the emitted alpha particle may change its trajectory and recollide with the daughter nucleus at sufficiently high energy to produce a nuclear reaction. Such laser-induced fast recollisions may probe in challenging experiments the short-lived excited nuclear states populated by alpha decay. Laser-driven nuclear recollisions in alpha decay thus allow the study of strong-field effects on a new

physical system and, in addition, open the possibility to investigate the interplay between the electromagnetic and the strong force in a new energy regime. As an important result, such recollisions were shown to be rare but detectable already at presently available laser intensities of 10^{22}–10^{23} W/cm² [4].

Shifting towards higher photon frequencies, the ongoing construction of the Nuclear Physics Pillar of ELI (the Extreme Light Infrastructure) offers exciting prospects and unprecedented possibilities for nuclear physics experiments. The facility holds promise to deliver in the not-too-distant future coherent gamma ray pulses with energies of several MeV per photon. Coherence strongly amplifies nuclear absorption and if the latter occurs comparably fast to nuclear equilibration, it leads to the formation of a compound nucleus with remarkably high excitation energy. Furthermore, the total angular momentum transferred in the process is much smaller than in typical heavy-ion reactions, as illustrated in Fig. 2. As a consequence, the excitation energy is several hundreds MeV above yrast, a totally unexplored regime where the most basic physical properties of nuclei are not known. For instance, a quantitative description of the absorption and equilibration processes requires knowledge of the density of states. Standard methods of calculation fail for the high excitation energies and large particle numbers that play a role here. The approach developed in Ref. [5] yields approximate analytical expressions for the total and partial level densities and allows the semiquantitative study of the competition between photon absorption, photon-induced nucleon emission, and neutron evaporation. With neutron evaporation overtaking photon absorption at energies below the saturation of the latter for medium-weight and heavy nuclei, the process promises to yield neutron-poor nuclei far from the valley of stability. Experiments planned at ELI thus promise to shed light on the structure of such nuclei and on the time scales that govern their production: the time scales for internal nuclear equilibration, for coherent photon absorption, and for neutron emission, all governed by the nuclear level density. Altogether the field constitutes a totally novel domain of laser-matter interaction.

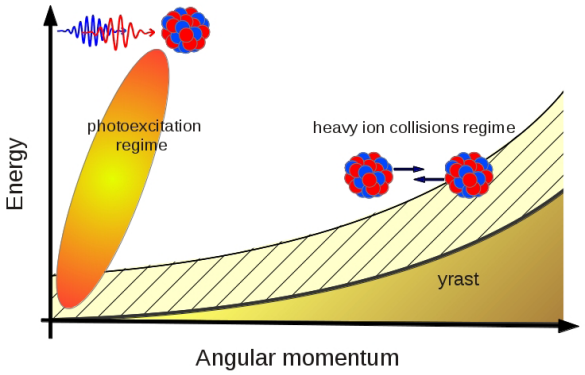

Fig. 2: Qualitative illustration of nuclear excitation regimes. The yrast line defines the minimum energy of a nuclear state with a certain angular momentum. Typically, heavy ion collisions produce excitation close to the yrast line, in the region depicted by the hatched area. Absorption of coherent MeV photons on the other hand can produce high excitation with low angular momentum transfer, leading to compound nuclei several hundred MeV above yrast.

Adriana Pálffy, Christoph H. Keitel, Hans-Arwed Weidenmüller

Quantum Radiation Reaction

In the realm of classical electrodynamics, when an electric charge, an electron for definiteness, is accelerated by a background electromagnetic field, it emits electromagnetic radiation and the associated energy-momentum loss alters the electron's trajectory [1]. The radiation-reaction problem is the determination of the equation of motion of an electron by including self-consistently the effects of the emitted radiation on the electron's motion. This problem has been investigated over many decades and there is a large consensus on the so-called Landau-Lifshitz equation as being the correct classical equation of motion, which includes self-consistently radiation-reaction effects. At a more fundamental level, we have been investigating the quantum origin of radiation reaction and its distinctive features in the quantum domain. After identifying quantum radiation reaction in the multiple incoherent emissions of photons by the electron driven by an external field, we have studied recently the role played by the stochastic nature of photon emission [6]. In classical electrodynamics, it is known that radiation-reaction effects can act as a beneficial, cooling mechanism. This has been observed, for example, in the energy spectrum of ions accelerated via laser-plasma interaction, in the so-called Radiation Pressure Acceleration regime. In fact, by including radiation-reaction effects, the energy spectra of the produced ion bunches resulted narrower than without such effects. However, we have seen that quantum mechanically the trend goes in the opposite direction, exactly due to the importance of the stochastic nature of photon emission in the quantum regime. In particular, we have seen that stochasticity effects broaden the energy distribution of an electron beam initially counter-propagating with respect to a strong laser field, whereas classical calculations would predict a narrowing of the energy distribution itself (see Fig. 3).

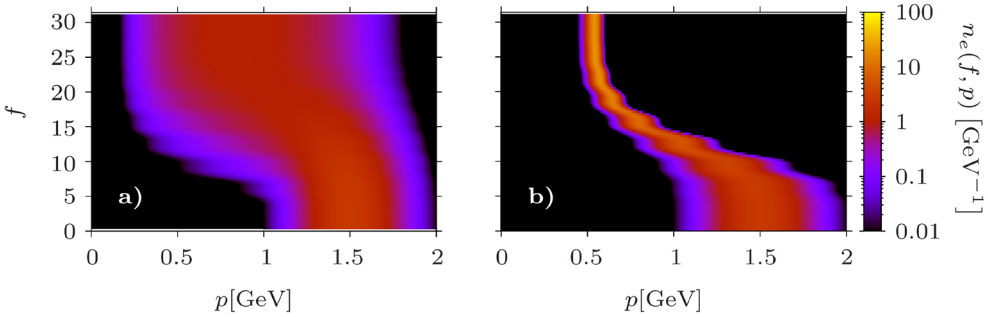

Fig. 3. Electron distribution function $n_e(f,p)$ as a function of the laser phase f and of the quantity p, representing approximately the electron energy. The left panel shows the evolution of the distribution function including self-consistently quantum effects and the right panel shows the corresponding evolution according to classical electrodynamics. The laser intensity in this numerical example is 3×10^{22} W/cm^2.

The connection between quantum radiation reaction and multiple photon emission has led us to study the fundamental process of nonlinear double Compton scattering in the full ultra-relativistic quantum regime from first principles [7]. In this process, two photons are emitted by a single electron, giving the possibility of investigating the effect of the first photon emission on the second one. We have shown that the angular distribution of nonlinear double Compton scattering is substantially different from that of nonlinear single Compton scattering, where only one photon is emitted by the electron. In fact, due to the recoil undergone by the electron in the emission of the first photon, the electron is slowed down and it is more effectively deflected by the laser field. As a result, the second photon is emitted in an angular region, which is broader than that of nonlinear single Compton scattering. We have shown that this feature can be exploited to detect for the first time nonlinear double Compton scattering experimentally already with available laser and electron technology [7].

The effect of the electromagnetic field produced by an electron on the motion of the electron itself is not only related to the resulting energy-momentum loss. The so-called "near field", produced by the electron close to its instantaneous position, can also alter the electron's dynamics. The effect of the near field onto the electron's dynamics is taken into account quantum mechanically by the so-called Schwinger-Dirac equation, which generalizes the Dirac equation. In Ref. [8], we have solved approximately the Schwinger-Dirac equation in the presence of a plane wave, by including leading-order near-field effects. The resulting electron states are a generalization of the so-called Volkov states, solutions of the Dirac equation for an electron in the presence of a plane wave. Now, for a plane-wave laser field the Dirac equation predicts that the average energy of the electron inside the laser-field is degenerated with respect to the spin quantum number. Similar to the Lamb-shift for electrons bound to a nucleus, near-field effects remove this degeneracy [8]. We have suggested an experiment which could measure this effect, in principle, with available technology. To this end, the spin asymmetry of electrons (which did not radiate) is measured after their interaction with a short laser-pulse. According to the Dirac equation, the calculated asymmetry should be zero. A measurement of a non-zero spin asymmetry would therefore be a clear signature for non-linear quantum effects induced by the electron's interaction with its own near field.

Antonino Di Piazza

Complex System Dynamics in Extreme Fields

In the previous section we have discussed various physical situations where radiation reaction plays a significant role in the dynamics of a single electron interacting with a strong laser radiation. In particular, the energy loss of the electron due to radiation reaction has been comparable with its initial energy in the so-called radiation dominated regime. In the case of collective particle dynamics in the laser-plasma interaction, the role of the radiation reaction force becomes more complex. In our recent work [9] we found a counter-intuitive effect of the radiation reaction force on the forward Raman scattering (FRS) of a strong laser radiation in a plasma. In the FRS, the impinging pump laser wave decays into

two electromagnetic sidebands (anti-Stokes and Stokes waves) and simultaneously generates a plasma wave. Usually, one relates the radiation reaction effect to a resulting damping and could expect that this would equally decrease the growth rate of the FRS. In contrast to this, our calculation shows a significant increase of the FRS growth rate, see Fig. 4. The reason for this unexpected effect is the nonlinear mixing of the two sidebands of the FRS. This nonlinear mixing is mediated by the radiation reaction force. In the absence of the radiation reaction force, nonlinear currents that drive the Stokes and the anti-Stokes modes have opposite polarizations. Inclusion of the radiation reaction force induces opposite phase shifts in these nonlinear currents causing an interaction between them. Our calculation shows that the indirect consequence of this interaction between the nonlinear currents leads to an enhancement in the growth rate of the FRS. One may understand this effect in an alternative way as follows: since the radiation reaction force causes damping of the pump laser pulse in a plasma, it facilitates an additional channel of the laser energy decay in the plasma. This channel of the laser energy decay becomes an additional source of the free energy for the anti-Stokes and the Stokes perturbations to grow in the plasma. This leads to the enhanced growth of the FRS.

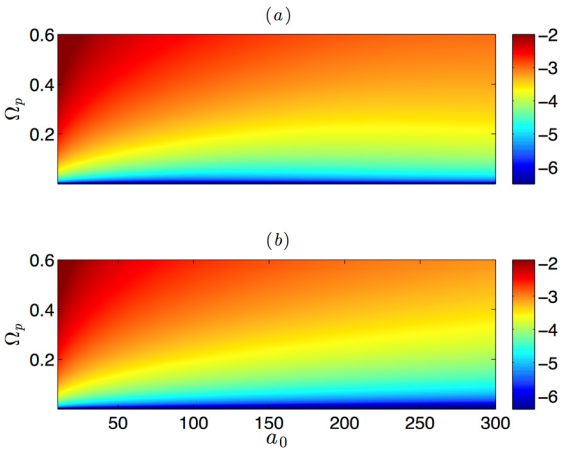

Fig. 4. Growth rate map of the forward Raman scattering as a function of the normalized plasma density Ω_p and normalized pump laser amplitude a_0 (a) including the radiation reaction force and (b) without the radiation reaction force. The colorbar is on the common logarithmic scale.

Super-strong laser fields furthermore offer unique possibilities for the investigation of the quantum vacuum in its full complexity. Different effects of vacuum QED nonlinearities induced by strong laser fields have been considered and elastic photon-photon scattering due to vacuum polarization is shown to be quite feasible for experimental observation [1]. When realizing photon-photon scattering via multiple laser beams the dynamics becomes more complex and interesting new possibilities arise for its enhancement (see also cover figure for the case of two beams). Thus, we have shown in [10] that multiple strong focused laser beams propagating in parallel modulate the vacuum polarization periodically in space which gives rise to constructive interference of the scattered light of a probe laser beam from different layers of the periodic "medium" (Bragg scattering). The Bragg interference arising at a specific impinging direction of the probe wave concentrates the scattered light due to vacuum polarization in specular directions. The interference maxima are enhanced with respect to the usual vacuum polarization effect proportional to the square of the number of modulation periods of the laser field amplitude within the interaction region. The enhancement of the photon-photon scattering rate is maintained also in the total probability of the scattering, integrated by the scattering angle. Thus, the Bragg scattering can be employed to detect the vacuum polarization effect in a setup of multiple crossed superstrong laser beams with parameters envisaged in the future Extreme Light Infrastructure. Similar enhancement effects will exist in all types of inelastic light-by-light scattering processes based on spatially modulated vacuum polarization.

Karen Z. Hatsagortsyan, Naveen Kumar, Christoph H. Keitel

References

[1] A. Di Piazza, C. Müller, K. Z. Hatsagortsyan, and C. H. Keitel, Rev. Mod. Phys. 84 (2012) 1177.
[2] M. Klaiber, E. Yakaboylu, H. Bauke, K. Z. Hatsagortsyan, C. H. Keitel, Phys. Rev. Lett. 110 (2013) 153004.
[3] S. Ahrens, H. Bauke, C. H. Keitel, C. Müller, Phys. Rev. Lett. 109 (2012) 043601.
[4] H. M. Castañeda Cortés, C. Müller, C. H. Keitel and A. Pálffy, Phys. Lett. B 723 (2013) 401.
[5] A. Pálffy and H.-A. Weidenmüller, Phys. Lett. B 718 (2013) 1105.
[6] N. Neitz and A. Di Piazza, Phys. Rev. Lett. 111 (2013) 054802.
[7] F. Mackenroth and A. Di Piazza, Phys. Rev. Lett. 110 (2013) 070402.
[8] S. Meuren and A. Di Piazza, Phys. Rev. Lett. 107 (2011) 260401.
[9] N. Kumar, K. Z. Hatsagortsyan, C. H. Keitel, Phys. Rev. Lett. 111 (2013) 105001.
[10] G. Yu. Kryuchkyan and K. Z. Hatsagortsyan, Phys. Rev. Lett. 107 (2011) 053604.